國 立 交 通 大 學

電信工程學系碩士班

碩士論文

在半正交空時區塊碼系統下之最小錯誤率功率分配法

Power Allocation for Minimum BER in Quasi-Orthogonal Space-Time Block Coded Systems

研 究 生：范盛博　　Student: Sheng-Po Fan

指導教授：李大嵩 博士　　Advisor: Dr. Ta-Sung Lee

中 華 民 國 九 十 五 年 六 月

在半正交空時區塊碼系統下之最小錯誤率功率分配法

Power Allocation for Minimum BER in Quasi-Orthogonal Space-Time Block Coded Systems

研 究 生：范盛博　　Student: Sheng-Po Fan

指導教授：李大嵩 博士　　Advisor: Dr. Ta-Sung Lee

國立交通大學

電信工程學系碩士班

碩士論文

A Thesis
Submitted to Institute of Communication Engineering
College of Electrical Engineering and Computer Science
National Chiao Tung University
in Partial Fulfillment of the Requirements
for the Degree of
Master of Science
in
Communication Engineering
June 2006
Hsinchu, Taiwan, Republic of China

中 華 民 國 九 十 五 年 六 月

在半正交空時區塊碼系統下之最小錯誤率功率分配法

學生：范盛博　　指導教授：李大嵩 博士

國立交通大學電信工程學系碩士班

摘要

在新一代無線通訊中，傳送多樣（Transmit Diversity）為一廣受矚目的技術，其中空時區塊碼尤其常被廣泛使用與討論。有別於常見的正交空時區塊碼(Orthogonal Space-Time Block Code, OSTBC)，在本論文中，吾人集中於探討一種特殊的半正交空時區塊碼 (Quasi-Orthogonal Space-Time Block Code, QOSTBC)，俗稱 ABBA 碼。半正交空時區塊碼的概念是藉由犧牲部分空時碼之間的正交性以換取較高的資料傳輸率。利用 ABBA 碼特有的通道代數架構，吾人在接收端利用 QR 分解來偵測訊號；而在傳送端，則提出一種最小錯誤率的功率分配法來改善平均的傳送錯誤率。一般而言，如果通道可事先得知，即可針對通道做功率分配；有別於此，吾人設計的方法是針對整體通道的平均錯誤率做功率的分配。在不考慮錯誤傳遞的情況下，吾人可推導出一個平均錯誤率的上界；此上界在針對通道特性做平均後，得到一個上界的平均錯誤率公式，進而對此上界的公式做最小錯誤率的功率分配。由模擬結果可以看出，吾人的方法在中高訊號與雜訊比的條件下，可以提供接近於聯合最大可能解碼的表現。

Power Allocation for Minimum BER in Quasi-Orthogonal Space-Time Block Coded Systems

Student: Sheng-Po Fan Advisor: Dr. Ta-Sung Lee

Department of Communication Engineering

National Chiao Tung University

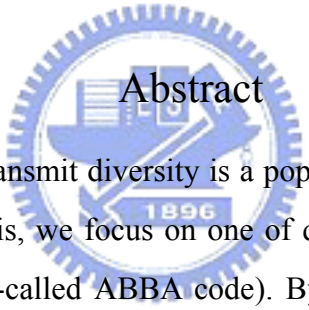

Abstract

It is well known that transmit diversity is a popular technique in modern wireless communication. In this thesis, we focus on one of quasi-orthogonal space-time block codes with full rate (the so-called ABBA code). By exploiting a distinctive channel matrix structure induced by the ABBA code, we derive an explicit formula of the associated QR-decomposition. We propose a minimal BER power allocation scheme for the ABBA code over i.i.d. Rayleigh fading channels under the QR-based successive detection framework. Under a fixed channel realization, we propose optimal power allocation schemes depending on whether or not inter-layer error propagation is taken into account first. Instead of relying on BER under a fixed channel realization, the design criterion adopted by us is the overall mean BER averaged with respect to the channel distribution. Without inter-layer error propagation, we derive an upper bound of the average BER. The closed-form formula is obtained by averaging the upper bound of mean BER with respect to the channel distribution. We then minimize the closed-form formula and an optimal power allocation scheme is obtained. Numerical simulation shows that the resultant performance is almost identical to that of the joint maximum-likelihood decoding in the medium-high SNR region.

Acknowledgement

I would like to express my deepest gratitude to my advisor, Dr. Ta-Sung Lee, for his enthusiastic guidance and great patience. I learn a lot from his positive attitude in many areas. Heartfelt thanks are also offered to all members in the Communication System Design and Signal Processing (CSDSP) Lab for their constant encouragement. Finally, I would like to show my sincere thanks to my parents and Nall for their invaluable love and love.

Contents

List of Figures

List of Tables

Acronym Glossary

AWGN	additive white Gaussian noise
BER	bit error rate
BPSK	binary phase shift keying
BLAST	Bell Lab Layered space time
BS	base station
CIR	channel impulse response
CSI	channel state information
EP	error propagation
EQ	equalizer
IEEE	institute of electrical and electronics engineers
ISI	intersymbol interference
LB	lower bound
LOS	line of sight
MIMO	multiple-input multiple-output
MISO	multiple-input single-output
ML	maximum likelihood
MMSE	minimum mean square error
MRC	maximal ratio combining
MS	mobile station
OSIC	ordered successive interference cancellation
OSTBC	orthogonal space-time block codes
PHY	physical layer
PL	power loading
QAM	quadrature amplitude modulation
QoS	quality of service

QPSK	quaternary phase shift keying
Q-OSTBC	quasi-orthogonal space-time block codes
RX	receiver
SD	spatial diversity
SIMO	single-input multiple-output
SISO	single-input single-output
SM	spatial multiplexing
SNR	signal-to-noise ratio
SIC	successive interference cancellation
STC	space-time coding
STBC	space-time block codes
TX	transmitter
V-BLAST	vertical Bell laboratory layered space-time
ZF	zero forcing

Notations

B	bandwidth
C	transmission code words matrix
E_b	bit energy
E_s	symbol energy
$h_t^{i,j}$	channel gain between the jth transmit and ith receive antenna at time t
M	modulation order
n_T	number of transmit antenna
n_R	number of receive antenna
N_0	noise power spectrum density
y_t^i	received data at the ith transmit at time t
R	rate of space-time block codes
r_b	bit rate
r_s	symbol rate
S	set of signal constellation
P	power loading matrix
p	number of time periods
x_t^j	transmitted signal form the jth transmit at time t
T_s	symbol duration
$\mathbf{w}_j$	weighting vector for the jth layer
n_t^i	additive white noise at the ith receive antenna at time t
η	spectral efficiency
σ_n^2	noise power
ρ	instantaneous SNR
λ	eigenvalue

Chapter 1

Introduction

Orthogonal space-time block codes (OSTBC) with full-rate and full-diversity for complex-valued constellations is well-known to exist only when the number of the transmit antennas is two [1]. Many alternative generalizations capable of boosting date rate at the expense of signal orthogonality have since been proposed, see [2], [3] for detailed literature survey. Among these the quasi-orthogonal space-time block code (Q-OSTBC) family [4], [5], originally tailored for the case with four transmit antennas, is one simple yet effective solution. With the Alamouti's codeword matrix [6] as the building block, Q-OSTBC shows great code construction flexibility for antenna arrays with more than four elements [4]. There have been many different forms for Q-OSTBC [4], [5]; all of them share a group-decoupled low-complexity decoding facility, and will result in comparable error rate performances [7].

This paper addresses the signal detection problem of a particular Q-OSTBC transmission introduced by [5], which is also termed as the ABBA scheme, over i.i.d. Rayleigh fading channels. In order to realize a bit-error-rate (BER) performance balance between linear equalization and joint maximum likelihood (ML) decoding, we propose to adopt QR-based successive detection with appropriate symbol power allocation. There have been many plausible performance measures for successive

signal recovery [8]-[11], depending on whether or not inter-layer error propagation is taken into account. The average BER with errorless front-layer decision feedback, although being merely a lower bound of the true mean error rate, remains simple to characterize and, moreover, is closely related to an upper bound of the block error probability when error-propagation occurs [10]: it thus serves as an efficient and meaningful performance metric accounting for the actual error rate outcome. Motivated by this fact and to also guarantee a performance improvement regardless of the instantaneous channel conditions, we propose to determine the power loading weights toward minimizing the overall such mean BER, averaged with respect to the channel distribution. Specific contributions of this paper include:

1. By exploiting a distinctive channel matrix structure induced by the ABBA code, we derive an explicit formula of the associated QR-decomposition.
2. With the established analytic QR solution and further leveraging the channel matrix structure, we then derive a closed-form upper bound for the considered BER metric.
3. By minimizing this upper bound the proposed optimal power allocation scheme is obtained through numerical search.

We note that performance enhancement of QR-based receiver via symbol power loading has been addressed in many previous works [8]-[13], almost all of them which are based on error rate criteria under a given channel realization known to the transmitter. Our solution strategy, on the other hand, is grounded on BER averaged over the channel distribution; it is thus universal (independent of the instantaneous channel state information) and does not call for any feedback message from the receiver. A similar design paradigm is also considered in [9] for general MIMO flat-fading channels; the criterion therein is instead via minimal average block error probability.

This thesis is organized as follows. In Chapter 2, the overview of space-time block coded system is introduced and the system model of the ABBA code is built. Moreover, the conventional decoding methods are also introduced here. In Chapter 3, under a fixed channel realization known to the transmitter, we design the transmit power allocation algorithms for minimum BER in a quasi-orthogonal dpace-time block code for the error propagation free and error propagation cases. In Chapter 4, the problem statement is formulated. The main result are presented and the numerical performance of the proposed scheme is illustrated. Finally, we conclude this thesis and propose some potential future works in Chapter 5.

Chapter 2

System Model of Quasi-Orthogonal Space-Time Block Codes

This chapter presents the overview of space-time block coded systems and quasi-orthogonal space-tome block codes (Q-OSTBC) will be introduced. Q-OSTBC can provide full rate but sacrifice their diversity. We focus on the ABBA code that is one of Q-OSTBC and discuss its conventional decoding methods and then extend the ABBA code to Alamouti scheme based multi-group systems. Afterwards, we will review the QR decomposition and introduce the QR decomposition of Alamouti scheme based on multi-group systems. The result of QR decomposition for Alamouti scheme based multi-group systems has a special structure. The received symbols are detected by exploiting this special structure and its performances are compared with conventional decoding methods. In addition, we find that diagonal entries of the upper triangular matrix under QR decomposition are associated with the entries of the Alamouti scheme based multi-group channel matrix. They can be written in terms of determinants of Alamouti scheme based multi-group channel matrix and its partitioned matrices. They are helpful for us to analyze the Alamouti scheme based multi-group systems.

2.1 Review of Space-Time Block Codes

In modern wireless communications, transmit diversity has been popular technique over fading channels especially when the power constraint and bandwidth efficiency are the major concerns. Sometimes, multiple antennas at the receiver may be often impractical. Therefore, this leads us to the use of multiple transmit antennas. Here, we only concentrate on one attractive approach to transmit diversity which is space-time coding (STC). Space-time coding introduces temporal and spatial correlations into signals transmitted from different antennas, so as to provide diversity at the receiver or coding gain without sacrificing the bandwidth. The concept of space-time coding was proposed by Tarokh, Seshadri and Calderbank first. This code is called space-time trellis codes. It can provide diversity gain but its decoding complexity grows with the number of antennas. In the issue of decoding complexity, the concept of space-time block codes was proposed by Tarokh, Jafarkhani and Calderbank [1]. The space-time block code matrices are orthogonal matrices and can provide full diversity gain. It is noted that full diversity gain is equal to the number of transmit antennas. It is convenient for us that a simple maximum-likelihood decoding algorithm is used at the receiver. A simple and famous space-time block codes is called Alamouti code [6] that can provide full rate and full diversity gain with two transmit antennas. In this section, we first review Alamouti scheme and Q-OSTBC, including their encoding and decoding methods.

2.1.1 Alamouti Space-Time Code

In the Alamouti space-time encoder, we assume that an *M*-ary modulation scheme is used and each group of m information bits is first modulated, where $m = \log_2 M$. The input symbols to the space-time encoder are divided into groups of two symbols in

each encoding operation. At a given symbol period, the two symbols in each group $\{x_1, x_2\}$ are transmitted simultaneously from the two antennas. The signal transmitted from antenna 1 is x_1 and the signal transmitter from antenna 2 is x_2. In the next symbol period, the signal x_2^* is transmitted from antenna 1 and the signal $-x_1^*$ is transmitted from antenna 2. Denote by $(.)^T$, $(.)^*$, and $(.)^H$, respectively the transpose, complex conjugate, and Hermitian operations. Two modulated symbols x_1 and x_2 are encoded and mapped to the transmit antennas according to a code matrix given by

$$\mathbf{X} = \begin{bmatrix} x_1 & x_2 \\ x_2^* & -x_1^* \end{bmatrix}. \tag{2.1}$$

The code matrix $\mathbf{X}$ is transmitted via the two transmit antennas and the transmit power must be normalized. Note that the rate of the Alamouti code is equal to one.

Let us denote the transmit sequences from antennas 1 and 2 by $\mathbf{x}^1$ and $\mathbf{x}^2$, and they are given by $\mathbf{x}^1 = \begin{bmatrix} x_1 & x_2^* \end{bmatrix}$ and $\mathbf{x}^2 = \begin{bmatrix} x_2 & -x_1^* \end{bmatrix}$, respectively. The key feature of the Alamouti scheme is that the transmit sequences from the two transmit antennas are orthogonal, since the inner product of the sequences $\mathbf{x}^1$ and $\mathbf{x}^2$ is zero, i.e.

$$\mathbf{x}^1 \left(\mathbf{x}^2\right)^H = x_1 x_2^* - x_2^* x_1 = 0. \tag{2.2}$$

The code matrix has the following property (orthogonal matrix)

$$\mathbf{X} \cdot \mathbf{X}^H = \begin{bmatrix} |x_1|^2 + |x_2|^2 & 0 \\ 0 & |x_1|^2 + |x_2|^2 \end{bmatrix} = \left(|x_1|^2 + |x_2|^2\right)\mathbf{I}_2, \tag{2.3}$$

where $\mathbf{I}_2$ is a 2×2 identity matrix.

Let $h_1(t)$ and $h_2(t)$ be the fading channel coefficients from the first and second transmit antennas to the receiver antenna respectively and they are constant over two

consecutive symbol periods. The real part and imaginary part of channel coefficients have the same variance 0.5. Assuming that there is only one receive antenna used at the receiver, we denote the received data over two consecutive symbol periods as y_1 and y_2. The received signals are expressed as

$$\begin{bmatrix} y_1 \\ y_2 \end{bmatrix} = \begin{bmatrix} x_1 & x_2 \\ x_2^* & -x_1^* \end{bmatrix} \begin{bmatrix} h_1 \\ h_2 \end{bmatrix} + \begin{bmatrix} n_1 \\ n_2 \end{bmatrix}, \tag{2.4}$$

where the noise samples n_1 and n_2 are independent complex Gaussian random variables with zero mean. They represent additive Gaussian samples at time t and $t+T$, respectively. The real part and imaginary part of noise have the same variance $n_T/(2\mathrm{SNR})$. The average energy of the symbols transmitted from each transmit antenna is normalized to be one. It is clear that the average power of the received signal at each receive antenna is n_T. Then, we arrange the received signals and have

$$\begin{bmatrix} y_1 \\ y_2^* \end{bmatrix} = \begin{bmatrix} h_1 & h_2 \\ -h_2^* & h_1^* \end{bmatrix} \begin{bmatrix} x_1 \\ x_2 \end{bmatrix} + \begin{bmatrix} n_1 \\ n_2^* \end{bmatrix} \rightarrow \mathbf{y} = \mathbf{H}\mathbf{x} + \mathbf{n}. \tag{2.5}$$

The block diagram that includes modulator, serial to parallel structure and Alamouti encoder is shown in Figure 2.1. The data stream is demultiplexed into two substreams which are converted from serial to parallel and mapped to Alamouti encoder.

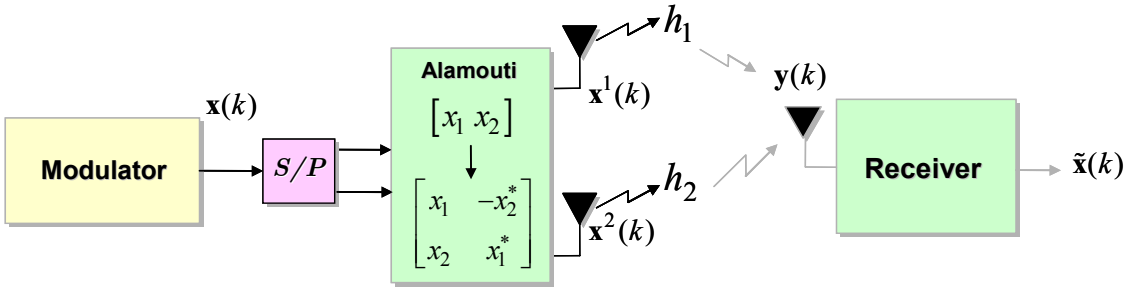

Figure 2.1: A block diagram of the Alamouti space-time coded system for two transmit antennas and single receive antenna

2.1.2 OSTBC for Real and Complex Signal Constellations

It is well known that the key feature of the Alamouti scheme is orthogonal between the sequences generated by the two transmit antennas. This scheme was generalized to more than two transmit antennas by applying the theory of orthogonal designs. The generalized schemes are referred to as space-time block codes (STBC) [1]. To design space-time block codes that provide the properties of the Alamouti code for more than two transmit antennas, let us assume that the signal constellations consists of 2^m points. A block of km information bits are mapped into the signal constellation to select k modulated signals x_1, x_2,…, x_k, where each group of m bits selects a constellation signal. The space-time block encoder encodes the k modulated signals to generate n_T parallel signal sequences of length p according to the transmission matrix $\mathbf{X}$. These sequences are transmitted through n_T antennas in p transmission symbol periods. The lth row of $\mathbf{X}$ is regarded as a space-time symbol transmitted at time l and the nth column of $\mathbf{X}$ is regarded as a space-time symbol transmitted from n th transmit antenna. In other words, there are p space-time symbols transmitted from each antennas for each block of k input symbols.

The rate of a space-time block code is defined as the ratio between the number of modulated symbols and the number of space-time coded symbols transmitted from each antenna. It is expressed as

$$R = \frac{k}{p}. \tag{2.6}$$

The spectral efficiency of the space-time block code is given by

$$\eta = \frac{r_b}{B} = \frac{r_s mR}{r_s} = \frac{km}{p} \text{ bits/s/Hz}, \tag{2.7}$$

where r_b and r_s are the bit and symbol rate, respectively, and B is the bandwidth.

In order to achieve the full transmit diversity of n_T, the transmission matrix $\mathbf{X}$ is constructed such that

$$\mathbf{X} \cdot \mathbf{X}^H = \left(|x_1|^2 + |x_2|^2 + \cdots + |x_k|^2 \right) \mathbf{I}_2 . \tag{2.8}$$

Due to the code orthogonality, the decoding preserves linear processing structure introduced later. The space-time block codes can be divided into space-time block codes with real signals and complex signals based on the type of the signal constellations. It is well-known that Tarokh's orthogonal designs are based on Radon-Hurwitz Theorem. Tarokh showed that the full rate OSTBC exist for some restricted antenna/modulation configurations. For any arbitrary real signal constellation, such as *M*-ASK, space-time block codes exist for any number of transmit antennas. These codes are full rate ($R = 1$) and offer the full transmit diversity of n_T. It is obvious that the number of symbols the encoder takes as its input is equal to the number of transmission symbol periods required to transmit these symbols. Therefore, these schemes don't require bandwidth expansion. For $R = 1$, OSTBC for complex constellations exists only for two transmit antennas. This is famous scheme that is called "Alamouti scheme". In other words, the Alamouti scheme is unique in the sense that it is the only space-time block code that provides the full diversity without loss of transmission rate for complex signal constellations. It has been proved that a complex orthogonal design and the corresponding space-time block code which provides the full diversity and full transmission rate is not possible for more than two antennas.

For any complex signal constellation, there are space-time block codes that can achieve a rate of $1/2$ for any given number of transmit antennas. We show Figure 2.2 as the block diagram of the OSTBC transmitter for four transmit antennas and one receive antenna. The data stream is demultiplexed into four substreams which are converted from serial to parallel and mapped in the OSTBC encoder.

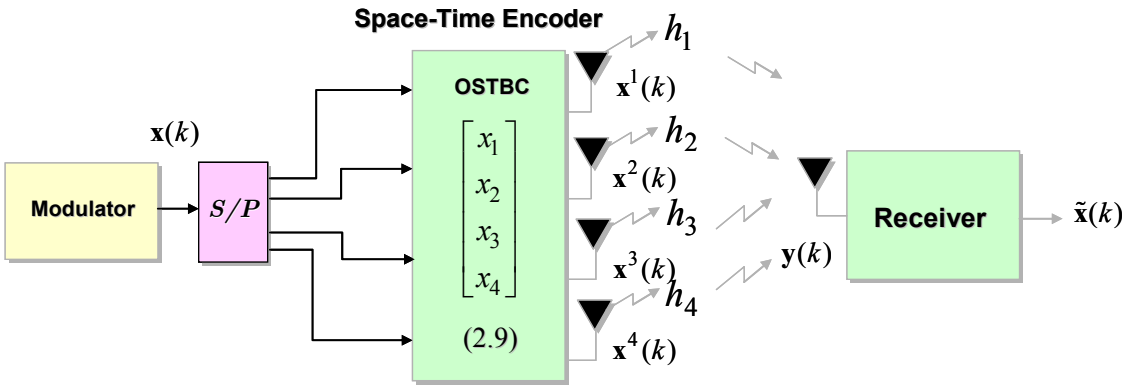

Figure 2.2: A block diagram of the orthogonal space-time block coded system for four transmit antennas and single receive antenna

For four transmit antennas, there are four symbols transmitted and the OSTBC matrix is given by

$$\mathbf{X}_4^C = \begin{bmatrix} x_1 & x_2 & x_3 & x_4 \\ -x_2 & x_1 & -x_4 & x_3 \\ -x_3 & x_4 & x_1 & -x_2 \\ -x_4 & -x_3 & x_2 & x_1 \\ x_1^* & x_2^* & x_3^* & x_4^* \\ -x_2^* & x_1^* & -x_4^* & x_3^* \\ -x_3^* & x_4^* & x_1^* & -x_2^* \\ -x_4^* & -x_3^* & x_2^* & x_1^* \end{bmatrix}, \tag{2.9}$$

where it is obvious that the inner product of any two columns of these matrices is zero. At the receiver, we obtain received signals and write them in terms of matrix. The system model is given by

$$\begin{bmatrix} y_1 \\ y_2 \\ y_3 \\ y_4 \\ y_5 \\ y_6 \\ y_7 \\ y_8 \end{bmatrix} = \begin{bmatrix} x_1 & x_2 & x_3 & x_4 \\ -x_2 & x_1 & -x_4 & x_3 \\ -x_3 & x_4 & x_1 & -x_2 \\ -x_4 & -x_3 & x_2 & x_1 \\ x_1^* & x_2^* & x_3^* & x_4^* \\ -x_2^* & x_1^* & -x_4^* & x_3^* \\ -x_3^* & x_4^* & x_1^* & -x_2^* \\ -x_4^* & -x_3^* & x_2^* & x_1^* \end{bmatrix} \begin{bmatrix} h_1 \\ h_2 \\ h_3 \\ h_4 \end{bmatrix} + \begin{bmatrix} n_1 \\ n_2 \\ n_3 \\ n_4 \\ n_5 \\ n_6 \\ n_7 \\ n_8 \end{bmatrix}. \tag{2.10}$$

We arrange the received signals and obtain

$$\begin{bmatrix} y_1 \\ y_2 \\ y_3 \\ y_4 \\ y_5^* \\ y_6^* \\ y_7^* \\ y_8^* \end{bmatrix} = \begin{bmatrix} h_1 & h_2 & h_3 & h_4 \\ h_2 & -h_1 & h_1 & -h_3 \\ h_3 & -h_4 & -h_1 & h_2 \\ h_4 & -h_3 & h_2 & -h_1 \\ h_1^* & h_2^* & h_3^* & h_4^* \\ h_2^* & -h_1^* & h_4^* & -h_3^* \\ h_3^* & -h_4^* & -h_1^* & h_2^* \\ h_4^* & h_3^* & -h_2^* & -h_1^* \end{bmatrix} \begin{bmatrix} x_1 \\ x_2 \\ x_3 \\ x_4 \end{bmatrix} + \begin{bmatrix} n_1 \\ n_2 \\ n_3 \\ n_4 \\ n_5^* \\ n_6^* \\ n_7^* \\ n_8^* \end{bmatrix} \rightarrow \mathbf{y} = \mathbf{H}\mathbf{x} + \mathbf{n}. \tag{2.11}$$

Now, we have the system model and channel matrix of OSTBC. The channel matrix of OSTBC preserves the property that the inner product of any two columns of channel matrix is zero. Then, this characteristic is exploited to discuss their decoding algorithms in the next section. We can see the advantage of the orthogonality of OSTBC and simplify the decoding process.

2.1.3 Decoding of OSTBC

The decoding algorithm of space-time block codes is introduced now. Assuming that the channel coefficients $h_{n,m}(t)$ are constant over p symbol time slots and the maximum likelihood decoding is used at the receiver. For simplicity, the decoding algorithm of Alamouti scheme is considered first. If the channel fading coefficients can

be perfectly known to the receiver, the decoder will use them as the channel state information (CSI). Assuming that all the signals in the modulation constellation are equiprobable, a maximum likelihood decoding chooses possible values from the signal modulation constellation to maximize

$$\sum_{m=1}^{n_R}\sum_{t=1}^{p}\left|y_{t,m}-\sum_{n=1}^{n_T}h_{n,m}(t)x_{t,n}\right|^2 . \tag{2.12}$$

where n_T and n_R represent the number of transmit antenna and receive antenna, respectively. After some manipulations, a simple form for the Alamouti scheme can be obtained. The maximum likelihood decoding chooses a pair of $(\tilde{x}_1,\tilde{x}_2)$ signal from the signal modulation constellation to minimize the distance metric

$$\begin{aligned} &d^2(y_1,h_1\tilde{x}_1+h_2\tilde{x}_2)+d^2(y_2,h_1\tilde{x}_2^*-h_2\tilde{x}_1^*) \\ &=\left|y_1-h_1\tilde{x}_1-h_2\tilde{x}_2\right|^2+\left|y_2-h_1\tilde{x}_2^*+h_2\tilde{x}_1^*\right|^2 . \end{aligned} \tag{2.13}$$

Due to the orthogonality from each of the antennas, we can exploit this important property to translate the maximum likelihood decoding into maximum ratio combining directly. The new decision statistics are constructed and can be given by

$$\hat{\mathbf{y}}=\mathbf{H}^H\mathbf{y}=\mathbf{H}^H(\mathbf{H}\mathbf{x}+\mathbf{n})=\left(|h_1|^2+|h_2|^2\right)\mathbf{x}+\hat{\mathbf{n}} . \tag{2.14}$$

It is clear that a two-dimensional minimization problem can be decoupled into two one-dimensional problems

$$\tilde{x}_1=\arg\min_{\tilde{x}_1}\left|\hat{y}_1-\left(|h_1|^2+|h_2|^2\right)\tilde{x}_1\right|^2 \quad , \quad \tilde{x}_2=\arg\min_{\tilde{x}_2}\left|\hat{y}_2-\left(|h_1|^2+|h_2|^2\right)\tilde{x}_2\right|^2 . \tag{2.15}$$

It is also obvious that each symbol is decoded separately using only linear processing. We apply the decoding process of the Alamouti scheme to the decoding process of space-time block codes. The case for four transmit antennas and one receive antenna is considered. The structure of maximum likelihood decoding is studied and the new decision statistics is constructed. The new decision statistics can be given by

$$\hat{\mathbf{y}} = \mathbf{H}^H \mathbf{y} = \mathbf{H}^H (\mathbf{H}\mathbf{x} + \mathbf{n}) = \left(|h_1|^2 + |h_2|^2 + |h_3|^2 + |h_4|^2 \right) \mathbf{x} + \hat{\mathbf{n}} . \quad (2.16)$$

A four-dimensional minimization problem can be decoupled into four one-dimensional problems as well

$$\begin{aligned}
\tilde{x}_1 &= \arg\min_{\tilde{x}_1} \left| \hat{y}_1 - \left(|h_1|^2 + |h_2|^2 + |h_3|^2 + |h_4|^2 \right) \tilde{x}_1 \right|^2 , \\
\tilde{x}_2 &= \arg\min_{\tilde{x}_2} \left| \hat{y}_2 - \left(|h_1|^2 + |h_2|^2 + |h_3|^2 + |h_4|^2 \right) \tilde{x}_2 \right|^2 , \\
\tilde{x}_3 &= \arg\min_{\tilde{x}_3} \left| \hat{y}_3 - \left(|h_1|^2 + |h_2|^2 + |h_3|^2 + |h_4|^2 \right) \tilde{x}_3 \right|^2 , \\
\tilde{x}_4 &= \arg\min_{\tilde{x}_4} \left| \hat{y}_4 - \left(|h_1|^2 + |h_2|^2 + |h_3|^2 + |h_4|^2 \right) \tilde{x}_4 \right|^2 . \quad (2.17)
\end{aligned}$$

It is emphasized that the space-time block codes provide two important properties

- Simple decoding：Each symbol is decoded separately by using linear processing.
- Diversity gain：The codes satisfy the rank criterion and provide the maximum possible diversity.

However, we know that "full rate" orthogonal designs with complex modulated symbols in its transmission matrix are impossible for more than two transmit antennas as discussed in Section 2.1.2. Sometimes, the transmission rate (spectral efficiency) is expected to be raised. Therefore, the concept of Q-OSTBC introduced in the next section resulted.

2.2 Quasi-Orthogonal Space-Time Block Codes

The main properties of an orthogonal design are simple separate decoding and full diversity. In order to design full-rate codes, the simple separate decoding property is relaxed. In Q-OSTBC, the transmission matrix columns are divided into groups. When columns in each group are not orthogonal to each other, different groups are orthogonal to each other. The application of a structure is to design codes which have higher transmission rates while sacrificing the full diversity. We will focus on the rate one

code which is quasi-orthogonal and provides partial diversity. In particular, Q-OSTBC for four transmit antennas and single receive antenna are introduced and its decoding algorithms are compared with the maximum likelihood decoding. The simplest form of this code can be expressed in terms of four copies of the Alamouti scheme. Here, we focus on the ABBA code proposed by Tirkkonen.

2.2.1 The ABBA Code

It is well-known that Tirkkonen proposed a full rate space-time block code for four transmit antennas that had partial diversity [5]. In order to measure the non-orthogonality, Tirkkonen defined the ratio of the squared magnitude of the off-diagonal entries to the squared magnitude of the diagonal entries in the Hermitian square of the code matrix. The expectation value is taken over all symbol constellations of the ratio of the squared Frobenius norms of the off-diagonal $\mathbf{N}$ and the diagonal value $\sum_{i=1}^{4}|x_i|^2$. The ratio is given by

$$\mu_{no} = \frac{1}{4} E\left\langle \left(\frac{\|\mathbf{N}\|_2}{\sum_{i=1}^{4}|x_i|^2} \right)^2 \right\rangle. \tag{2.18}$$

Tirkkonen tried to minimize the ratio by choosing the appropriate code. The minimal value of μ_{no} for a four by four block code of the form is 0.25. In the simplest form of the minimal non-orthogonality code, we consider a wireless link, with four transmit antennas and single receive antenna, which adopts the Q-OSTBC transmission [5]. Four transmitted symbols from the four transmit antennas are given by

$$\begin{bmatrix} x_1 & x_2 & x_3 & x_4 \\ x_2^* & -x_1^* & x_4^* & -x_3^* \\ x_3 & x_4 & x_1 & x_2 \\ x_4^* & -x_3^* & x_2^* & -x_1^* \end{bmatrix}. \tag{2.19}$$

It is obvious that it has two copies of the 2×2 Alamouti block code with symbols x_1, x_2 on the block diagonal, and two copies of the Alamouti code with symbols x_3, x_4 on the block anti-diagonal. The scheme is called "ABBA" and can be expressed as

$$\begin{bmatrix} \mathbf{A} & \mathbf{B} \\ \mathbf{B} & \mathbf{A} \end{bmatrix}. \tag{2.20}$$

Multiplying the Hermitian of the ABBA code matrix with the ABBA code matrix, the result is given by

$$\begin{aligned} &\begin{bmatrix} x_1 & x_2 & x_3 & x_4 \\ x_2^* & -x_1^* & x_4^* & -x_3^* \\ x_3 & x_4 & x_1 & x_2 \\ x_4^* & -x_3^* & x_2^* & -x_1^* \end{bmatrix}^H \begin{bmatrix} x_1 & x_2 & x_3 & x_4 \\ x_2^* & -x_1^* & x_4^* & -x_3^* \\ x_3 & x_4 & x_1 & x_2 \\ x_4^* & -x_3^* & x_2^* & -x_1^* \end{bmatrix} \\ &= \left(|h_1|^2 + |h_2|^2 + |h_3|^2 + |h_4|^2\right)\mathbf{I}_4 + 2\,\mathrm{Re}[x_1 x_3^* + x_2 x_4^*] \begin{bmatrix} 0 & 0 & 1 & 0 \\ 0 & 0 & 0 & 1 \\ 1 & 0 & 0 & 0 \\ 0 & 1 & 0 & 0 \end{bmatrix}. \end{aligned} \tag{2.21}$$

It is emphasized that the non-orthogonality of the ABBA code is shown as follows

$$\mathbf{N} = 2\,\mathrm{Re}[x_1 x_3^* + x_2 x_4^*] \begin{bmatrix} 0 & 0 & 1 & 0 \\ 0 & 0 & 0 & 1 \\ 1 & 0 & 0 & 0 \\ 0 & 1 & 0 & 0 \end{bmatrix}. \tag{2.22}$$

From the above equation, it is obvious that the interferences exist between symbols x_1, x_3 and x_2, x_4; the encoding of the ABBA code is very similar to the encoding of OSTBC. Therefore, we show Figure 2.3 as the block diagram of the ABBA code and introduce its decoding in the next section.

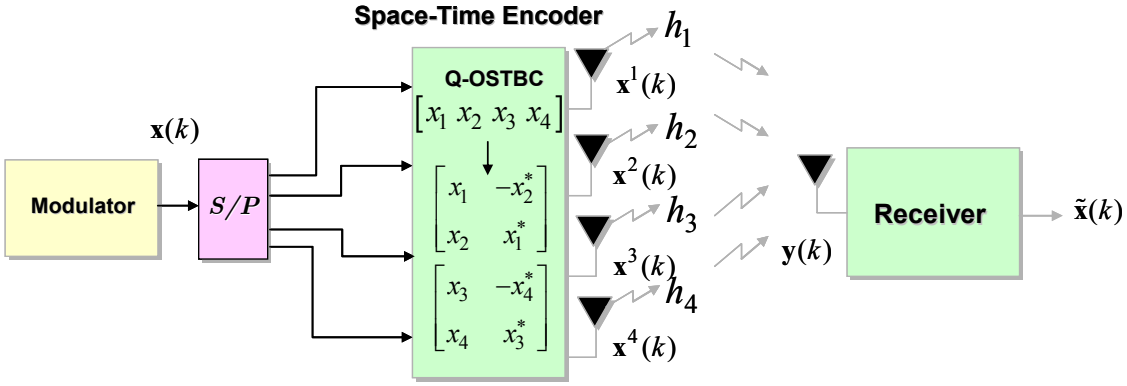

Figure 2.3: A block diagram of the quasi-orthogonal space-time block coded system for four transmit antennas and single receive antenna

2.2.2 Least Minimal Mean Square Estimate (LMMSE)

The decoding of the ABBA code is introduced and compared with the maximum likelihood decoding. Under flat fading channel assumption, the temporal received signal vector is given by

$$\begin{bmatrix} y_1 \\ y_2 \\ y_3 \\ y_4 \end{bmatrix} = \begin{bmatrix} x_1 & x_2 & x_3 & x_4 \\ x_2^* & -x_1^* & x_4^* & -x_3^* \\ x_3 & x_4 & x_1 & x_2 \\ x_4^* & -x_3^* & x_2^* & -x_1^* \end{bmatrix} \underbrace{\begin{bmatrix} h_1 \\ h_2 \\ h_3 \\ h_4 \end{bmatrix}}_{\mathbf{h}} + \begin{bmatrix} n_1 \\ n_2 \\ n_3 \\ n_4 \end{bmatrix}. \tag{2.23}$$

where y_i and n_i are, respectively, the ith received signal and the corresponding noise component, and h_i is the channel gain between the ith transmit antenna and the receive antenna. The signal model (2.23) can be further rearranged into

$$\begin{bmatrix} y_1 \\ y_2^* \\ y_3 \\ y_4^* \end{bmatrix} = \begin{bmatrix} h_1 & h_2 & h_3 & h_4 \\ -h_2^* & h_1^* & -h_4^* & h_3^* \\ h_3 & h_4 & h_1 & h_2 \\ -h_4^* & h_3^* & -h_2^* & h_1^* \end{bmatrix} \begin{bmatrix} x_1 \\ x_2 \\ x_3 \\ x_4 \end{bmatrix} + \begin{bmatrix} n_1 \\ n_2^* \\ n_3 \\ n_4^* \end{bmatrix} \rightarrow \mathbf{y} = \mathbf{H}\mathbf{x} + \mathbf{n}, \tag{2.24}$$

where the channel matrix is expressed as

$$\mathbf{H} = \begin{bmatrix} h_1 & h_2 & h_3 & h_4 \\ -h_2^* & h_1^* & -h_4^* & h_3^* \\ h_3 & h_4 & h_1 & h_2 \\ -h_4^* & h_3^* & -h_2^* & h_1^* \end{bmatrix}. \tag{2.25}$$

The following assumptions are made in the sequel:

1. The channel $\mathbf{h}$ is i.i.d. zero-mean complex white Gaussian with covariance $\mathbf{I}$
2. The noise $\mathbf{n}$ is i.i.d. zero-mean complex white Gaussian with covariance $N_0\mathbf{I}$

Now, we process the channel with the Hermitian conjugate of the channel matrix and obtain

$$\mathbf{H}^H \begin{bmatrix} y_1 \\ y_2^* \\ y_3 \\ y_4^* \end{bmatrix} = \left(\sum_{i=1}^{4} |h_i|^2 \, \mathbf{I} + \tilde{\mathbf{N}} \right) \begin{bmatrix} x_1 \\ x_2 \\ x_3 \\ x_4 \end{bmatrix} + \text{noise}, \tag{2.26}$$

where the non-vanishing correlation matrix $\tilde{\mathbf{N}}$ that is similar to (2.22) is given by

$$\tilde{\mathbf{N}} = 2\,\mathrm{Re}[h_1 h_3^* + h_2 h_4^*] \begin{bmatrix} 0 & 0 & 1 & 0 \\ 0 & 0 & 0 & 1 \\ 1 & 0 & 0 & 0 \\ 0 & 1 & 0 & 0 \end{bmatrix}. \tag{2.27}$$

In the non-vanishing correlation matrix $\tilde{\mathbf{N}}$, the non-diagonal entries show the non-orthogonality and the corresponding decorrelating matrix is shown as:

$$\mathbf{D} = \frac{1}{1-a^2} \begin{bmatrix} 1 & 0 & -a & 0 \\ 0 & 1 & 0 & -a \\ -a & 0 & 1 & 0 \\ 0 & -a & 0 & 1 \end{bmatrix}, \tag{2.28}$$

$$a = \frac{2\,\mathrm{Re}[h_1 h_3^* + h_2 h_4^*]}{h_1 h_1^* + h_2 h_2^* + h_3 h_3^* + h_4 h_4^* + b}. \tag{2.29}$$

where we select different values of b for different estimates of the symbols. Compared the least minimal mean squares estimate with the maximum likelihood decoding, the decision metric is in the form (2.12) if perfect channel state information is available. The maximum likelihood decision metric can be calculated as the sum of

two terms $f_{13}(x_1,x_3)+f_{24}(x_2,x_4)$, where $f_{13}(x_1,x_3)$ is independent of x_2 and x_4 and $f_{24}(x_2,x_4)$ is independent of x_1 and x_3. Minimizing $f_{13}(x_1,x_3)+f_{24}(x_2,x_4)$ is equivalent to minimizing $f_{13}(x_1,x_3)$ and $f_{24}(x_2,x_4)$, respectively. After some manipulations, $f_{13}(x_1,x_3)$ and $f_{24}(x_2,x_4)$ are given by

$$\begin{aligned} f_{13}(x_1,x_3) &= \left(\sum_{i=1}^{4}|h_i|^2\right)\left(|x_1|^2+|x_3|^2\right) \\ &+2\,\mathrm{Re}\left\{\left(-h_1y_1^*-h_2^*y_2-h_3y_3^*-h_4^*y_4\right)x_1+\left(-h_3y_1^*-h_4^*y_2-h_1y_3^*-h_2^*y_4\right)x_3\right\} \\ &+4\,\mathrm{Re}\left(h_1h_3^*+h_2h_4^*\right)\mathrm{Re}\left(x_1x_3^*\right), \end{aligned} \tag{2.30}$$

$$\begin{aligned} f_{24}(x_1,x_3) &= \left(\sum_{i=1}^{4}|h_i|^2\right)\left(|x_2|^2+|x_4|^2\right) \\ &+2\,\mathrm{Re}\left\{\left(-h_2y_1^*+h_1^*y_2-h_4y_3^*+h_3^*y_4\right)x_2+\left(-h_4y_1^*+h_3^*y_2-h_2y_3^*+h_1^*y_4\right)x_4\right\} \\ &+4\,\mathrm{Re}\left(h_1h_3^*+h_2h_4^*\right)\mathrm{Re}\left(x_2x_4^*\right). \end{aligned} \tag{2.31}$$

From (2.30) and (2.31), it is obvious that the decoding of $f_{13}(x_1,x_3)$ and $f_{24}(x_2,x_4)$ is more complicated than the maximum likelihood decoding of OSTBC because we must have decoding pairs for the ABBA code. If $\mathrm{Re}(x_1x_3^*)=0$ and $\mathrm{Re}(x_2x_4^*)=0$, the decoding equations can be simplified, the symbols x_1, x_2, x_3, x_4 can be detected separately. For instance, when x_1 and x_2 are real numbers while x_3 and x_4 are imaginary numbers, it is possible for $\mathrm{Re}(x_1x_3^*)=\mathrm{Re}(x_2x_4^*)=0$. It is well known that iterative methods may be used to improve the performance in multiuse interference cancellation but it brings to higher complexity. We avoid adopting these methods here.

There are some examples of Q-OSTBC which have similar properties with the ABBA code. A common example proposed by Jafarkhani is

$$\begin{bmatrix} \mathbf{A} & \mathbf{B} \\ -\mathbf{B}^* & \mathbf{A}^* \end{bmatrix}, \tag{2.32}$$

where $(.)^*$ denotes the complex conjugate of the matrix. Other examples with similar

behaviors are shown as

$$\begin{bmatrix} \mathbf{A} & \mathbf{B} \\ \mathbf{B}^* & -\mathbf{A}^* \end{bmatrix}, \begin{bmatrix} \mathbf{A} & \mathbf{B} \\ -\mathbf{B} & \mathbf{A} \end{bmatrix}, \text{ and } \begin{bmatrix} \mathbf{A} & \mathbf{B} \\ \mathbf{B} & -\mathbf{A} \end{bmatrix}. \tag{2.33}$$

It is easily seen that the main idea of any similar structures for Q-OSTBC can be factorized as four Alamouti schemes. In Section 2.5, the performances of the ABBA code and Jafarkhani code are obtained and they are almost the same. Further, these examples for a rate one code with four transmit antennas are extended into other structures different rates and different number of transmit antennas. For example, a rate $3/4$ code with eight transmit antennas is given by

$$\begin{bmatrix} x_1 & x_2 & x_3 & 0 & x_4 & x_5 & x_6 & 0 \\ -x_2^* & x_1^* & 0 & -x_3 & x_5 & -x_4^* & 0 & x_6 \\ x_3^* & 0 & -x_1^* & -x_2 & -x_6^* & 0 & x_4^* & x_5 \\ 0 & -x_3^* & x_2^* & -x_1 & 0 & x_6^* & -x_5^* & x_4 \\ -x_4 & -x_5 & -x_6 & 0 & x_1 & x_2 & x_3 & 0 \\ -x_5^* & x_4^* & 0 & x_6 & -x_2^* & x_1^* & 0 & x_3 \\ x_6^* & 0 & -x_4^* & x_5 & x_3^* & 0 & -x_1^* & x_2 \\ 0 & x_6^* & -x_5^* & -x_4 & 0 & x_3^* & -x_2^* & -x_1 \end{bmatrix}. \tag{2.34}$$

Then $\mathbf{C}_i$ is defined as the ith column. The inner products with these columns are given by

$$\begin{aligned} &\langle \mathbf{C}_1, \mathbf{C}_i \rangle = 0, i \neq 5 \quad &&\langle \mathbf{C}_2, \mathbf{C}_i \rangle = 0, i \neq 6 \\ &\langle \mathbf{C}_3, \mathbf{C}_i \rangle = 0, i \neq 7 \quad &&\langle \mathbf{C}_4, \mathbf{C}_i \rangle = 0, i \neq 8 \\ &\langle \mathbf{C}_5, \mathbf{C}_i \rangle = 0, i \neq 1 \quad &&\langle \mathbf{C}_6, \mathbf{C}_i \rangle = 0, i \neq 2 \\ &\langle \mathbf{C}_7, \mathbf{C}_i \rangle = 0, i \neq 3 \quad &&\langle \mathbf{C}_8, \mathbf{C}_i \rangle = 0, i \neq 4. \end{aligned} \tag{2.35}$$

The decorrelating matrix for non-vanishing correlation entries is designed similar to (2.28). Compared it with the maximum likelihood decoding, the ML decision metric can be calculated as the sum of $f_{14}(x_1, x_4) + f_{25}(x_2, x_5) + f_{36}(x_3, x_6)$. It is known that to increase the rate is to sacrifice the orthogonality. This is a conflict, but we can select a proper rate for given transmit antennas to obtain the required performance.

2.2.3 Alamouti Scheme Based Multi-Group Systems

In this section, the general form for Q-OSTBC with four transmit antennas is found. Without loss of generality, we can write these structures as

$$\begin{bmatrix} \mathbf{A} & \mathbf{B} \\ \mathbf{C} & \mathbf{D} \end{bmatrix}, \tag{2.36}$$

where $\mathbf{A}$, $\mathbf{B}$, $\mathbf{C}$, and $\mathbf{D}$ are Alamouti schemes individually. This structure is called "Alamouti scheme based on multi-group systems" by us. From Equation (2.23)-(2.25), the similar channel matrix can be obtained as follows

$$\mathbf{H} = \begin{bmatrix} h_{11} & h_{12} & h_{13} & h_{14} \\ -h_{12}^* & h_{11}^* & -h_{14}^* & h_{13}^* \\ h_{31} & h_{32} & h_{33} & h_{34} \\ -h_{32}^* & h_{31}^* & -h_{34}^* & h_{33}^* \end{bmatrix}, \tag{2.37}$$

where h_{mn} represents the fading channel coefficient for the nth transmit antenna and mth transmission symbol slot. If $\mathbf{A}$ and $\mathbf{B}$ are not related to $\mathbf{C}$ and $\mathbf{D}$, it is seen that the rate is two because the meaningful eight symbols transmitted at four transmission symbol slots and this structure is modeled as the framework with four transmit antennas and two receive antennas. In the concept of multiusers, this structure can be imagined that two users have single receive antenna respectively and the base station have four transmit antennas. The different Alamouti schemes are transmitted at the first two symbol time slots and the last two symbol time slots. It is why this structure is called "Alamouti scheme based on multi-group systems". If $\mathbf{C}$ and $\mathbf{D}$ are dependent on $\mathbf{B}$ and $\mathbf{A}$, the rate is one because there are only the meaningful four symbols transmitted at four transmission symbol slots. For example, the form with $\mathbf{C} = -\mathbf{B}^*$ and $\mathbf{D} = \mathbf{A}^*$ which is proposed by Jafarkhani is one of Q-OSTBC. In the next section, the QR decomposition is exploited to the channel matrix of Alamouti scheme based on multi-group systems.

2.3 QR Decomposition of Channel Matrix

First of all, the QR decomposition of Alamouti scheme based on multi-group systems is introduced. The result of QR decomposition for Alamouti scheme based multi-group systems has a special structure. The special structure is exploited to detect the received symbols and the performance is compared with the methods introduced in Section 2.2.2. In addition, the diagonal entries of the upper triangular matrix under QR decomposition are found that they are associated with the entries of the Alamouti scheme based multi-group channels and can be written in terms of determinants of Alamouti scheme based multi-group channels and its partitioned matrices.

2.3.1 Review of QR Decomposition

QR decomposition is one of the well-known decompositions. It is noted that it can be derived from the Gram-Schmidt algorithm straightforwardly. It is well known that the formulation of Gram-Schmidt procedure is to find an orthonormal basis for the space spanned by the original linearly independent basis. The Gram-Schmidt process frequently appears in the matrix form. It is equivalent to QR decomposition. Let us show the lemma of QR decomposition and apply it to Alamouti scheme based multi-group systems.

Lemma 2.1: Every matrix $\mathbf{H}_{m\times n}$ with linearly independent columns can be uniquely factored as $\mathbf{H}=\mathbf{QR}$ in which the columns of $\mathbf{Q}_{m\times n}$ are an orthogonal basis for $R(\mathbf{H})$ and $\mathbf{R}_{n\times n}$ is an upper-triangular matrix with positive diagonal entries.

Based on Lemma 2.1, the QR decomposition is applied to the Alamouti scheme based multi-group channel matrices. The process is presented in the next section.

2.3.2 Channel Matrix Under QR Decomposition

The properties of Alamouti scheme is introduced first. It is important for us to derive the QR composition of Alamouti scheme based multi-group systems. Therefore, the fundamental properties are listed as follows

- The sum of two Alamouti matrices is another Alamouti matrix.
- The product of two Alamouti matrices is another Alamouti matrix.
- The inverse of an Alamouti matrix is another Alamouti matrix.

It is easy to derive the above results and the proofs of them are ignored. From above properties, it is obvious that the Alamouti structure for block matrices is preserved if the matrix operation is used. We arrange them and show Lemma 2.2 and Lemma 2.3. [14].

Lemma 2.2: For a square matrix $\mathbf{H}_{n\times n}$, it is constructed by 2×2 Alamouti sub-blocks. The inverse of $\mathbf{H}_{n\times n}$ is also constructed by 2×2 Alamouti sub-blocks. That is, it is a block matrix with 2×2 Alamouti sub-blocks.

We give the following example in order to explain the above lemma. Consider a matrix $\mathbf{H}_{4\times 4}$ (2.37) with four sub-blocks and it is given by

$$\mathbf{H}=\begin{bmatrix}\mathbf{H}_1 & \mathbf{H}_2\\ \mathbf{H}_3 & \mathbf{H}_4\end{bmatrix}, \tag{2.38}$$

where $\mathbf{H}_1$, $\mathbf{H}_2$, $\mathbf{H}_3$, and $\mathbf{H}_4$ are all 2×2 Alamouti schemes, e.g.,

$$\mathbf{H}_1=\begin{pmatrix}h_{11} & h_{12}\\ -h_{12}^* & h_{11}^*\end{pmatrix}, \text{ and } \mathbf{H}_2=\begin{pmatrix}h_{13} & h_{14}\\ -h_{14}^* & h_{13}^*\end{pmatrix},$$

and

$$\mathbf{H}_3=\begin{pmatrix}h_{31} & h_{32}\\ -h_{32}^* & h_{31}^*\end{pmatrix}, \text{ and } \mathbf{H}_4=\begin{pmatrix}h_{33} & h_{34}\\ -h_{34}^* & h_{33}^*\end{pmatrix}. \tag{2.39}$$

Under some manipulations, all the sub-blocks in $\mathbf{H}^{-1}$ are also 2×2 Alamouti

schemes by using the fundamental properties of the Alamouti matrix. Therefore, we can see that the inverse of the Alamouti scheme based multi-group channel matrix has the same structure.

Lemma 2.3: For a square matrix $\mathbf{H}_{n\times n}$, it is constructed by 2×2 Alamouti sub-blocks. It is noted that $R(\mathbf{H}) = n$. Assume $\mathbf{H}_{n\times n}$ is factored as $\mathbf{H} = \mathbf{QR}$, where the columns of $\mathbf{Q}_{n\times n}$ are an orthogonal basis and $\mathbf{Q}_{n\times n}$ is a square unitary matrix. $\mathbf{R}_{n\times n}$ is an upper-triangular matrix with positive diagonal entries. Then, $\mathbf{Q}_{n\times n}$ is also constructed by 2×2 Alamouti sub-blocks. $\mathbf{R}_{n\times n}$ has a special structure that is a block matrix with multiples of $\mathbf{I}_2$ along its diagonal and with 2×2 Alamouti sub-blocks in its upper triangular part. For instance,

$$\mathbf{H} = \begin{pmatrix} h_{11} & h_{12} & h_{13} & h_{14} \\ -h_{12}^* & h_{11}^* & -h_{14}^* & h_{13}^* \\ h_{31} & h_{32} & h_{33} & h_{34} \\ -h_{32}^* & h_{31}^* & -h_{34}^* & h_{33}^* \end{pmatrix} \tag{2.40}$$

The result under QR decomposition is expressed as

$$\mathbf{Q} = \begin{bmatrix} q_{11} & q_{12} & q_{13} & q_{14} \\ -q_{12}^* & q_{11}^* & -q_{14}^* & q_{13}^* \\ q_{31} & q_{32} & q_{33} & q_{34} \\ -q_{32}^* & q_{31}^* & -q_{34}^* & q_{33}^* \end{bmatrix} \text{ and } \mathbf{R} = \begin{bmatrix} R_{11} & 0 & R_{13} & R_{14} \\ 0 & R_{22} & -R_{14}^* & R_{13}^* \\ 0 & 0 & R_{33} & 0 \\ 0 & 0 & 0 & R_{44} \end{bmatrix}. \tag{2.41}$$

where all 2×2 sub-blocks are Alamouti. It is important for us to emphasize that $R_{11} = R_{22}$ and $R_{33} = R_{44}$.

In [14], we follow the proof and revise the error.

Proof:

First, let us define the Hermitian of the channel matrix as follows:

$$\mathbf{H}^H = \begin{bmatrix} \mathbf{H}_1^H & \mathbf{H}_2^H \\ \mathbf{H}_3^H & \mathbf{H}_4^H \end{bmatrix} \overset{\text{def}}{=} \begin{bmatrix} \mathbf{H}_5 & \mathbf{H}_6 \\ \mathbf{H}_7 & \mathbf{H}_8 \end{bmatrix}. \tag{2.42}$$

The following two observations are introduced. They are useful to complete this Proof.

1. A unitary matrix $\mathbf{Q}_1$ with 2×2 Alamouti sub-blocks is shown by

$$\mathbf{Q}_1 = \frac{1}{\sqrt{\alpha_{\mathbf{H}_5}+\alpha_{\mathbf{H}_6}}}\begin{bmatrix}\mathbf{H}_5^H & -\mathbf{H}_6 \\ \mathbf{H}_6^H & \mathbf{H}_6^{-1}\mathbf{H}_5\mathbf{H}_6\end{bmatrix},$$

and it satisfies that

$$\begin{bmatrix}\mathbf{H}_5 & \mathbf{H}_6\end{bmatrix}\frac{1}{\sqrt{\alpha_{\mathbf{H}_5}+\alpha_{\mathbf{H}_6}}}\begin{bmatrix}\mathbf{H}_5^H & -\mathbf{H}_6 \\ \mathbf{H}_6^H & \mathbf{H}_6^{-1}\mathbf{H}_5\mathbf{H}_6\end{bmatrix} = \begin{bmatrix}\gamma\mathbf{I}_2 & \mathbf{0}\end{bmatrix}. \quad (2.43)$$

2. A unitary matrix $\mathbf{Q}_2$ with 2×2 Alamouti sub-blocks is shown by

$$\mathbf{Q}_2 = \begin{bmatrix}\mathbf{I}_2 & \mathbf{0} \\ \mathbf{0} & \mathbf{H}_8^H/\sqrt{\alpha_{\mathbf{H}_8}}\end{bmatrix},$$

and it satisfies that

$$\begin{bmatrix}\mathbf{H}_7 & \mathbf{H}_8\end{bmatrix}\begin{bmatrix}\mathbf{I}_2 & \mathbf{0} \\ \mathbf{0} & \mathbf{H}_8^H/\sqrt{\alpha_{\mathbf{H}_8}}\end{bmatrix} = \begin{bmatrix}\mathbf{H}_7 & \sqrt{\alpha_{\mathbf{H}_8}}\mathbf{I}_2\end{bmatrix}. \quad (2.44)$$

where $\alpha_{\mathbf{H}_5} = |h_{11}|^2 + |h_{12}|^2$, $\alpha_{\mathbf{H}_6} = |h_{13}|^2 + |h_{14}|^2$, $\alpha_{\mathbf{H}_7} = |h_{31}|^2 + |h_{32}|^2$, and $\alpha_{\mathbf{H}_8} = |h_{33}|^2 + |h_{34}|^2$. It is noted that they are the determinants of $\mathbf{H}_5$, $\mathbf{H}_6$, $\mathbf{H}_7$, and $\mathbf{H}_8$, respectively. That is,

$$\alpha_{\mathbf{H}_5} = \det(\mathbf{H}_5),\ \alpha_{\mathbf{H}_6} = \det(\mathbf{H}_6),\ \alpha_{\mathbf{H}_7} = \det(\mathbf{H}_7), \text{ and } \alpha_{\mathbf{H}_8} = \det(\mathbf{H}_8). \quad (2.45)$$

The error in observation 1 [14, e.q. (9)-(10)] must be revised from $\begin{bmatrix}\mathbf{B} & \mathbf{C}\end{bmatrix}\frac{1}{\sqrt{\alpha_{\mathbf{B}}+\alpha_{\mathbf{C}}}}\begin{bmatrix}\mathbf{B}^H & -\mathbf{C} \\ \mathbf{C}^H & \mathbf{B}\end{bmatrix} = \begin{bmatrix}\sqrt{\alpha_{\mathbf{B}}+\alpha_{\mathbf{C}}}\mathbf{I}_2 & \mathbf{0}\end{bmatrix}$ to (2.43). We must revise the second diagonal matrix $\mathbf{B}$ to $\mathbf{C}^{-1}\mathbf{B}\mathbf{C}$. It is wrong because the product of matrices is not interchangeable such as $\mathbf{B}\mathbf{C} \neq \mathbf{C}\mathbf{B}$.

It is assumed that there is a matrix with Alamouti sub-blocks, e.g., $\mathbf{H}^H = \begin{bmatrix}\mathbf{H}_5 & \mathbf{H}_6 \\ \mathbf{H}_7 & \mathbf{H}_8\end{bmatrix}$. With observation 1, we select

$$\mathbf{Q}_1 = \frac{1}{\sqrt{\alpha_{\mathbf{H}_5} + \alpha_{\mathbf{H}_6}}} \begin{bmatrix} \mathbf{H}_5^H & -\mathbf{H}_6 \\ \mathbf{H}_6^H & \mathbf{H}_6^{-1}\mathbf{H}_5\mathbf{H}_6 \end{bmatrix}, \tag{2.46}$$

and the first step is given by

$$\begin{aligned} &\begin{bmatrix} \mathbf{H}_5 & \mathbf{H}_6 \\ \mathbf{H}_7 & \mathbf{H}_8 \end{bmatrix} \frac{1}{\sqrt{\alpha_{\mathbf{H}_5} + \alpha_{\mathbf{H}_6}}} \begin{bmatrix} \mathbf{H}_5^H & -\mathbf{H}_6 \\ \mathbf{H}_6^H & \mathbf{H}_6^{-1}\mathbf{H}_5\mathbf{H}_6 \end{bmatrix} \\ &= \begin{bmatrix} \gamma\mathbf{I}_2 & \mathbf{0} \\ \frac{1}{\gamma}\left(\mathbf{H}_7\mathbf{H}_5^H + \mathbf{H}_8\mathbf{H}_6^H\right) & \frac{1}{\gamma}\left(-\mathbf{H}_7\mathbf{H}_6 + \mathbf{H}_8\mathbf{H}_6^{-1}\mathbf{H}_5\mathbf{H}_6\right) \end{bmatrix}, \end{aligned} \tag{2.47}$$

where γ is a positive constant defined by $\gamma = \sqrt{\alpha_{\mathbf{H}_5} + \alpha_{\mathbf{H}_6}}$. After that, let us define the matrix $\mathbf{H}_9 = -\mathbf{H}_7\mathbf{H}_6 + \mathbf{H}_8\mathbf{H}_6^{-1}\mathbf{H}_5\mathbf{H}_6$. The result from the first step is reduced to

$$\begin{bmatrix} \gamma\mathbf{I}_2 & \mathbf{0} \\ \frac{1}{\gamma}\left(\mathbf{H}_7\mathbf{H}_5^H + \mathbf{H}_8\mathbf{H}_6^H\right) & \frac{\mathbf{H}_9}{\gamma} \end{bmatrix}. \tag{2.48}$$

With observation 2, we select $\mathbf{Q}_2 = \begin{bmatrix} \mathbf{I}_2 & \mathbf{0} \\ \mathbf{0} & \mathbf{H}_9^H / \sqrt{\alpha_{\mathbf{H}_9}} \end{bmatrix}$ and the second step is given by

$$\begin{bmatrix} \gamma\mathbf{I}_2 & \mathbf{0} \\ \frac{1}{\gamma}\left(\mathbf{H}_7\mathbf{H}_5^H + \mathbf{H}_8\mathbf{H}_6^H\right) & \frac{\mathbf{H}_9}{\gamma} \end{bmatrix} \begin{bmatrix} \mathbf{I}_2 & \mathbf{0} \\ \mathbf{0} & \mathbf{H}_9^H / \sqrt{\alpha_{\mathbf{H}_9}} \end{bmatrix} = \begin{bmatrix} \gamma\mathbf{I}_2 & \mathbf{0} \\ \frac{1}{\gamma}\left(\mathbf{H}_7\mathbf{H}_5^H + \mathbf{H}_8\mathbf{H}_6^H\right) & \frac{\mathbf{H}_9\mathbf{H}_9^H}{\gamma\sqrt{\alpha_{\mathbf{H}_9}}} \end{bmatrix}, \tag{2.49}$$

where $\mathbf{H}_9\mathbf{H}_9^H = \left(\alpha_{\mathbf{H}_9}\right)\mathbf{I}_2 = \left(\det(\mathbf{H}_9)\right)\mathbf{I}_2$. The result from the second step is reduced to

$$\begin{bmatrix} \gamma\mathbf{I}_2 & \mathbf{0} \\ \frac{1}{\gamma}\left(\mathbf{H}_7\mathbf{H}_5^H + \mathbf{H}_8\mathbf{H}_6^H\right) & \frac{\sqrt{\alpha_{\mathbf{H}_9}}}{\gamma}\mathbf{I}_2 \end{bmatrix}. \tag{2.50}$$

The above two processes are arranged as follows

$$\begin{bmatrix}\mathbf{H}_5 & \mathbf{H}_6\\ \mathbf{H}_7 & \mathbf{H}_8\end{bmatrix}\frac{1}{\sqrt{\alpha_{\mathbf{H}_5}+\alpha_{\mathbf{H}_6}}}\begin{bmatrix}\mathbf{H}_5^H & -\mathbf{H}_6\\ \mathbf{H}_6^H & \mathbf{H}_6^{-1}\mathbf{H}_5\mathbf{H}_6\end{bmatrix}\begin{bmatrix}\mathbf{I}_2 & \mathbf{0}\\ \mathbf{0} & \mathbf{H}_9^H/\sqrt{\alpha_{\mathbf{H}_9}}\end{bmatrix}$$

$$=\begin{bmatrix}\gamma\mathbf{I}_2 & \mathbf{0}\\ \frac{1}{\gamma}\left(\mathbf{H}_7\mathbf{H}_5^H+\mathbf{H}_8\mathbf{H}_6^H\right) & \frac{1}{\gamma}\left(-\mathbf{H}_7\mathbf{H}_6+\mathbf{H}_8\mathbf{H}_6^{-1}\mathbf{H}_5\mathbf{H}_6\right)\end{bmatrix}\begin{bmatrix}\mathbf{I}_2 & \mathbf{0}\\ \mathbf{0} & \mathbf{H}_9^H/\sqrt{\alpha_{\mathbf{H}_9}}\end{bmatrix} \quad (2.51)$$

$$=\begin{bmatrix}\gamma\mathbf{I}_2 & \mathbf{0}\\ \frac{1}{\gamma}\left(\mathbf{H}_7\mathbf{H}_5^H+\mathbf{H}_8\mathbf{H}_6^H\right) & \frac{\mathbf{H}_9\mathbf{H}_9^H}{\gamma\sqrt{\alpha_{\mathbf{H}_9}}}\end{bmatrix}=\begin{bmatrix}\gamma\mathbf{I}_2 & \mathbf{0}\\ \frac{1}{\gamma}\left(\mathbf{H}_7\mathbf{H}_5^H+\mathbf{H}_8\mathbf{H}_6^H\right) & \frac{\sqrt{\alpha_{\mathbf{H}_9}}}{\gamma}\mathbf{I}_2\end{bmatrix}.$$

Let us combine $\mathbf{Q}=\mathbf{Q}_1\mathbf{Q}_2=\frac{1}{\sqrt{\alpha_{\mathbf{H}_5}+\alpha_{\mathbf{H}_6}}}\begin{bmatrix}\mathbf{H}_5^H & -\mathbf{H}_6\\ \mathbf{H}_6^H & \mathbf{H}_6^{-1}\mathbf{H}_5\mathbf{H}_6\end{bmatrix}\begin{bmatrix}\mathbf{I}_2 & \mathbf{0}\\ \mathbf{0} & \mathbf{H}_9^H/\sqrt{\alpha_{\mathbf{H}_9}}\end{bmatrix}$

and define the lower triangular matrix $\mathbf{L}=\begin{bmatrix}\gamma\mathbf{I}_2 & \mathbf{0}\\ \frac{1}{\gamma}\left(\mathbf{H}_7\mathbf{H}_5^H+\mathbf{H}_8\mathbf{H}_6^H\right) & \frac{\sqrt{\alpha_{\mathbf{H}_9}}}{\gamma}\mathbf{I}_2\end{bmatrix}$. The result (2.51) can translated into $\mathbf{H}^H\mathbf{Q}=\mathbf{L}$. We rewirte $\mathbf{H}^H\mathbf{Q}=\mathbf{L}$ as $\left(\mathbf{H}^H\mathbf{Q}\right)^H=\mathbf{Q}^H\mathbf{H}=\mathbf{L}^H=\mathbf{R}$ and obtain the final result $\mathbf{H}=\mathbf{Q}\mathbf{R}$ equivalently, where

$$\mathbf{Q}=\frac{1}{\sqrt{\det(\mathbf{H}_5)+\det(\mathbf{H}_6)}}\begin{bmatrix}\mathbf{H}_5^H & -\mathbf{H}_6\\ \mathbf{H}_6^H & \mathbf{H}_6^{-1}\mathbf{H}_5\mathbf{H}_6\end{bmatrix}\begin{bmatrix}\mathbf{I}_2 & \mathbf{0}\\ \mathbf{0} & \mathbf{H}_9^H/\sqrt{\alpha_{\mathbf{H}_9}}\end{bmatrix}, \quad (2.52)$$

and

$$\mathbf{R}=\begin{bmatrix}\gamma\mathbf{I}_2 & \mathbf{0}\\ \frac{1}{\gamma}\left(\mathbf{H}_7\mathbf{H}_5^H+\mathbf{H}_8\mathbf{H}_6^H\right) & \frac{\sqrt{\alpha_{\mathbf{H}_9}}}{\gamma}\mathbf{I}_2\end{bmatrix}^H=\begin{bmatrix}\gamma\mathbf{I}_2 & \frac{1}{\gamma}\left(\mathbf{H}_7\mathbf{H}_5^H+\mathbf{H}_8\mathbf{H}_6^H\right)^H\\ \mathbf{0} & \frac{\sqrt{\alpha_{\mathbf{H}_9}}}{\gamma}\mathbf{I}_2\end{bmatrix}$$

$$=\begin{bmatrix}\sqrt{\det(\mathbf{H}_5)+\det(\mathbf{H}_6)}\mathbf{I}_2 & \frac{\left(\mathbf{H}_7\mathbf{H}_5^H+\mathbf{H}_8\mathbf{H}_6^H\right)^H}{\sqrt{\det(\mathbf{H}_5)+\det(\mathbf{H}_6)}}\\ \mathbf{0} & \frac{\sqrt{\det(\mathbf{H}_9)}}{\sqrt{\det(\mathbf{H}_5)+\det(\mathbf{H}_6)}}\mathbf{I}_2\end{bmatrix}$$

$$=\begin{bmatrix}\sqrt{\det(\mathbf{H}_5)+\det(\mathbf{H}_6)}\mathbf{I}_2 & \frac{\left(\mathbf{H}_7\mathbf{H}_5^H+\mathbf{H}_8\mathbf{H}_6^H\right)^H}{\sqrt{\det(\mathbf{H}_5)+\det(\mathbf{H}_6)}}\\ \mathbf{0} & \frac{\sqrt{\det(\mathbf{H}_9)}}{\sqrt{\det(\mathbf{H}_5)+\det(\mathbf{H}_6)}}\mathbf{I}_2\end{bmatrix}. \quad (2.53)$$

The proof is completed and it is easy to check that the matrix $\mathbf{Q}$ preserves the structure of 2×2 Alamouti sub-blocks and the right upper part of the matrix $\mathbf{R}$ is another Alamouti scheme.

It is obvious that the diagonal entries of matrix $\mathbf{R}$ are related to the determinants of the partitioned matrices. Because $\mathbf{Q}$ is a unitary matrix, the determinant of $\mathbf{Q}$ is equal to one. It is easy to see that the determinant of $\mathbf{H}$ is equal to the determinant of $\mathbf{R}$. Because $\mathbf{R}$ is an upper triangular matrix, the determinant of $\mathbf{R}$ is equal to the products of the diagonal entries. Then, we calculate the determinant of $\mathbf{R}$, and have the following relationship between $\mathbf{R}$ and $\mathbf{H}_9$:

$$\det(\mathbf{H})=\det(\mathbf{R})=(\gamma)^2\left(\frac{\sqrt{\alpha_{\mathbf{H}_9}}}{\gamma}\right)^2=\alpha_{\mathbf{H}_9}=\det(\mathbf{H}_9). \quad (2.54)$$

From the definition of (2.42), the relations are obtained as follows:

$$\det(\mathbf{H}_5)=\det(\mathbf{H}_1^H)=\det(\mathbf{H}_1),\ \ \det(\mathbf{H}_6)=\det(\mathbf{H}_2^H)=\det(\mathbf{H}_2),$$

$$\det(\mathbf{H}_7)=\det(\mathbf{H}_3^H)=\det(\mathbf{H}_3),\ \ \det(\mathbf{H}_8)=\det(\mathbf{H}_4^H)=\det(\mathbf{H}_4). \quad (2.55)$$

Therefore, the determinants of $\mathbf{H}_1$, $\mathbf{H}_2$, and $\mathbf{H}$ are substituted for the determinant of

$\mathbf{H}_5$, $\mathbf{H}_6$, and $\mathbf{H}_9$, respectively. We rewrite $\mathbf{R}$ as

$$\mathbf{R} = \begin{bmatrix} \sqrt{\det(\mathbf{H}_1) + \det(\mathbf{H}_2)}\mathbf{I}_2 & \dfrac{\left(\mathbf{H}_1^H \mathbf{H}_3 + \mathbf{H}_2^H \mathbf{H}_4\right)}{\sqrt{\det(\mathbf{H}_1) + \det(\mathbf{H}_2)}} \\ \mathbf{0} & \dfrac{\sqrt{\det(\mathbf{H})}}{\sqrt{\det(\mathbf{H}_1) + \det(\mathbf{H}_2)}}\mathbf{I}_2 \end{bmatrix}. \tag{2.56}$$

It is noted that the diagonal entries of matrix $\mathbf{R}$ are positive and written in terms of the determinants of the partitioned matrices. Finally, the above derivation for the channel matrix of Alamouti scheme based multi-group systems is arranged and some important properties are listed as follows:

- The channel matrix of Alamouti scheme based multi-group systems is given by

$$\mathbf{H} = \begin{pmatrix} h_{11} & h_{12} & h_{13} & h_{14} \\ -h_{12}^* & h_{11}^* & -h_{14}^* & h_{13}^* \\ h_{31} & h_{32} & h_{33} & h_{34} \\ -h_{32}^* & h_{31}^* & -h_{34}^* & h_{33}^* \end{pmatrix}. \tag{2.57}$$

  It can be factorized as

$$\mathbf{H} = \mathbf{QR} = \begin{bmatrix} q_{11} & q_{12} & q_{13} & q_{14} \\ -q_{12}^* & q_{11}^* & -q_{14}^* & q_{13}^* \\ q_{31} & q_{32} & q_{33} & q_{34} \\ -q_{32}^* & q_{31}^* & -q_{34}^* & q_{33}^* \end{bmatrix} \begin{bmatrix} R_{11} & 0 & R_{13} & R_{14} \\ 0 & R_{11} & -R_{14}^* & R_{13}^* \\ 0 & 0 & R_{33} & 0 \\ 0 & 0 & 0 & R_{33} \end{bmatrix}. \tag{2.58}$$

- The diagonal entries of matrix $\mathbf{R}$ is described as

$$R_{11} = R_{22} = \sqrt{\det(\mathbf{H}_1) + \det(\mathbf{H}_2)}, \tag{2.59}$$

$$R_{33} = R_{44} = \sqrt{\frac{\det(\mathbf{H})}{\det(\mathbf{H}_1) + \det(\mathbf{H}_2)}}, \tag{2.60}$$

  where $\mathbf{H}_1$, $\mathbf{H}_2$, $\mathbf{H}_3$, and $\mathbf{H}_4$ are 2×2 Alamouti schemes in the form (2.39), and the determinants of them are given by

$$\det(\mathbf{H}_1) = |h_{11}|^2 + |h_{12}|^2, \quad \det(\mathbf{H}_2) = |h_{13}|^2 + |h_{14}|^2,$$

$$\det(\mathbf{H}_3) = |h_{31}|^2 + |h_{32}|^2, \quad \det(\mathbf{H}_4) = |h_{33}|^2 + |h_{34}|^2. \tag{2.61}$$

2.4 System Model of the ABBA Code with QR Based Successive Detection

From the above discussions, considering the simple case such as the ABBA code, the channel matrix of the ABBA code is given by

$$\mathbf{H} = \begin{bmatrix} \mathbf{H}_1 & \mathbf{H}_2 \\ \mathbf{H}_2 & \mathbf{H}_1 \end{bmatrix}. \tag{2.62}$$

where

$$\mathbf{H}_1 = \begin{bmatrix} h_1 & h_2 \\ -h_2^* & h_1^* \end{bmatrix} \text{ and } \mathbf{H}_2 = \begin{bmatrix} h_3 & h_4 \\ -h_4^* & h_3^* \end{bmatrix}. \tag{2.63}$$

It can be also factorized as

$$\mathbf{H} = \mathbf{QR} = \begin{bmatrix} q_1 & q_2 & q_3 & q_4 \\ -q_2^* & q_1^* & -q_4^* & q_3^* \\ q_3 & q_4 & q_1 & q_2 \\ -q_4^* & q_3^* & -q_2^* & q_1^* \end{bmatrix} \begin{bmatrix} R_{11} & 0 & R_{13} & 0 \\ 0 & R_{11} & 0 & R_{13} \\ 0 & 0 & R_{33} & 0 \\ 0 & 0 & 0 & R_{33} \end{bmatrix}. \tag{2.64}$$

It is noted that the right upper part of $\mathbf{R}$ is not an Alamouti scheme but a multiples of $\mathbf{I}_2$ along its diagonal. The diagonal entries of matrix $\mathbf{R}$ are described in the same way. There are only six nonzero entries in the upper triangular matrix $\mathbf{R}$ and they are real number.

Since $\mathbf{R}$ is upper triangular, successive symbol detection through canceling the contributions of the previously detected components can be performed, as in [10], [15]. From Equations (2.24) and (2.64), the received signals are multiplied by unitary matrix $\mathbf{Q}^H$ and we obtain

$$\begin{bmatrix} \tilde{y}_1 \\ \tilde{y}_2 \\ \tilde{y}_3 \\ \tilde{y}_4 \end{bmatrix} = \begin{bmatrix} R_{11} & 0 & R_{13} & 0 \\ 0 & R_{11} & 0 & R_{13} \\ 0 & 0 & R_{33} & 0 \\ 0 & 0 & 0 & R_{33} \end{bmatrix} \begin{bmatrix} x_1 \\ x_2 \\ x_3 \\ x_4 \end{bmatrix} + \begin{bmatrix} \tilde{n}_1 \\ \tilde{n}_2 \\ \tilde{n}_3 \\ \tilde{n}_4 \end{bmatrix} \rightarrow \tilde{\mathbf{y}} = \mathbf{R}\mathbf{x} + \tilde{\mathbf{n}}. \tag{2.65}$$

where $\tilde{\mathbf{y}} = \mathbf{Q}^H \mathbf{y}$ and $\tilde{\mathbf{n}} = \mathbf{Q}^H \mathbf{n}$. Assuming that the $\tilde{\mathbf{n}}$ is also complex Gaussian distributed with the same variance as $\mathbf{n}$, Equation (2.65) is equally expressed as

$$\begin{aligned} \tilde{y}_1 &= R_{11}\tilde{x}_1 + R_{13}\tilde{x}_3, \\ \tilde{y}_2 &= R_{11}\tilde{x}_2 + R_{13}\tilde{x}_4, \\ \tilde{y}_3 &= R_{33}\tilde{x}_3, \\ \tilde{y}_4 &= R_{33}\tilde{x}_4. \end{aligned} \tag{2.66}$$

Then, the modified received signals $\hat{y}_i$ is created as follows

$$\hat{y}_i = \tilde{y}_i - \sum_{j=i+1}^{4} R_{ij}\tilde{x}_j = R_{ii}x_i + \sum_{j=i+1}^{4} R_{ij}\left(x_j - \tilde{x}_j\right) + \tilde{n}_i. \tag{2.67}$$

Since $\mathbf{R}$ is upper triangular, successive symbol detection through canceling the contributions of previously detected components can be preformed. That is, the modified received signals $\hat{y}_i$ are detected from the third and fourth rows and the hard decisions are made. Then, we substitute the estimated symbol back into the first and second row so as to remove the interference term and make the hard decisions. The above procedure is described by the following formulas:

$$\tilde{x}_4 = \text{Quant}\left[\frac{\tilde{y}_4}{R_{33}}\right], \quad \tilde{x}_3 = \text{Quant}\left[\frac{\tilde{y}_3}{R_{33}}\right],$$

$$\tilde{x}_2 = \text{Quant}\left[\frac{\tilde{y}_2 - R_{13}\tilde{x}_4}{R_{11}}\right], \text{ and } \tilde{x}_1 = \text{Quant}\left[\frac{\tilde{y}_1 - R_{13}\tilde{x}_3}{R_{11}}\right]. \tag{2.68}$$

where the function $t = \text{Quant}[q]$ sets t to the element of signal constellations that is closest to q. Assuming that these decisions are correct ($x_j = \tilde{x}_j$), Equation (2.66) is simplified into $\hat{y}_i = R_{ii}x_i + \tilde{n}$; that is, the detection procedure turn out to be $\tilde{x}_i = \text{Quant}[\hat{y}_i / R_{ii}]$. It is convenient for us to detect the received signals. The simulations are provided and compared with the LMMSE decoding and ML decoding.

2.5 Computer Simulations

In this section, four transmit antennas and single antenna are used in the transmitter and receiver, respectively. For the transmission rate 2 bits/s/Hz, it is assumed that the rate one Q-OSTBC with QPSK modulation is used and the channel fading is flat over four consecutive transmission symbol slots in Q-OSTBC. The fading channel is i.i.d. complex Gaussian variables with zero mean and half variance per dimension. Noise is i.i.d. complex Gaussian variables while the real part and imaginary part of noise are the same variance $n_T/(2\mathrm{SNR})$. In Figure 2.4, the simulations for the ABBA code and the code proposed by Jafarkhani are presented. It is found that their average BER performances are almost the same.

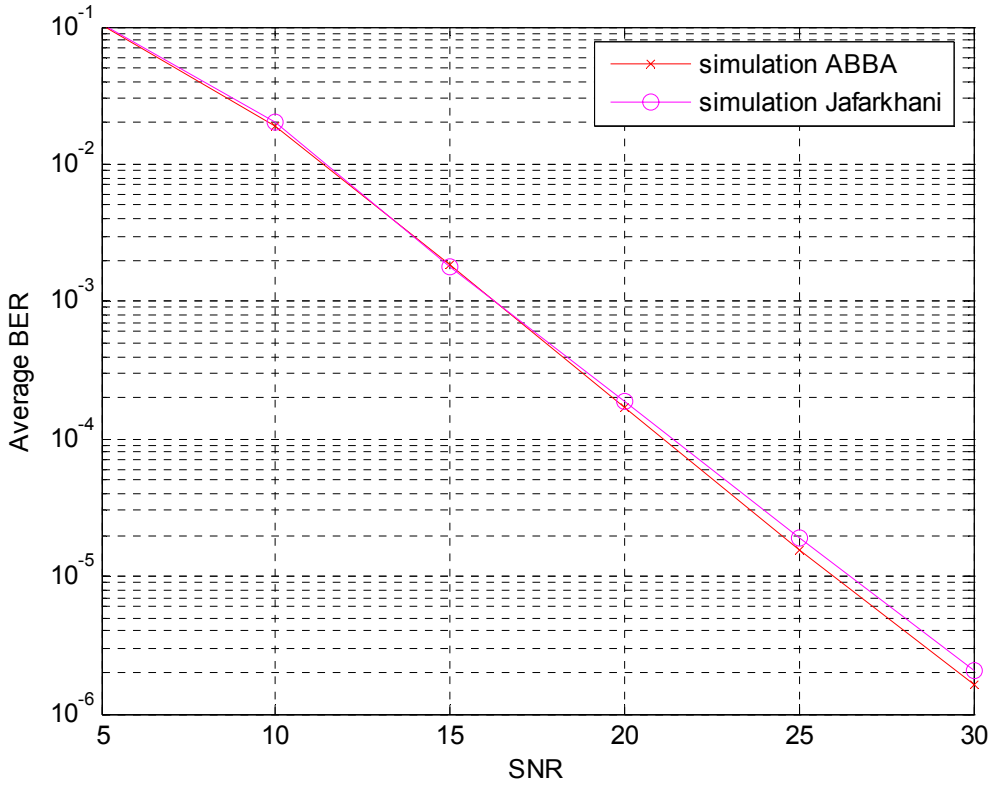

Figure 2.4: Average BER performances of the ABBA code and the code proposed by Jafarkhani

The simulation for the ABBA code with LMMSE and ML decoding are presented and compared with the result for OSTBC. For the transmission rate 2 bits/s/Hz, it is assumed that the rate 1/2 full diversity OSTBC with 16-QAM modulation is used and the channel fading is flat over eight consecutive transmission symbol slots in OSTBC. In Figure 2.5, it is easy to see that the full diversity OSTBC has better performance than the full rate Q-OSTBC in the high SNR region. On the contrary, the full rate Q-OSTBC has better performance than the full diversity OSTBC in the low SNR region. Because the influence on slope of the BER-SNR curve in the high SNR region is the degree of diversity, it is why the full diversity OSTBC has lower bit error rate in the high SNR region. The full rate Q-OSTBC uses a lower modulation order, so the better performance is obtained in the low SNR region.

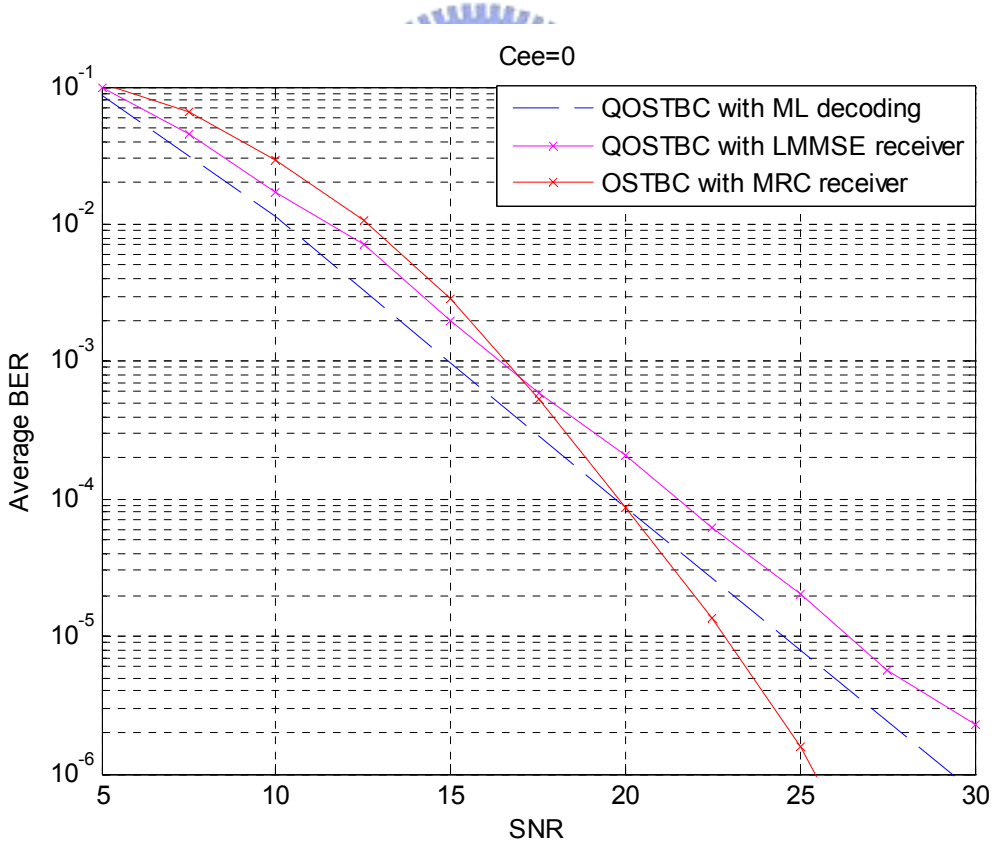

Figure 2.5: Average BER performances of OSTBC and Q-OSTBC

From the point of view in complexity, it is noted that the decoding complexity of Q-OSTBC is higher than OSTBC but the encoding complexity of two codes is similar.

Figure 2.6 shows the average BER performance of the ABBA code with QR-based successive detection compared with the conventional decoding methods. The performance with QR-based successive detection is almost identical to that with the LMMSE receiver and the analysis of the average BER in Figure 2.6 is similar to that in Figure 2.5. It is obvious that we can provide the similar average BER performance with QR-based successive detection compared with the LMMSE receiver.

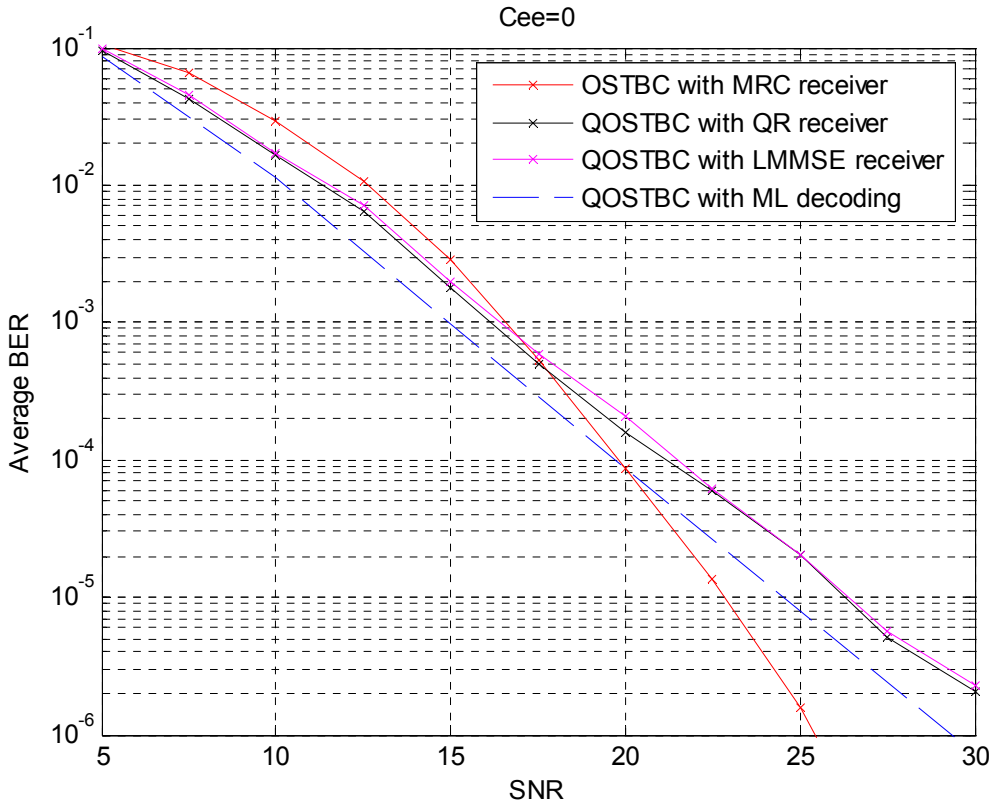

Figure 2.6: Average BER performances of OSTBC and Q-OSTBC with different receivers

After that, one example for channel matrix of Q-OSTBC is given and its QR decomposition results are shown in Table 2.1-2.4. The results are used to detect the received signals and this method is similar to BLAST based on QR decomposition. It is famous that a vertical Bell Laboratories Layered space-time (V-BLAST) system has an optimal ordered detection algorithm. In the ABBA code system, we don't consider the ordered successive cancellation detection because the permutation behavior at the transmitter is able to destroy the special structure of the unitary matrix **Q** and upper triangular matrix **R** under QR decomposition. In a special case, from Table 2.5-2.7, we obtain the same upper triangular matrix **R'** as **R** by exchanging the first two columns and last two columns. In other conditions, the triangular matrix that permutes its columns will destroy its special structure in (2.65).

Table 2.1: Channel state information

h	h_1	h_2	h_3	h_4
	0.4763 + 0.7564i	0.1507 - 0.8355i	-0.3749 + 1.3065i	0.0776 - 1.7238i

Table 2.2: Channel matrix **H** of the ABBA code

H				
	0.4763 + 0.7564i	0.1507 - 0.8355i	-0.3749 + 1.3065i	0.0776 - 1.7238i
	-0.1507 - 0.8355i	0.4763 - 0.7564i	-0.0776 - 1.7238i	-0.3749 - 1.3065i
	-0.3749 + 1.3065i	0.0776 - 1.7238i	0.4763 + 0.7564i	0.1507 - 0.8355i
	-0.0776 - 1.7238i	-0.3749 - 1.3065i	-0.1507 - 0.8355i	0.4763 - 0.7564i

Table 2.3: Unitary matrix **Q** under QR decomposition

Q				
	0.1891 + 0.3003i	0.0598 - 0.3317i	-0.1488 +0.5187i	0.0308 - 0.6843i
	-0.0598 - 0.3317i	0.1891 - 0.3003i	-0.0308- 0.6843i	-0.1488 - 0.5187i
	-0.1488 +0.5187i	0.0308- 0.6843i	0.1891 + 0.3003i	0.0598 - 0.3317i
	-0.0308- 0.6843i	-0.1488 - 0.5187i	-0.0598 - 0.3317i	0.1891 - 0.3003i

Table 2.4: Upper triangular matrix **R** under QR decomposition

R				
	2.5189	0	1.7958	0
	0	2.5189	0	1.7958
	0	0	1.7664	0
	0	0	0	1.7664

Table 2.5: Channel matrix **H'** of the ABBA code

H'				
	-0.3749 + 1.3065i	0.0776 - 1.7238i	0.4763 + 0.7564i	0.1507 - 0.8355i
	-0.0776 - 1.7238i	-0.3749 - 1.3065i	-0.1507 - 0.8355i	0.4763 - 0.7564i
	0.4763 + 0.7564i	0.1507 - 0.8355i	-0.3749 + 1.3065i	0.0776 - 1.7238i
	-0.1507 - 0.8355i	0.4763 - 0.7564i	-0.0776 - 1.7238i	-0.3749 - 1.3065i

Table 2.6: Unitary matrix **Q'** under QR decomposition

Q'				
	-0.1488 +0.5187i	0.0308- 0.6843i	0.1891 + 0.3003i	0.0598 - 0.3317i
	-0.0308- 0.6843i	-0.1488 - 0.5187i	-0.0598 - 0.3317i	0.1891 - 0.3003i
	0.1891 + 0.3003i	0.0598 - 0.3317i	-0.1488 +0.5187i	0.0308 - 0.6843i
	-0.0598 - 0.3317i	0.1891 - 0.3003i	-0.0308- 0.6843i	-0.1488 - 0.5187i

Table 2.7: Upper triangular matrix **R'** under QR decomposition

R'				
	2.5189	0	1.7958	0
	0	2.5189	0	1.7958
	0	0	1.7664	0
	0	0	0	1.7664

2.6 Smmary

In wireless communication systems, diversity techniques are widely used to reduce the effects of multipath fading and improve the reliability of transmission without increasing the transmitted power or sacrificing the bandwidth. It is well-known that diversity techniques are classified into time, frequency, and space diversity. Without increasing the bandwidth and decreasing the transmission rate, it is popular to make use of space diversity which can be classified into two categories, transmit diversity and receive diversity. In this chapter, we focus on transmit diversity such as OSTBC and Q-OSTBC. They can improve the performance by exploiting the structure of the codes and provide the simple linear decoding methods compared with the maximum likelihood decoding. It is mentioned that diversity order determines the slope of BER-SNR curve in the high SNR region. Therefore, the better performance for OSTBC can be obtained in the high SNR region because OSTBC has the full diversity gain. With introduction of non-orthogonality, the better performance is obtained in the lower SNR region because a lower modulation order is used in the low SNR region.

Then, the QR decomposition of the ABBA code is introduced in Section 2.3. Under the result of QR decomposition, the special structure of the upper triangular matrix is shown in Equation (2.64). It is useful for us to detect the received signals and provide better performance. Further, the diagonal entries of the upper triangular matrix are derived and expressed in terms of the determinants of the channel matrix and its partitioned matrices. Compared the QR-based successive cancellation detector with the LMMSE and ML receivers, the performance with QR-based successive cancellation detection is slightly better than that with LMMSE but worse than that with the ML decoding. This simulation is helpful to confirm our derivation in this chapter. In the

next chapter, the precoding matrix is exploited to allocate the transmit power and the average bit error rate is expected to reduce. That is, we focus on the power allocation scheme by using the special structure with QR-based successive interference cancellation detection.

Chapter 3

Transmit Power Allocation for Minimum BER in a Quasi-Orthogonal Space-Time Block Code

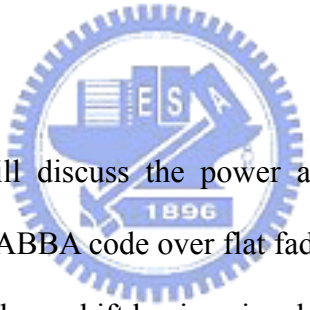

In this chapter, we will discuss the power allocation scheme with QR-based successive detection for the ABBA code over flat fading channels. Our consideration is confined to uncoded quadriphase-shift keying signals and the channels are independent and identically distributed Rayleigh fading. Given that the channel state information (CSI) is perfectly available at the receiver and transmitter, we design a precoding matrix to allocate transmit power under a fixed channel realization at the transmitter. Furthermore, at the receiver, the signals are detected with a QR-based successive cancellation detection mentioned in the previous chapter. For simplicity, the precoding matrix is restricted to be a power loading diagonal matrix so as to reduce the computational complexity. We minimize the average bit error rate (BER) of the received signals but the error propagation is not considered first. From the theory in [10], the design of the precoding matrix is based on the minimization of the lower bound of average BER. It can be proved that minimizing the lower bound of the

average BER leads to minimizing the upper bound of the block error rate. For the error propagation free case (no error propagation), some closed-form solutions of power allocation schemes are provided in [16]. Then, we consider the error propagation effect, which is modeled into the error probability. Finally, we exploit the modified error probability to determine power allocation factors. The performances of the error propagation free and error propagation cases will be discussed in Sections 3.2 and 3.3.

3.1 Bound for BER of QR Based Successive Detection

Power loading schemes allocate the transmit power across symbols under the constraint of constant power per block. At the transmitter per block of four symbols x_i, $1 \le i \le 4$, we denote the transmitted power allocated to the ith symbol as p_i^2 and define the power loading matrix as below:

$$\mathbf{P} = \begin{bmatrix} p_1 & 0 & 0 & 0 \\ 0 & p_2 & 0 & 0 \\ 0 & 0 & p_3 & 0 \\ 0 & 0 & 0 & p_4 \end{bmatrix}. \tag{3.1}$$

where $p_i > 0$ is power loading factor and it is mentioned that the block power constraint must be normalized as

$$\text{trace}\{\mathbf{P}^2\} = \sum_{i=1}^{4} p_i^2 = 4. \tag{3.2}$$

Under flat-fading channel assumption, the power loading matrix is inserted into the system model (2.65). If the receiver replies the channel state information (CSI) to the transmitter, the transmitter can determine the power loading factors by CSI. The block diagram with transmit power allocation scheme is shown in Figure 3.1.

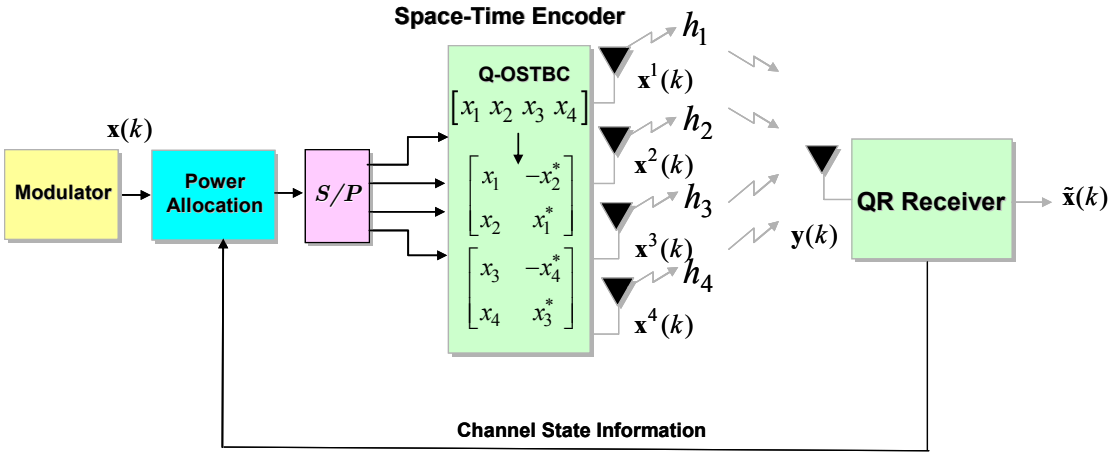

Figure 3.1: A block diagram of the quasi-orthogonal space-time block coded system with transmit power allocation scheme

The received signals are multiplied from the left by unitary matrix $\mathbf{Q}^H$ and shown as below:

$$\begin{bmatrix} \tilde{y}_1 \\ \tilde{y}_2 \\ \tilde{y}_3 \\ \tilde{y}_4 \end{bmatrix} = \begin{bmatrix} R_{11} & 0 & R_{13} & 0 \\ 0 & R_{11} & 0 & R_{13} \\ 0 & 0 & R_{33} & 0 \\ 0 & 0 & 0 & R_{33} \end{bmatrix} \begin{bmatrix} p_1 & 0 & 0 & 0 \\ 0 & p_2 & 0 & 0 \\ 0 & 0 & p_3 & 0 \\ 0 & 0 & 0 & p_4 \end{bmatrix} \begin{bmatrix} x_1 \\ x_2 \\ x_3 \\ x_4 \end{bmatrix} + \begin{bmatrix} \tilde{n}_1 \\ \tilde{n}_2 \\ \tilde{n}_3 \\ \tilde{n}_4 \end{bmatrix} \rightarrow \tilde{\mathbf{y}} = \mathbf{RPx} + \tilde{\mathbf{n}} . \quad (3.3)$$

where $\tilde{\mathbf{y}} = \mathbf{Q}^H \mathbf{y}$ and $\tilde{\mathbf{n}} = \mathbf{Q}^H \mathbf{n}$. The *i*th element of modified received signals is detected as follows:

$$\hat{y}_i = \tilde{y}_i - \sum_{j=i+1}^{4} R_{ij} p_j \tilde{x}_j = R_{ii} p_i x_i + \sum_{j=i+1}^{4} R_{ij} p_j \left(x_j - \tilde{x}_j \right) + \tilde{n}_i . \quad (3.4)$$

Assuming there is no error determined in the previous symbols. Then, we obtain $\hat{y}_i = R_{ii} p_i x_i + \tilde{n}_i$. It is obvious that the *i*th modified signal is affected by the *i*th transmitted symbol and channel noise. As long as the symbol in each stage is correctly detected and, hence, there is no layer-wise error propagation, the space-time model decouples into four independent links. The power loading factor p_i^2 represents the transmit power allocated to the ith subchannel and R_{ii} is the *i*th subchannel gain.

The average energy of the symbols transmitted from each antenna is normalized to be one. Therefore, total symbol energy E_s is equal to n_T, so that the average power of received signal at each receive antenna is also n_T. The real part and imaginary part of noise have the same variance n_T /(2SNR). The signal to noise ratio (SNR) is denoted by $\rho \overset{\text{def}}{=} \frac{E_s}{N_0}$, where the total symbol energy and noise variance are defined as $E\left[\mathbf{x}\mathbf{x}^H\right] = E_s\mathbf{I}_{n_T} = n_T\mathbf{I}_{n_T} = 4\mathbf{I}_4$ and $E\left[\mathbf{n}\mathbf{n}^H\right] = N_0\mathbf{I}_p = N_0\mathbf{I}_4$, respectively. The decision point SNR of the *i*th symbol is given by $\rho\left|p_i R_{ii}\right|^2$. Then, we compute the bit error rate of the *i*th subchannel and the instantaneous BER is given by

$$P_{ei} = Q\left(\sqrt{\rho}\left|p_i R_{ii}\right|\right), \tag{3.5}$$

where $Q(x) \overset{\text{def}}{=} \frac{1}{\sqrt{2\pi}}\int_x^\infty e^{-y^2/2}dy$ and the QPSK modulation is adopted. Therefore, the average instantaneous BER for the symbols block given a channel realization is given by

$$P_e = \frac{1}{4}\sum_{i=1}^{4} P_{ei} = \frac{1}{4}\sum_{i=1}^{4} Q\left(\sqrt{\rho}\left|p_i R_{ii}\right|\right). \tag{3.6}$$

It is noted that Equation (3.6) is discussed in the error propagation free case, that is, error propagation is not considered, so Equation (3.6) merely is a lower bound of average BER. The average instantaneous BER (lower bound of average BER) is rewritten as

$$P_{eL} = \frac{1}{4}\sum_{i=1}^{4} P_{eLi} = \frac{1}{4}\sum_{i=1}^{4} Q\left(\sqrt{\rho}\left|p_i R_{ii}\right|\right), \tag{3.7}$$

where the subscript L indicates the lower bound of the BER. This is a lower bound with QR-based successive interference cancellation detection due to neglecting of error propagation, which is also an accurate approximate at the moderate to high SNR region. The approximation is reasonable since error propagation is minimal. If the error propagation is considered, the detection error of previous symbols will affect the

detection of present symbol. This will increase the BER and the average BER is slightly higher than the average BER in the error propagation free case. The lower bound of average BER has been presented; we then introduce the upper bound of average BER. First, let us define the detection error in the *i*th symbols x_i when there may be errors in the detection of previous symbols. We denote by $\tilde{\mathbf{x}}_{ai} = \left[\tilde{x}_{i+1} \ldots, \tilde{x}_4\right]^T$ and $\mathbf{x}_{ai} = \left[x_{i+1} \ldots, x_4\right]^T$ represent the signal vector detected before x_i and the transmitted signal vector, respectively. For the detection of the *i*th symbol x_i, from the Bayes' theorem, we obtain

$$\begin{aligned} P(x_i \neq \tilde{x}_i) = & P(x_i \neq \tilde{x}_i \left| \mathbf{x}_{ai} = \tilde{\mathbf{x}}_{ai} \right.) P(\mathbf{x}_{ai} = \tilde{\mathbf{x}}_{ai}) \\ & + P(x_i \neq \tilde{x}_i \left| \mathbf{x}_{ai} \neq \tilde{\mathbf{x}}_{ai} \right.) P(\mathbf{x}_{ai} \neq \tilde{\mathbf{x}}_{ai}) \end{aligned} . \tag{3.8}$$

Here, $P(x_i \neq \tilde{x}_i \left| \mathbf{x}_{ai} = \tilde{\mathbf{x}}_{ai} \right.)$ is equivalent to Equation (3.5) for the error propagation free case. Equation (3.8) can be rewritten as

$$\begin{aligned} P(x_i \neq \tilde{x}_i) &= P_{eLi} P(\mathbf{x}_{ai} = \tilde{\mathbf{x}}_{ai}) + P(x_i \neq \tilde{x}_i \left| \mathbf{x}_{ai} \neq \tilde{\mathbf{x}}_{ai} \right.) P(\mathbf{x}_{ai} \neq \tilde{\mathbf{x}}_{ai}) \\ &\leq P_{eLi} + P(\mathbf{x}_{ai} \neq \tilde{\mathbf{x}}_{ai}). \end{aligned} \tag{3.9}$$

In the above formula, the last inequality is the fact that $P(x_i \neq \tilde{x}_i \left| \mathbf{x}_{ai} \neq \tilde{\mathbf{x}}_{ai} \right.) \leq 1$ and $P(\mathbf{x}_{ai} = \tilde{\mathbf{x}}_{ai}) \cong 1$ for high SNR. Furthermore,

$$\begin{aligned} & P(\mathbf{x}_{ai} \neq \tilde{\mathbf{x}}_{ai}) = 1 - P(\mathbf{x}_{ai} = \tilde{\mathbf{x}}_{ai}) \\ & = 1 - P(x_4 = \tilde{x}_4) P(x_3 = \tilde{x}_3 \left| x_4 = \tilde{x}_4 \right.) \cdots P(x_{i+1} = \tilde{x}_{i+1} \left| \mathbf{x}_{ai+1} = \tilde{\mathbf{x}}_{ai+1} \right.) \\ & = 1 - \prod_{j=i+1}^{4} \left(1 - P_{eLj}\right) \leq \sum_{j=i+1}^{4} P_{eLj}. \end{aligned} \tag{3.10}$$

Because $P(x_{i+1} = \tilde{x}_{i+1} \left| \mathbf{x}_{ai+1} = \tilde{\mathbf{x}}_{ai+1} \right.)$ is written as $1 - P(x_i \neq \tilde{x}_i \left| \mathbf{x}_{ai} = \tilde{\mathbf{x}}_{ai} \right.)$ $= 1 - P_{eLj}$, the last equality is established. The last inequality is easily derived by some manipulations.

Combining (3.9) and (3.10), the result is shown as

$$P(x_i \neq \tilde{x}_i) \leq P_{eLi} + P(\mathbf{x}_{ai} \neq \tilde{\mathbf{x}}_{ai}) \leq P_{eLi} + \sum_{j=i+1}^{4} P_{eLj} = \sum_{j=i}^{4} P_{eLj} = P_{eUi}. \tag{3.11}$$

where the subscript U indicates the upper bound of the BER. Equation (3.11) represents the upper bound of the BER based on the consideration that there may be detection errors in the previous symbols. The upper bound of the average BER of four symbols is given by

$$\begin{aligned} P_{eU} &= \frac{1}{4}\sum_{i=1}^{4} P_{eUi} = \frac{1}{4}\sum_{i=1}^{4}\sum_{j=i}^{4} P_{eLj} \\ &= \frac{1}{4}\sum_{i=1}^{4} iP_{eLi} = \frac{1}{4}\sum_{i=1}^{4} iQ\left(\sqrt{\rho}\,|p_i R_{ii}|\right). \end{aligned} \tag{3.12}$$

The last equality is because the detection order follows the upper triangular structure of the matrix. In view of the block error rate, let $i = 0$ in (3.11), we have

$$P(\mathbf{x} \neq \tilde{\mathbf{x}}) = P(\mathbf{x}_{a0} \neq \tilde{\mathbf{x}}_{a0}) \leq \sum_{j=1}^{4} P_{eLj} = 4P_{eL}\,. \tag{3.13}$$

It is obvious that the block error rate $P(\mathbf{x} \neq \tilde{\mathbf{x}})$ is upper bounded by four times the lower bound of the average BER P_{eL}. This is an important result for us to determine the power allocation factors. If a power allocation matrix is designed to minimize the lower bound of the average BER, it simultaneously minimizes the upper bound of the block error rate as well. From the above derivations, the minimization of lower bound for average BER is reasonable because the upper bound of the block error rate is minimized at the same time. It implies that the decision performance can be potentially improved even in the presence of inter-layer error propagation. In the next section, the lower bound of the average BER is exploited to design the power loading matrix and some different closed-form expressions for different criteria are presented.

3.2 Power Allocation Algorithms with QR-Based Successive Detection: Error Propagation Free Case

An proper power allocation matrix is chosen to minimize the lower bound of the average BER for different criteria. Combining the transmit power constraint (3.2) and the lower bound of average instantaneous BER Equation (3.7), the optimization problem results. The lower bound of average instantaneous BER Equation (3.7) is called “cost function” or “objective function” here. Subject to “power constraint”, the average instantaneous BER with power allocation can be written as

$$P_{eL} = \frac{1}{4}\sum_{i=1}^{4} P_{eLi} = \frac{1}{4}\sum_{i=1}^{4} Q\left(\sqrt{\rho}\,|p_i R_{ii}|\right) \quad \text{subject to } \sum_{i=1}^{4} p_i^2 = 4 \qquad (3.14)$$

Then, three common strategies are shown as below [16]-[18]:

1. Optimal Minimum BER Power Allocation.
2. Approximate Minimum BER Power Allocation.
3. Equal Gain (Equal SNR) Power Allocation.

Furthermore, their closed-form solutionss are introduced in the later section. We assume that the channel state information is perfectly available with no error, although it is not realistic.

3.2.1 Optimal Minimum BER Power Allocation

A direct method is to minimize the problem (3.14). Then, the optimum minimum BER power allocation strategy is expressed as

$$\begin{cases} \min P_{eL} = \dfrac{1}{4}\sum_{i=1}^{4} Q\left(\sqrt{\rho}\,|p_i R_{ii}|\right) \\ \text{subject to } \sum_{i=1}^{4} p_i^2 = 4 \end{cases}. \tag{3.15}$$

Because the average instantaneous BER P_{eL} is a convex function, minimizing the problem (3.14) is difficult. It is a convex programming problem which consists of many computational complexities. Its closed-form solution can't be derived but the global minimum solution is unique and satisfies [19]

$$\sqrt{\frac{\rho\,|R_{ii}|^2}{2p_i^2}} e^{-\frac{1}{2}\rho|R_{ii}|^2 p_i^2} = \mu\,. \tag{3.16}$$

The parameter μ is chosen numerically such that the transmit power constraint is fulfilled. Minimizing the convex problem requires an iterative procedure to obtain the optimum solution and we must solve nonlinear equations numerically. It is clear that the slow convergence and high computational complexity in this strategy are obtained. In order to reduce the computational complexity, approximate minimum BER will be proposed in the next section.

3.2.2 Approximate Minimum BER Power Allocation

In order to avoid computing numerically, the approach is adopted in [16]. The cost function is approximated to an exponential form. The approximate BER can be written as

$$P_e = Q\left(\sqrt{2c\rho}\right) = \frac{1}{5}\exp(-c\rho), \tag{3.17}$$

where c is a constellation-specific constant, For BPSK and QPSK modulations, $c = 1$ and $c = 1/2$, respectively. Therefore, the optimal minimum BER power allocation is reformulated as the approximate minimum BER power allocation as follows:

$$\begin{cases} \min P_{eL} = \dfrac{1}{20}\sum_{i=1}^{4} \exp(-\dfrac{1}{2}\rho \left|R_{ii}\right|^2 p_i^2) \\ \text{subject to } \sum_{i=1}^{4} p_i^2 = 4 \end{cases} . \tag{3.18}$$

It is mentioned that when we minimize (3.15) under transmit power constraint, no closed-form solution exists. However, the corresponding closed-form solution in (3.18) can be obtained by using Lagrange method. The closed-form solution of the approximate minimum BER power allocation is obtained as

$$p_i^2 = \left(\frac{\ln \left|R_{ii}\right|^2 + \mu}{\frac{1}{2}\rho \ln \left|R_{ii}\right|^2} \right)_+ , \tag{3.19}$$

where $(x)_+ = \max\{0, x\}$ and the parameter μ is chosen such that the transmit power constraint is satisfied, as be shown as below:

$$\mu \overset{\text{def}}{=} \frac{\frac{1}{2}\rho - \frac{1}{4}\sum_{l=1}^{4} \frac{\ln \left|R_{ii}\right|^2}{\left|R_{ll}\right|^2}}{\frac{1}{4}\sum_{l=1}^{4} \frac{1}{\left|R_{ll}\right|^2}} . \tag{3.20}$$

It is noted that μ is unique and can be obtained rapidly. Therefore, the total transmit power in four transmit antennas is given by

$$\sum_{i=1}^{4} p_i^2 = \sum_{i=1}^{4} \left(\frac{\ln \left|R_{ii}\right|^2 + \mu}{\frac{1}{2}\rho \ln \left|R_{ii}\right|^2} \right)_+ , \tag{3.21}$$

which is a piecewise-linear function in μ. Compared with the optimum minimum BER power allocation, the approximate minimum BER power allocation doesn't require numerical solution of nonlinear equations. It is effective to reduce the computational complexity. It is found that the performance of approximate minimum BER strategy is very close to that of optimum minimum BER strategy. If

$\ln\left|R_{ii}\right|^2 + \mu \le 0$ $(-\ln\left|R_{ii}\right|^2 \ge \mu)$, the case implies that the symbol with weaker channel gain is dropped. The concept of the above solution (3.19) is similar to that of the waterfilling solution but there is a different viewpoint. The characteristics of the transmit power allocation strategy derived above differ from those of the waterfilling scheme that maximizes the capacity. In view of power allocation strategy, symbols with high channel gain can share power with other symbols to improve the average BER. The waterfilling scheme is that symbols with high channel gain can acquire more power in order to achieve maximum system capacity.

3.2.3 Equal Gain (Equal SNR) Power Allocation

It is well-known that the BER is often dominated by certain terms with smallest channel gain because the $Q(\cdot)$ function decreases as its argument increases. In order to avoid this condition, we pre-equalize the transmitted symbols so that all gain of received signals is equal. The equal gain power allocation strategy is given by

$$\begin{cases} \left|R_{ii}^2\right| p_i^2 = \text{constant}, \forall i \\ \text{subject to } \sum_{i=1}^{4} p_i^2 = 4 \end{cases}. \tag{3.22}$$

Under some manipulations, the closed-form solution is easily derived and given by

$$p_{eg,i}^2 = \frac{1}{\frac{1}{4}\left|R_{ii}\right|^2 \sum_{l=1}^{4} \frac{1}{\left|R_{ll}\right|^2}}. \tag{3.23}$$

It is obvious that the equal gain power allocation scheme requires the less computational complexity compared with the optimum and approximate minimum BER power allocation and the performance is indeed improved. The equal gain power allocation strategy allocates transmit power $p_{eg,i}^2$ inversely proportional to the channel state information $\left|R_{ii}\right|^2$, and more transmit power is allocated to the more

attenuated subchannel. From the above discussions, three strategies are provided and some closed-form solutions are presented. In the next section, the error propagation is considered and the corresponding analysis is presented.

3.3 Power Allocation Algorithms with QR-Based Successive Detection: Error Propagation Case

It is well-known that the detection with decision feedback suffers form error propagation. It implies that the cancellation of an erroneously detected symbol will cause significant performance degradation. In the previous discussions, no error propagation is considered. Here, based on the assumption that there is error propagation, it is clear that the detection error of previous symbols will increase the BER. Take into account the effects of error propagation, the exact expressions for the error probability is difficult. A simple approach to estimate the probabilities is presented. It is shown that their performances are very close to the simulation results. Writing (3.4) in terms of the vector and matrix, we have

$$\hat{\mathbf{y}} = \begin{bmatrix} \hat{y}_1 \\ \hat{y}_2 \\ \hat{y}_3 \\ \hat{y}_4 \end{bmatrix} = \begin{bmatrix} \tilde{y}_1 \\ \tilde{y}_2 \\ \tilde{y}_3 \\ \tilde{y}_4 \end{bmatrix} - \begin{bmatrix} 0 & 0 & R_{13}p_3 & 0 \\ 0 & 0 & 0 & R_{13}p_4 \\ 0 & 0 & 0 & 0 \\ 0 & 0 & 0 & 0 \end{bmatrix} \begin{bmatrix} \tilde{x}_1 \\ \tilde{x}_2 \\ \tilde{x}_3 \\ \tilde{x}_4 \end{bmatrix}$$

$$= \begin{bmatrix} R_{11}p_1 & 0 & 0 & 0 \\ 0 & R_{11}p_2 & 0 & 0 \\ 0 & 0 & R_{33}p_3 & 0 \\ 0 & 0 & 0 & R_{33}p_4 \end{bmatrix} \begin{bmatrix} x_1 \\ x_2 \\ x_3 \\ x_4 \end{bmatrix} + \begin{bmatrix} 0 & 0 & R_{13}p_3 & 0 \\ 0 & 0 & 0 & R_{13}p_4 \\ 0 & 0 & 0 & 0 \\ 0 & 0 & 0 & 0 \end{bmatrix} \begin{bmatrix} x_1 - \tilde{x}_1 \\ x_2 - \tilde{x}_2 \\ x_3 - \tilde{x}_3 \\ x_4 - \tilde{x}_4 \end{bmatrix} + \begin{bmatrix} \tilde{n}_1 \\ \tilde{n}_2 \\ \tilde{n}_3 \\ \tilde{n}_4 \end{bmatrix}. \tag{3.24}$$

Divide the modified received signal $\hat{\mathbf{y}}$ into two groups as below:

$$\begin{bmatrix} \hat{y}_3 \\ \hat{y}_4 \end{bmatrix} = \begin{bmatrix} R_{33}p_3 & 0 \\ 0 & R_{33}p_4 \end{bmatrix} \begin{bmatrix} x_3 \\ x_4 \end{bmatrix} + \begin{bmatrix} \tilde{n}_3 \\ \tilde{n}_4 \end{bmatrix}, \tag{3.25}$$

$$\begin{bmatrix}\hat{y}_1\\ \hat{y}_2\end{bmatrix}=\begin{bmatrix}R_{11}p_1 & 0\\ 0 & R_{11}p_2\end{bmatrix}\begin{bmatrix}x_1\\ x_2\end{bmatrix}+\begin{bmatrix}R_{13}p_3 & 0\\ 0 & R_{13}p_4\end{bmatrix}\begin{bmatrix}x_3-\tilde{x}_3\\ x_4-\tilde{x}_4\end{bmatrix}+\begin{bmatrix}\tilde{n}_1\\ \tilde{n}_2\end{bmatrix}. \quad (3.26)$$

It is clear that the third and fourth symbols in (3.25) are detected directly without error propagation, but the first and second symbols in (3.26) are detected with error propagation. In [20], the error on the previous symbol can be regarded as an additional disturbance. We rewrite (3.26) as

$$\begin{aligned}\hat{y}_2 &= R_{11}p_2x_2+\underbrace{R_{13}p_4\left(x_4-\tilde{x}_4\right)+\tilde{n}_2}_{n_{eq}}\\ \hat{y}_1 &= R_{11}p_1x_1+\underbrace{R_{13}p_3\left(x_3-\tilde{x}_3\right)+\tilde{n}_1}_{n_{eq}}.\end{aligned} \quad (3.27)$$

where $\tilde{x}_3$ and $\tilde{x}_4$ are the erroneous decision regarding x_3 and x_4. To estimate this error propagation effect, the term n_{eq} is approximated as a Gaussian random variable. The mean and variance of n_{eq} are given by

$$E\left[n_{eq}\right]=0 \quad \text{and} \quad E\left[n_{eq}n_{eq}\right]=\left|R_{13}p_i\right|^2E\left\{\left|x_i-\tilde{x}_i\right|^2\right\}+N_0,\ i=3,4. \quad (3.28)$$

Without loss of generality, most of the errors $\tilde{x}_i$ ($i=3,4$) are considered as one of the neighboring symbol $\tilde{x}_i$ in the high SNR region, that is ,

$$\left|x_i-\tilde{x}_i\right|^2=4\sin^2\left(\pi/M\right)=d_{MPSK}^2. \quad (3.29)$$

Therefore, we have

$$E\left[n_{eq}n_{eq}\right]=\left|R_{13}p_i\right|^2\left(4\sin^2\left(\pi/M\right)\right)+N_0=\left|R_{13}p_i\right|^2d_{MPSK}^2+N_0. \quad (3.30)$$

In other words, the error propagation effect is modeled as $E\left[n_{eq}n_{eq}\right]=\left|R_{13}p_i\right|^2d_{MPSK}^2+N_0$, which differs from the original noise power $E[nn]=N_0$. For QPSK modulation, the square minimum distance is given by $d_{QPSK}^2=2$. Denote by σ_{13}^2 and σ_{24}^2, respectively that the noise power of the first symbol with considering error propagation of the third symbol and the noise power of

the second symbol with considering error propagation of the fourth symbol shown as below:

$$\sigma_{13}^2 = \left|R_{13}p_3\right|^2 d_{MPSK}^2 + N_0 \text{, and } \sigma_{24}^2 = \left|R_{13}p_4\right|^2 d_{MPSK}^2 + N_0 . \quad (3.31)$$

Therefore, the average BER [21] for the error propagation effect is expressed as

$$P_e = \frac{1}{4}\left\{P\left(x_1 \neq \tilde{x}_1\right) + P\left(x_2 \neq \tilde{x}_2\right) + P\left(x_3 \neq \tilde{x}_3\right) + P\left(x_4 \neq \tilde{x}_4\right)\right\}, \quad (3.32)$$

where

$$P\left(x_4 \neq \tilde{x}_4\right) = Q\left(\sqrt{\frac{E_s}{N_0}}\left|p_4 R_{33}\right|\right), \quad (3.33)$$

$$P\left(x_3 \neq \tilde{x}_3\right) = Q\left(\sqrt{\frac{E_s}{N_0}}\left|p_3 R_{33}\right|\right), \quad (3.34)$$

$$\begin{aligned}
&P\left(x_2 \neq \tilde{x}_2\right) = P\left(x_2 \neq \tilde{x}_2 \left| x_4 = \tilde{x}_4\right.\right) P\left(x_4 = \tilde{x}_4\right) + P\left(x_2 \neq \tilde{x}_2 \left| x_4 \neq \tilde{x}_4\right.\right) P\left(x_4 \neq \tilde{x}_4\right) \\
&= Q\left(\sqrt{\frac{E_s}{N_0}}\left|p_2 R_{11}\right|\right)\left(1 - Q\left(\sqrt{\frac{E_s}{N_0}}\left|p_4 R_{33}\right|\right)\right) + Q\left(\sqrt{\frac{E_s}{\sigma_{24}^2}}\left|p_2 R_{11}\right|\right) Q\left(\sqrt{\frac{E_s}{N_0}}\left|p_4 R_{33}\right|\right) \\
&= Q\left(\sqrt{\frac{E_s}{N_0}}\left|p_2 R_{11}\right|\right) + Q\left(\sqrt{\frac{E_s}{N_0}}\left|p_4 R_{33}\right|\right)\left(Q\left(\sqrt{\frac{E_s}{\sigma_{24}^2}}\left|p_2 R_{11}\right|\right) - Q\left(\sqrt{\frac{E_s}{N_0}}\left|p_2 R_{11}\right|\right)\right),
\end{aligned} \quad (3.35)$$

and

$$\begin{aligned}
&P\left(x_1 \neq \tilde{x}_1\right) = P\left(x_1 \neq \tilde{x}_1 \left| x_3 = \tilde{x}_3\right.\right) P\left(x_3 = \tilde{x}_3\right) + P\left(x_1 \neq \tilde{x}_1 \left| x_3 \neq \tilde{x}_3\right.\right) P\left(x_3 \neq \tilde{x}_3\right) \\
&= Q\left(\sqrt{\frac{E_s}{N_0}}\left|p_1 R_{11}\right|\right)\left(1 - Q\left(\sqrt{\frac{E_s}{N_0}}\left|p_3 R_{33}\right|\right)\right) + Q\left(\sqrt{\frac{E_s}{\sigma_{13}^2}}\left|p_1 R_{11}\right|\right) Q\left(\sqrt{\frac{E_s}{N_0}}\left|p_3 R_{33}\right|\right) \\
&= Q\left(\sqrt{\frac{E_s}{N_0}}\left|p_1 R_{11}\right|\right) + Q\left(\sqrt{\frac{E_s}{N_0}}\left|p_3 R_{33}\right|\right)\left(Q\left(\sqrt{\frac{E_s}{\sigma_{13}^2}}\left|p_1 R_{11}\right|\right) - Q\left(\sqrt{\frac{E_s}{N_0}}\left|p_1 R_{11}\right|\right)\right).
\end{aligned} \quad (3.36)$$

Inserting (3.33)-(3.36) into (3.32), the average BER with considering error propagation is expressed as

$$
\begin{aligned}
P_e &= \frac{1}{4}\left\{P\left(x_1 \neq \tilde{x}_1\right) + P\left(x_2 \neq \tilde{x}_2\right) + P\left(x_3 \neq \tilde{x}_3\right) + P\left(x_4 \neq \tilde{x}_4\right)\right\} \\
&= \frac{1}{4}\left\{Q\left(\sqrt{\frac{E_s}{N_0}}\left|p_1 R_{11}\right|\right) + Q\left(\sqrt{\frac{E_s}{N_0}}\left|p_2 R_{11}\right|\right) + Q\left(\sqrt{\frac{E_s}{N_0}}\left|p_3 R_{33}\right|\right) + Q\left(\sqrt{\frac{E_s}{N_0}}\left|p_4 R_{33}\right|\right)\right. \\
&\quad + Q\left(\sqrt{\frac{E_s}{N_0}}\left|p_3 R_{33}\right|\right)\left(Q\left(\sqrt{\frac{E_s}{\sigma_{13}^2}}\left|p_1 R_{11}\right|\right) - Q\left(\sqrt{\frac{E_s}{N_0}}\left|p_1 R_{11}\right|\right)\right) \\
&\quad \left. + Q\left(\sqrt{\frac{E_s}{N_0}}\left|p_4 R_{33}\right|\right)\left(Q\left(\sqrt{\frac{E_s}{\sigma_{24}^2}}\left|p_2 R_{11}\right|\right) - Q\left(\sqrt{\frac{E_s}{N_0}}\left|p_2 R_{11}\right|\right)\right)\right\}.
\end{aligned}
\tag{3.37}
$$

The last two terms are regarded as the addition error probabilities due to the error propagation effect. From the concept of Section 3.2, the power allocation matrix is designed to minimize the average instantaneous BER (3.37) with considering error propagation. The average BER performance is shown in the next section.

3.4 Computer Simulations

In this section, we use the "fmincon" function of Matlab [22] which employs sequential quadratic programming to find the optimal power loading factors that minimize the average instantaneous BER. It is proved that the approximate minimum BER solution is very close to that of the minimum BER solution in [16]. Therefore, we ignore the simulation of approximate minimum BER scheme and present the equal gain scheme and minimum BER scheme compared with the conventional QR receiver without power allocation scheme in the error propagation free case in Figures 3.2 and 3.3. It is noted that the transmit power is allocated for each channel realization, that is, the channel state information is perfectly known to the transmitter and receiver. From the simulation results, we can see that the power loading factors p_1 and p_2 are almost equal to each other, and the same condition holds for the power loading factors p_3 and p_4 because $R_{11} = R_{22}$ and $R_{33} = R_{44}$.

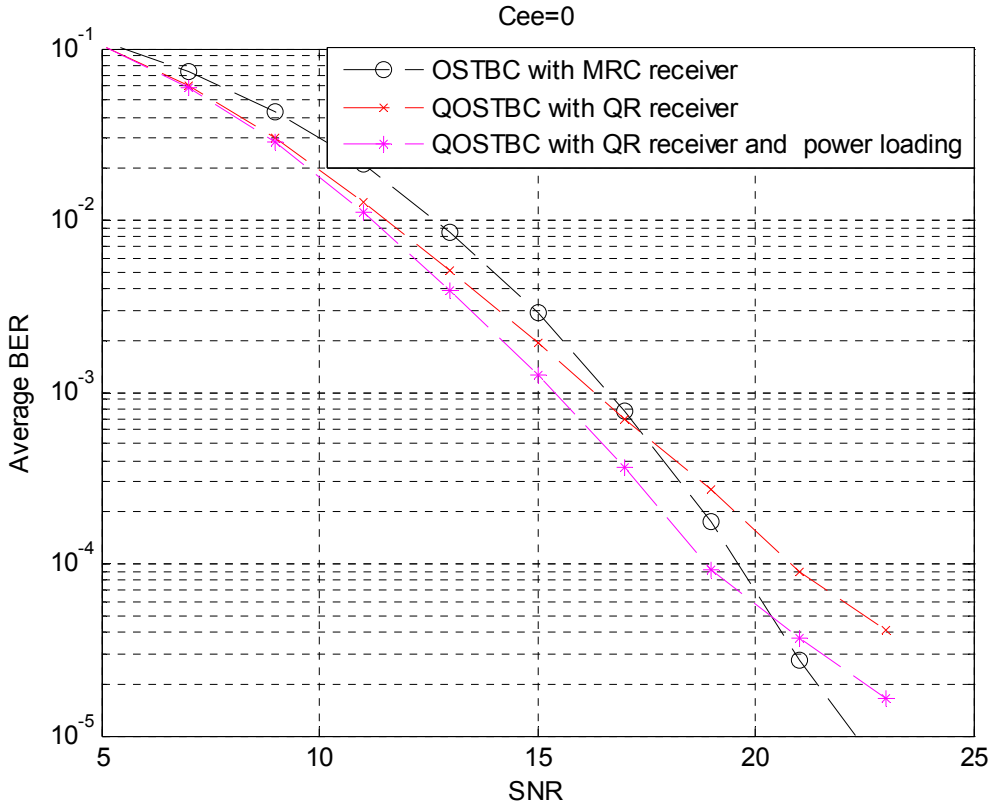

Figure 3.2: Average BER performances of OSTBC and Q-OSTBC with power loading

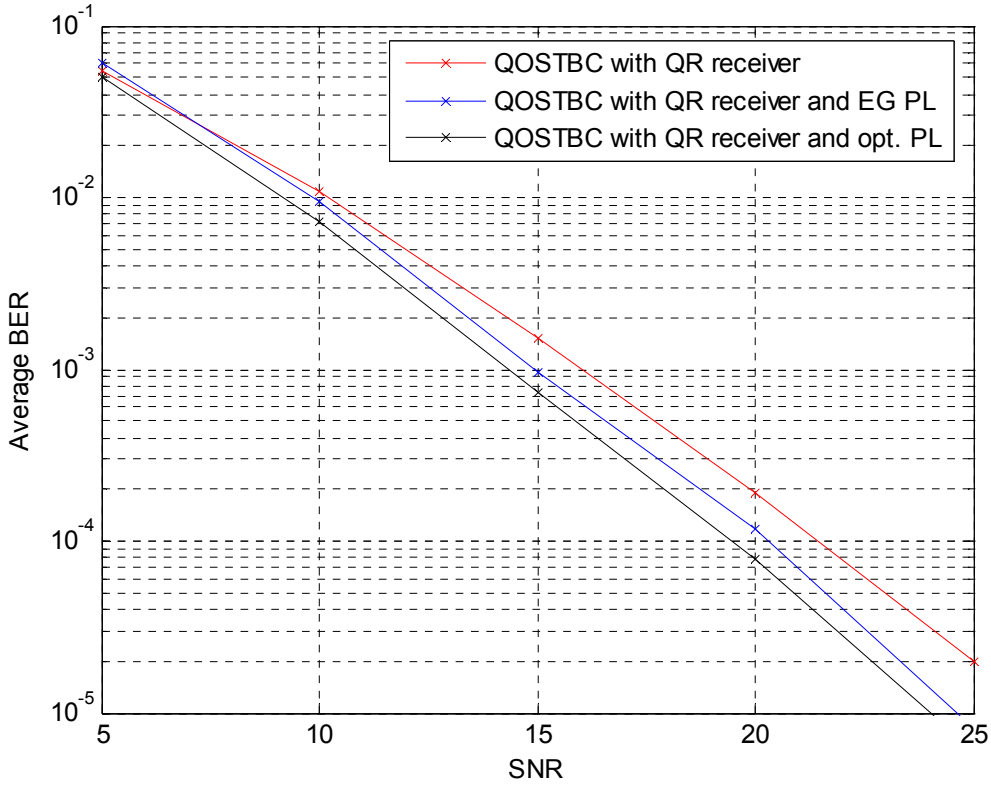

Figure 3.3: Average BER performances of Q-OSTBC with different power loading

In Figure 3.2, we observe that the average BER performance improvement with the optimal power loading scheme is at least 2 dB better than that without power loading scheme in the medium-to-high SNR region. Figure 3.3 illustrates the average BER performances with different power loading schemes; the average BER performance with equal gain power loading scheme is about 1 dB better than that without power loading scheme but is still 1 dB worse than that with optimal power loading scheme (numerical method). In Figures 3.4 and 3.5, we present simulation results in the error propagation free and error propagation cases. Compared with the simulated performance and analytic performance, it is shown that the simulated performance degrades due to the erroneous assumption in the error propagation free case. Therefore, the error propagation effect is considered in Figure 3.5, in which the analytic performance degrades. However, the performance improvement up to about 2 dB is achieved in both cases.

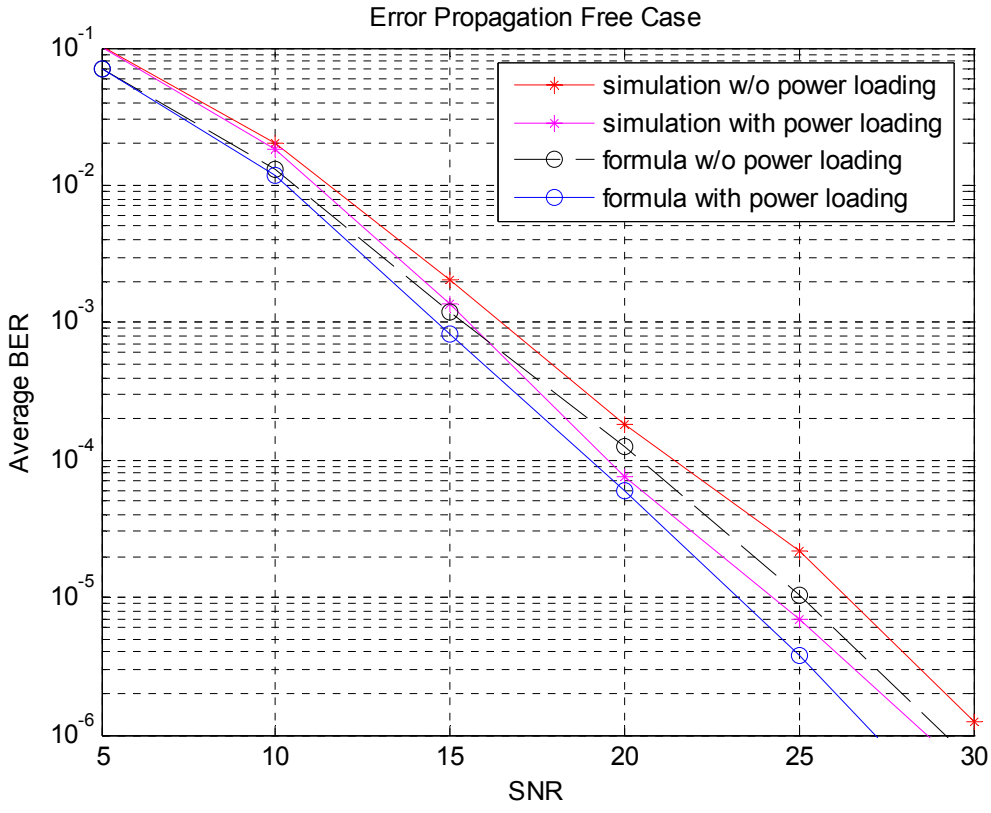

Figure 3.4: Average BER performances without error propagation

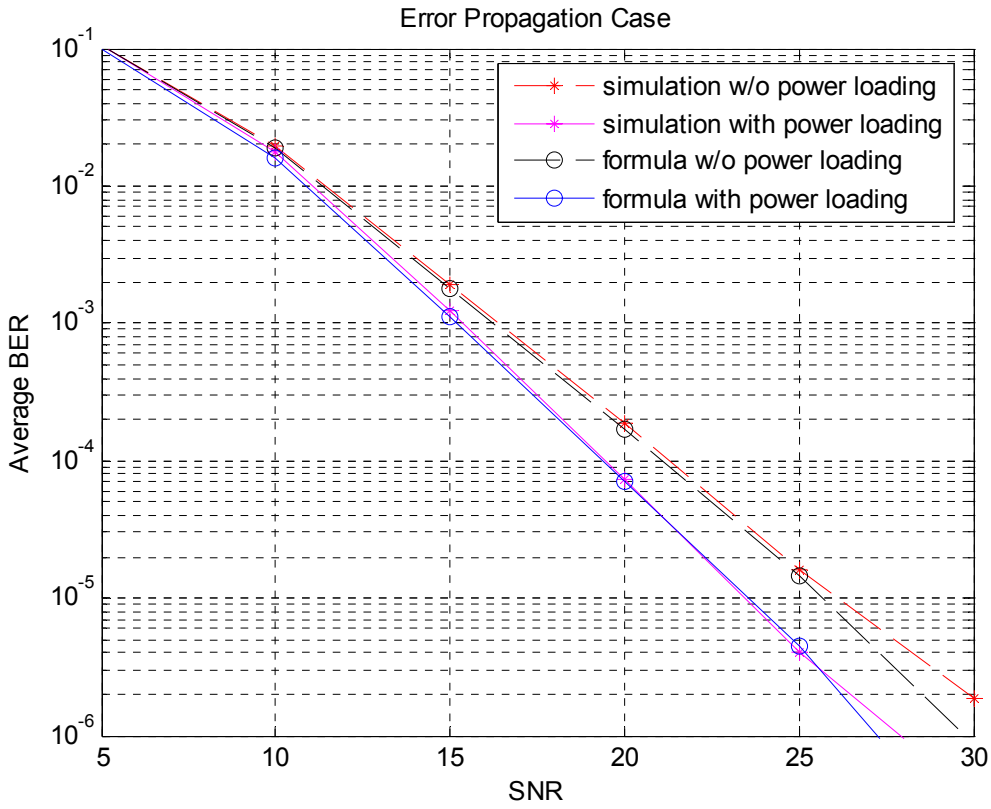

Figure 3.5: Average BER performances with error propagation

In Figure 3.6, we show different performances such as OSTBC, Q-OSTBC (4×1), and Alamouti scheme based multi-group (4×2). Given a fixed channel realization, the average BER performance of Q-OSTBC (4×1) is almost identical to that of Alamouti scheme based multi-group (4×2) in the high SNR region because the diversity and spectral efficiency are the same whether the power loading schemes are considered or not. The analysis of BER performances in Figure 3.6 is similar to that in Figure 3.2. In the low SNR region, the performance of Alamouti scheme based multi-group (4×2) is better than others because a lower modulation order (BPSK modulation) is used. We assume that BPSK modulation is used with the same average symbol power as QPSK and 16-QAM. In the high SNR region, the diversity affects the BER-SNR curve and the performance of OSTBC is better than other codes in Figure 3.6.

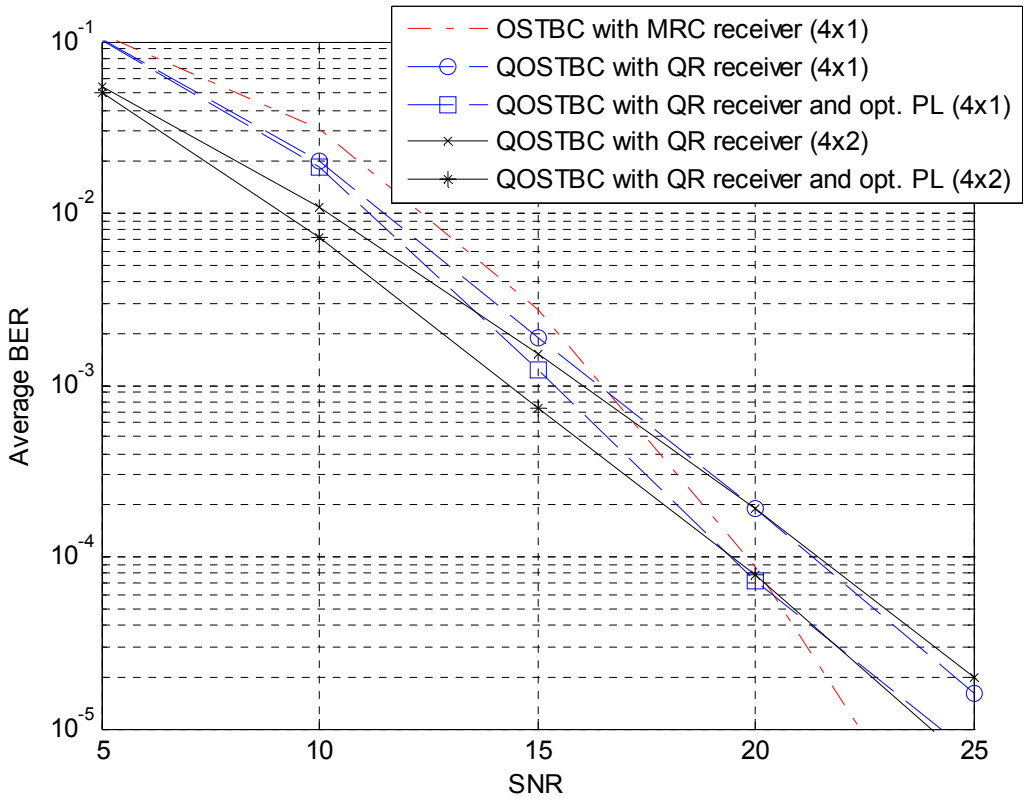

Figure 3.6: Comparison of average BER performances for OSTBC and Q-OSTBC

In [10], it is proved that minimizing the lower bound of the average BER leads to minimizing the upper bound of the block error rate. In Figure 3.8 and 3.9, the above description is confirmed. The power loading factors are determined by minimizing the average BER performance and the block error rate can be minimized by using the same power loading factors. It is thus a reasonable approach to determine the power loading factors by minimizing the lower bound of the average BER. We observe that at error probability of about 10^{-4} in Figure 3.7, we obtain up to 2 dB improvement in SNR compared with the original equal power scheme.

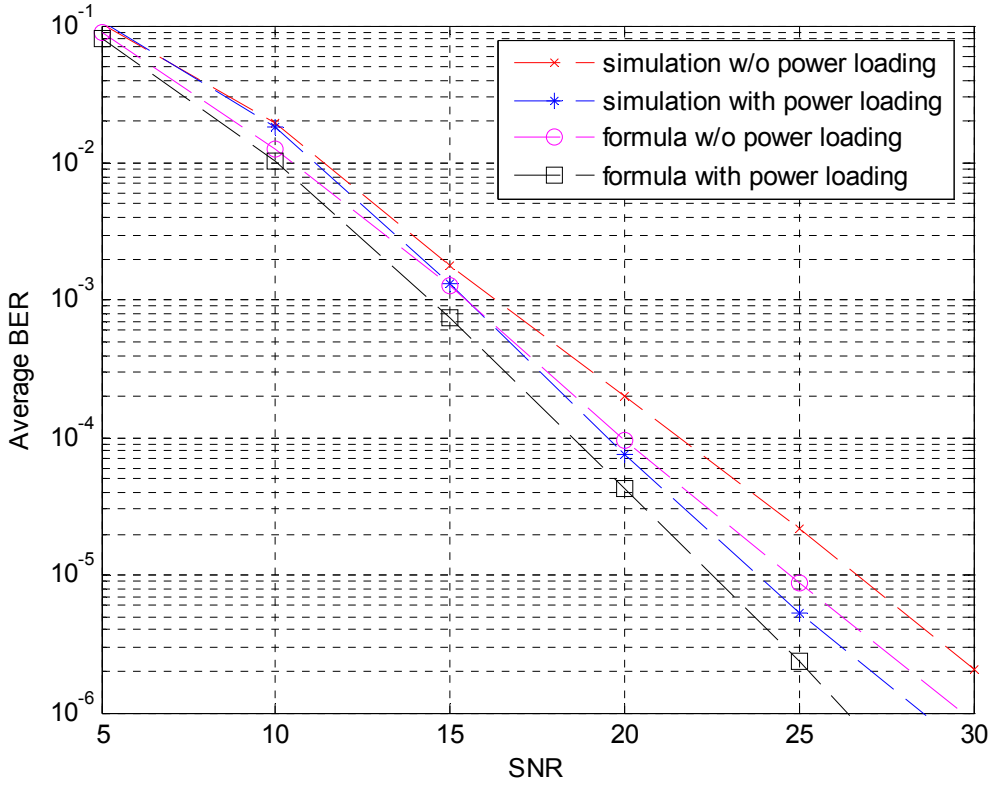

Figure 3.7: Average BER performances of Q-OSTBC with power loading

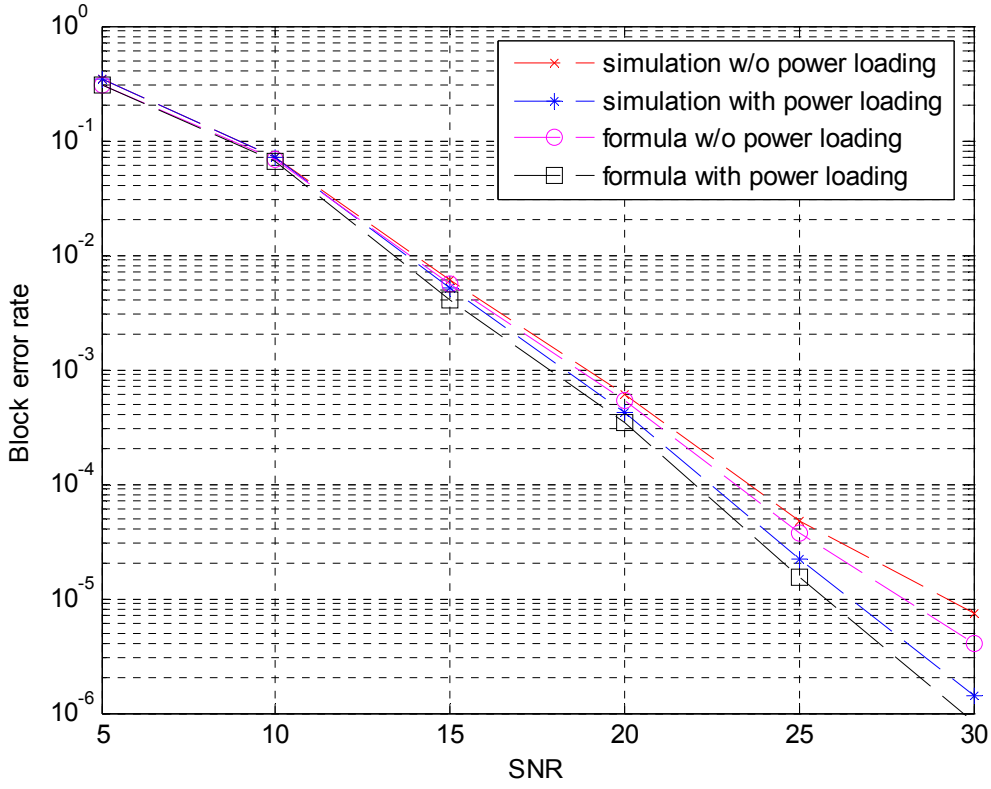

Figure 3.8: Block error rate performances of Q-OSTBC with power loading

Finally, Figure 3.10 illustrates that the ABBA code has performance close to the code proposed by Jafarkhani because the code proposed by Jafarkhani has a structure of the triangular matrix $\mathbf{R}$ similar to the ABBA code. Therefore, the power allocation schemes can be extended directly.

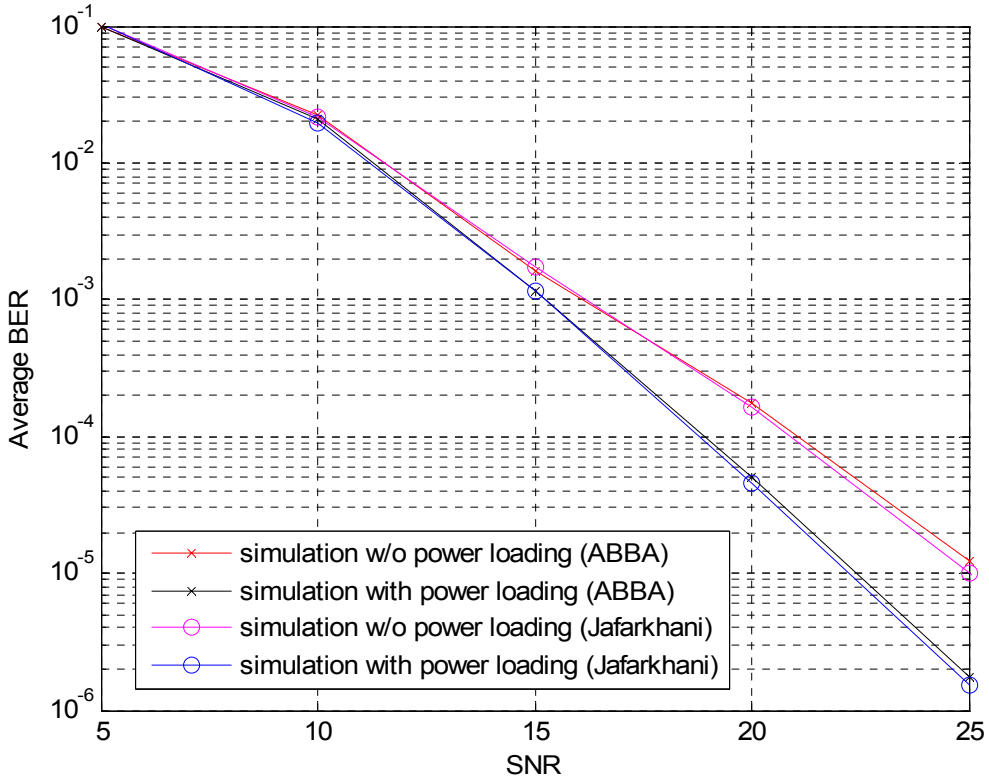

Figure 3.9: Comparison of average BER performances for ABBA code and the code proposed by Jafarkhani with and without power loading

3.5 Summary

In this chapter, we introduce transmit power allocation for minimum average BER with QR-based successive detection. For simplicity, we discuss the error propagation free case first and minimize the lower bound of average BER. It can be proved that minimizing the lower bound of the average BER leads to minimizing the upper bound of the block error rate. For the error propagation free case, we exploit some closed-form expressions of power allocation algorithms provided in [16] to allocate

transmit power. By means of power allocation, we can improve the performance in the high SNR region. Then, we model the error propagation effect as an additional disturbance approximated as a Gaussian random variable. Under such modeling, we determine power allocation factors to minimize the average BER. It can be seen that the better performance is obtained. In the above, we focus on the power allocation schemes under a fixed channel realization known to the transmitter. It is sometimes difficult for us to allocate transmit power if the accurate channel realization is not known at the transmitter. In order to extend our power allocation schemes, we will consider the channel probability density function (pdf) in the error probability formula in the next chapter.

Chapter 4

Robust Transmit Power Allocation for Minimum BER in a Quasi-Orthogonal Space-Time Block Code

In general, the average BER performance will degrade if the channel statistics is not taken into account. In this chapter, we will consider the channel probability density function (pdf) in deriving the error probability. In this case, the instantaneous average BER is no longer considered. Motivated by this fact and to deliver a performance merit over different channel realizations, we evaluate the average BER for the channel estimation. Combining Chapter 3, we propose to determine power loading factors by minimizing the error probability averaged with respect to the channel distribution. It is known that channel estimation can be classified into two categories, perfect channel estimation and imperfect channel estimation. We will discuss perfect channel estimation first and derive an upper bound of average BER for the error propagation free case. Taking into account that the channel pdf is Gaussian with zero mean and covariance matrix $\sum = E\left[\mathbf{h}\mathbf{h}^H\right]$, we evaluate the average BER for the error propagation free case and exploit the corresponding closed-form expression provided

in [23] into the upper bound of average BER formula. Therefore, we change our design rule to minimize the upper bound of average BER for the error propagation free case. The transmit power is allocated in order to minimize the closed-form expression for the upper bound of average BER in the error propagation free case. In this closed-form expression, the channel state information is unnecessary but SNR is necessary. In other words, we only require SNR instead of the channel realization mentioned known to the transmitter in Chapter 3. Furthermore, we introduce the upper bound of the average BER when the channel state information is not perfectly known. Finally, both categories are compared and their performances discussed.

4.1 Evaluation of Overall Average BER

First, the common methods used to analyze the evaluation of overall average BER are introduced. Here, two methods are shown as follows. One [10] is that for a complex circular Gaussian distribution channel, $|R_{ii}|^2$ is χ^2-distributed such that

$$p(|R_{ii}|) = \frac{\left(|R_{ii}|^2\right)^{n_T - i} e^{-|R_{ii}|^2}}{(n_T - i)!}. \tag{4.1}$$

The overall average BER is evaluated by averaging the distribution of $|R_{ii}|$ as follows:

$$P_e = \frac{1}{4}\sum_{i=1}^{4} P_{ei} = \frac{1}{4}\sum_{i=1}^{4} \int Q\left(\sqrt{\rho}\,|R_{ii}|\right) p(|R_{ii}|) d|R_{ii}|, \tag{4.2}$$

where P_{ei} represent that the *i*th symbol is erroneous. Hence, we obtain

$$P_e = \frac{1}{4}\sum_{i=1}^{4} P_{ei} = \frac{1}{4}\sum_{i=1}^{4} \int Q\left(\sqrt{\rho}\,|R_{ii}|\right) \frac{\left(|R_{ii}|^2\right)^{n_T - i} e^{-|R_{ii}|^2}}{(n_T - i)!} d|R_{ii}|. \tag{4.3}$$

The closed-form expression can be derived. However, it is a pity that the assumption is not held in the channel matrix of the ABBA code because the channel matrix has a

special structure and $|R_{ii}|^2$ is not χ^2-distributed. The above method can't be exploited to evaluate overall average BER. The other is that the channel pdf $f(\mathbf{h})$ is assumed to be Gaussian with zero mean and variance $\sum = E\left[\mathbf{h}\mathbf{h}^H\right]$ as below:

$$f(\mathbf{h}) = \frac{1}{\pi^4 \det(\sum)} \exp\left(-\mathbf{h}^H \sum^{-1} \mathbf{h}\right), \tag{4.4}$$

where $\mathbf{h}$ is the column vector representing the four channel coefficients. The overall mean BER is evaluated by averaging the channel pdf $f(\mathbf{h})$ as follows:

$$P_e = \frac{1}{4}\sum_{i=1}^{4} P_{ei} = \frac{1}{4}\sum_{i=1}^{4} \int Q\left(\sqrt{\rho}\,|R_{ii}|\right) \frac{1}{\pi^4 \det(\sum)} \exp\left(-\mathbf{h}^H \sum^{-1} \mathbf{h}\right) d\mathbf{h}\,. \tag{4.5}$$

It is obvious that $|R_{ii}|$ can be expressed in terms of $\mathbf{h}$ and the integral can be computed. Here, the alternative expression differs from $Q(x) \stackrel{\text{def}}{=} \frac{1}{\sqrt{2\pi}} \int_x^\infty e^{-y^2/2} dy$ for the $\mathrm{Q}(\cdot)$ function is given by [24]

$$Q(x) = \frac{1}{\pi} \int_0^{\pi/2} \exp\left(-\frac{x^2}{2\sin^2\theta}\right) d\theta \quad . \tag{4.6}$$

Hence, P_e can be rewritten as

$$\begin{aligned} P_e &= \frac{1}{4}\sum_{i=1}^{4} P_{ei} \\ &= \frac{1}{4}\sum_{i=1}^{4} \int \frac{1}{\pi} \int_0^{\pi/2} \exp\left(-\frac{\left(\sqrt{\rho}\,|R_{ii}|\right)^2}{2\sin^2\theta}\right) d\theta \frac{1}{\pi^4 \det(\sum)} \exp\left(-\mathbf{h}^H \sum^{-1} \mathbf{h}\right) d\mathbf{h}. \end{aligned} \tag{4.7}$$

In general, when the output SNR is in quadratic form ($|R_{ii}|^2 = \mathbf{h}^H \mathbf{h}$, where $\mathbf{h} = \begin{bmatrix} h_1 & h_2 & h_3 & h_4 \end{bmatrix}^H$), and P_e can be computed as follows:

$$P_e = \frac{1}{4}\sum_{i=1}^{4} P_{ei} = \frac{1}{4}\sum_{i=1}^{4} \int \frac{1}{\pi} \int_0^{\pi/2} \exp\left(-\frac{\rho \mathbf{h}^H \mathbf{h}}{2\sin^2\theta}\right) d\theta \frac{1}{\pi^4 \det(\sum)} \exp\left(-\mathbf{h}^H \sum^{-1} \mathbf{h}\right) d\mathbf{h}, \tag{4.8}$$

and it provides the close-form expression [25]. It is useful for us to evaluate the overall average BER. Furthermore, the BER is not a function of the channel realization, i.e.,

we don't require the channel realization in each iteration computation in order to determine power allocation factors. Instead of the channel realization known to the transmitter, it is necessary to know SNR here. Then, the derivation of the closed-form expression is shown as below:

$$
\begin{aligned}
P_{ei} &= \int_{\mathbf{h}} Q\left(\sqrt{\rho}\,|R_{ii}|\right) \frac{1}{\pi^4 \det(\sum)} \exp\left(-\mathbf{h}^H \sum^{-1} \mathbf{h}\right) d\theta d\mathbf{h} \\
&= \int_{\mathbf{h}} \frac{1}{\pi} \int_0^{\pi/2} \exp\left(-\frac{\rho |R_{ii}|^2}{2\sin^2\theta}\right) d\theta \frac{1}{\pi^4 \det(\sum)} \exp\left(-\mathbf{h}^H \sum^{-1} \mathbf{h}\right) d\theta d\mathbf{h} \\
&= \int_{\mathbf{h}} \frac{1}{\pi} \int_0^{\pi/2} \exp\left(-\frac{\rho \mathbf{h}^H \mathbf{h}}{2\sin^2\theta}\right) \frac{1}{\pi^4 \det(\sum)} \exp\left(-\mathbf{h}^H \sum^{-1} \mathbf{h}\right) d\theta d\mathbf{h} \\
&= \frac{1}{\pi} \int_0^{\pi/2} \int_{\mathbf{h}} \frac{1}{\pi^4 \det(\sum)} \exp\left(-\mathbf{h}^H \left(\frac{\rho \sum}{2\sin^2\theta} + \mathbf{I}_4\right) \sum^{-1} \mathbf{h}\right) d\mathbf{h}\, d\theta \\
&\underset{(a)}{=} \frac{1}{\pi} \int_0^{\pi/2} \left\{ \det\left[\frac{\rho \sum}{2\sin^2\theta} + \mathbf{I}_4\right] \right\}^{-1} d\theta = \frac{1}{\pi} \int_0^{\pi/2} \left\{ \prod_{n=1}^{4} \left(\frac{\lambda_n}{\sin^2\theta} + 1\right) \right\}^{-1} d\theta \\
&= \frac{1}{\pi} \int_0^{\pi/2} \left[\sum_{i=1}^{K} \sum_{n=1}^{N_i} \mu_{i,n} \left(\frac{\lambda_i}{\sin^2\theta} + 1\right)^{-n} \right] d\theta \\
&\underset{(b)}{=} \sum_{i=1}^{K} \sum_{n=1}^{N_i} \mu_{i,n} \sum_{k=0}^{n-1} \binom{n-1+k}{k} \left[1 - G(\lambda_i)\right]^k \left[G(\lambda_i)\right]^n .
\end{aligned}
\tag{4.9}
$$

where (a) is obtained by performing integration with respect to $\mathbf{h}$ [23], [25], and (b) follows from [25, e.q.(38)]. These parameters are defined as that λ_i ($i = 1, 2, \ldots, K$) is the eigenvalues of $\frac{\rho \sum}{2}$, K is the number of distinct eigenvalues, N_i is the eigenvalue's multiplicity, $\mu_{i,n}$ is the ith residue associated with nth power in the partial-fraction expansion, and the function $G(\lambda)$ is given by

$$
G(\lambda) = \frac{1}{2}\left(1 - \sqrt{\frac{\lambda}{1+\lambda}}\right). \tag{4.10}
$$

If four eigenvalues are equal to λ, partial expansion is not necessary, and Equation (4.9) can be obtained as

$$P_{ei} = \sum_{k=0}^{3} \binom{3+k}{k} [1 - G(\lambda)]^k [G(\lambda)]^4. \tag{4.11}$$

Combining Equations (4.8) and (4.11), the mean BER averaged with respect to the channel distribution is obtained as

$$P_e = \frac{1}{4} \sum_{i=1}^{4} P_{ei} = \frac{1}{4} \sum_{i=1}^{4} \sum_{k=0}^{3} \binom{3+k}{k} [1 - G(\lambda_i)]^k [G(\lambda_i)]^4, \tag{4.12}$$

where λ_i is the duplicate eigenvalue of $\frac{\rho \sum}{2}$ for P_{ei} (i = 1, 2,…, 4). However, in the ABBA code channel, $|R_{33}|^2$ is not χ^2-distributed and can't be written as a quadratic form, that is, we can't consider our condition to the above closed-form expression in (4.12) directly. In place of this condition, the relationship between quadratic form of the channel vector $\mathbf{h}$ and diagonal entry ($|R_{33}|$) is found. It is possible to exploit the relationship to use the above closed-form expression in (4.12).

4.2 Bound of the Channel Determinant

From Section 4.1, the diagonal entries are important for us to evaluate the overall average BER. In order to understand the diagonal entries of the upper triangular matrix $\mathbf{R}$, it is interesting for us to calculate the determinant of the channel matrix for the ABBA code. For the channel matrix of the ABBA code, some simple derivations are given as follows:

$$\begin{aligned}
\det(\mathbf{H}) &= \det\left(\begin{bmatrix} \mathbf{H}_1 & \mathbf{H}_2 \\ \mathbf{H}_2 & \mathbf{H}_1 \end{bmatrix}\right) = \det\left(\begin{bmatrix} \mathbf{I}_2 & \mathbf{I}_2 \\ \mathbf{0} & \mathbf{I}_2 \end{bmatrix}\right) \det\left(\begin{bmatrix} \mathbf{H}_1 & \mathbf{H}_2 \\ \mathbf{H}_2 & \mathbf{H}_1 \end{bmatrix}\right) \det\left(\begin{bmatrix} \mathbf{I}_2 & -\mathbf{I}_2 \\ \mathbf{0} & \mathbf{I}_2 \end{bmatrix}\right) \\
&= \det\left(\begin{bmatrix} \mathbf{I}_2 & \mathbf{I}_2 \\ \mathbf{0} & \mathbf{I}_2 \end{bmatrix} \begin{bmatrix} \mathbf{H}_1 & \mathbf{H}_2 \\ \mathbf{H}_2 & \mathbf{H}_1 \end{bmatrix} \begin{bmatrix} \mathbf{I}_2 & -\mathbf{I}_2 \\ \mathbf{0} & \mathbf{I}_2 \end{bmatrix}\right) = \det\left(\begin{bmatrix} \mathbf{H}_1 + \mathbf{H}_2 & \mathbf{H}_1 + \mathbf{H}_2 \\ \mathbf{H}_2 & \mathbf{H}_1 \end{bmatrix} \begin{bmatrix} \mathbf{I}_2 & -\mathbf{I}_2 \\ \mathbf{0} & \mathbf{I}_2 \end{bmatrix}\right) \\
&= \det\left(\begin{bmatrix} \mathbf{H}_1 + \mathbf{H}_2 & \mathbf{0} \\ \mathbf{H}_2 & \mathbf{H}_1 - \mathbf{H}_2 \end{bmatrix}\right) = \det(\mathbf{H}_1 + \mathbf{H}_2) \times \det(\mathbf{H}_1 - \mathbf{H}_2).
\end{aligned} \tag{4.13}$$

It is important for us that $\det(\mathbf{H}) = \det(\mathbf{H}_1 + \mathbf{H}_2) \times \det(\mathbf{H}_1 - \mathbf{H}_2)$, the diagonal entries of matrix $\mathbf{R}$ in (2.59) and (2.60) can be rewritten as

$$R_{11} = R_{22} = \sqrt{\det(\mathbf{H}_1) + \det(\mathbf{H}_2)}, \tag{4.14}$$

$$R_{33} = R_{44} = \sqrt{\frac{\det(\mathbf{H}_1 + \mathbf{H}_2) \times \det(\mathbf{H}_1 - \mathbf{H}_2)}{\det(\mathbf{H}_1) + \det(\mathbf{H}_2)}}, \tag{4.15}$$

where

$$\det(\mathbf{H}_1) + \det(\mathbf{H}_2) = |h_1|^2 + |h_2|^2 + |h_3|^2 + |h_4|^2, \tag{4.16}$$

$$\det(\mathbf{H}_1 + \mathbf{H}_2) = |h_1 + h_3|^2 + |h_2 + h_4|^2, \tag{4.17}$$

$$\det(\mathbf{H}_1 - \mathbf{H}_2) = |h_1 - h_3|^2 + |h_2 - h_4|^2. \tag{4.18}$$

In Equations (4.14) and (4.15), the relationship between channel coefficients and the diagonal entries of $\mathbf{R}$ is obtained; the diagonal entries can be written in terms of the determinants of the partitioned matrices. Then, the bound of the channel determinant is derived from the above relationship.

Now, we attempt to find the bound of the channel determinant because some diagonal entries of the upper triangular matrix are deeply affected by determinants of channel matrix. The purpose of the bounds is to simply the expression in (4.15). The simple expressions are exploited to determine power loading factors in order to achieve better performance. Under some manipulations, we have

$$\begin{aligned}
\det(\mathbf{H}_1 + \mathbf{H}_2) &= |h_1 + h_3|^2 + |h_2 + h_4|^2 \\
&= |h_1|^2 + |h_1|^2 + |h_3|^2 + |h_4|^2 + 2\,\mathrm{Re}\left(h_1^* h_3 + h_2^* h_4\right) \\
&= \det(\mathbf{H}_1) + \det(\mathbf{H}_2) + 2\,\mathrm{Re}\left(h_1^* h_3 + h_2^* h_4\right),
\end{aligned} \tag{4.19}$$

$$\begin{aligned}
\det(\mathbf{H}_1 - \mathbf{H}_2) &= |h_1 - h_3|^2 + |h_2 - h_4|^2 \\
&= |h_1|^2 + |h_1|^2 + |h_3|^2 + |h_4|^2 - 2\,\mathrm{Re}\left(h_1^* h_3 + h_2^* h_4\right) \\
&= \det(\mathbf{H}_1) + \det(\mathbf{H}_2) - 2\,\mathrm{Re}\left(h_1^* h_3 + h_2^* h_4\right).
\end{aligned} \tag{4.20}$$

It is obvious that the term $\mathrm{Re}(h_1^* h_3 + h_2^* h_4)$ will affect the value of determinants in (4.19) and (4.20). With a careful observation, we generalize a conclusion as follows:

If $\mathrm{Re}(h_1^* h_3 + h_2^* h_4) \geq 0$, we have

$$\det(\mathbf{H}_1 - \mathbf{H}_2) \leq \det(\mathbf{H}_1) + \det(\mathbf{H}_2) \leq \det(\mathbf{H}_1 + \mathbf{H}_2). \tag{4.21}$$

Combining Equations (4.15) and (4.21), the result is given by

$$\det(\mathbf{H}_1 - \mathbf{H}_2) \leq \frac{\det(\mathbf{H}_1 + \mathbf{H}_2)\det(\mathbf{H}_1 - \mathbf{H}_2)}{\det(\mathbf{H}_1) + \det(\mathbf{H}_2)} \leq \det(\mathbf{H}_1 + \mathbf{H}_2). \tag{4.22}$$

On the contrary, if $\mathrm{Re}(h_1^* h_3 + h_2^* h_4) < 0$, we have

$$\det(\mathbf{H}_1 + \mathbf{H}_2) \leq \det(\mathbf{H}_1) + \det(\mathbf{H}_2) \leq \det(\mathbf{H}_1 - \mathbf{H}_2). \tag{4.23}$$

Combining Equations (4.15) and (4.23), the result is given by

$$\det(\mathbf{H}_1 + \mathbf{H}_2) \leq \frac{\det(\mathbf{H}_1 + \mathbf{H}_2)\det(\mathbf{H}_1 - \mathbf{H}_2)}{\det(\mathbf{H}_1) + \det(\mathbf{H}_2)} \leq \det(\mathbf{H}_1 - \mathbf{H}_2). \tag{4.24}$$

As a result, $|R_{33}|^2$ must satisfy either (4.22) or (4.24), depending on whether $\Lambda \geq 0$ or $\Lambda < 0$, where $\Lambda = \mathrm{Re}(h_1^* h_3 + h_2^* h_4)$. For simplicity, Equations (4.22) and (4.24) are translated into

$$\det(\mathbf{H}_1 - \mathbf{H}_2) \leq |R_{33}|^2 \leq \det(\mathbf{H}_1 + \mathbf{H}_2)$$

and

$$\det(\mathbf{H}_1 + \mathbf{H}_2) \leq |R_{33}|^2 \leq \det(\mathbf{H}_1 - \mathbf{H}_2), \text{ respectively.} \tag{4.25}$$

From the above equation, it is the fact the larger term of $\det(\mathbf{H}_1 - \mathbf{H}_2)$ and $\det(\mathbf{H}_1 + \mathbf{H}_2)$ is the upper bound of $|R_{33}|^2$ while the smaller term of $\det(\mathbf{H}_1 - \mathbf{H}_2)$ and $\det(\mathbf{H}_1 + \mathbf{H}_2)$ is the lower bound of $|R_{33}|^2$. In terms of the channel coefficients ($\mathbf{h} = \begin{bmatrix} h_1 & h_2 & h_3 & h_4 \end{bmatrix}^T$), the diagonal entries can be expressed as follows:

$$|R_{11}|^2 = \det(\mathbf{H}_1) + \det(\mathbf{H}_2) = \mathbf{h}^H \mathbf{h}, \tag{4.26}$$

$$\left|R_{33}\right|^2 = \frac{\det(\mathbf{H})}{\det(\mathbf{H}_1)+\det(\mathbf{H}_2)} \geq \det(\mathbf{H}_1 - \mathbf{H}_2) = \mathbf{h}^H \Delta\_\mathbf{h}\,, \tag{4.27}$$

and

$$\left|R_{33}\right|^2 = \frac{\det(\mathbf{H})}{\det(\mathbf{H}_1)+\det(\mathbf{H}_2)} \geq \det(\mathbf{H}_1 + \mathbf{H}_2) = \mathbf{h}^H \Delta_+ \mathbf{h}\,, \tag{4.28}$$

where

$$\det(\mathbf{H}_1 + \mathbf{H}_2) = \left|h_1 + h_3\right|^2 + \left|h_2 + h_4\right|^2 = \mathbf{h}^H \begin{bmatrix} 1 & 0 & 1 & 0 \\ 0 & 1 & 0 & 1 \\ 1 & 0 & 1 & 0 \\ 0 & 1 & 0 & 1 \end{bmatrix} \mathbf{h} = \mathbf{h}^H \Delta_+ \mathbf{h}\,, \tag{4.29}$$

and

$$\det(\mathbf{H}_1 - \mathbf{H}_2) = \left|h_1 - h_3\right|^2 + \left|h_2 - h_4\right|^2 = \mathbf{h}^H \begin{bmatrix} 1 & 0 & -1 & 0 \\ 0 & 1 & 0 & -1 \\ -1 & 0 & 1 & 0 \\ 0 & -1 & 0 & 1 \end{bmatrix} \mathbf{h} = \mathbf{h}^H \Delta\_\mathbf{h}\,. \tag{4.30}$$

It is well-known that the signal to noise ratio (SNR) at the receiver (decision-point SNR) is often a function of the channel gain such as $\left|R_{11}\right|^2$, $\left|R_{33}\right|^2$ and so on. The instantaneous bit error rate is determined by the decision-point SNR, so the diagonal entries play an important role in the instantaneous bit error rate. Combining Sections 4.1 and 4.2, a power allocation scheme for Q-OSTBC is proposed by exploiting the bound of diagonal entries and the corresponding closed-form expression is introduced in Section 4.1.

4.3 Evaluation of Overall Average BER for Upper Bound and its Closed-Form Expression

The channel estimation can be classified into two categories, perfect channel estimation and imperfect channel estimation. The perfect channel estimation is discussed in Section 4.3.1 and an upper bound of average BER for the error propagation free case is derived. Then, the imperfect channel estimation is extended in

Section 4.3.2. The average BER for the error propagation free case is evaluated and the corresponding closed-form expression is exploited into the upper bound of average BER formula.

4.3.1 Perfect Channel Estimation Case

To facilitate the derivation of diagonal entries $\mathbf{R}$ and based on design procedure of Section 4.1, an upper bound of average BER for the error propagation free case is derived in closed-form. As $R_{11} = R_{22}$ and $R_{33} = R_{44}$, it is more convenient to decompose P_e in (4.7) into

$$\begin{aligned} P_e &= \frac{1}{4}\sum_{i=1}^{4} P_{ei} = \frac{1}{4}\sum_{i=1}^{4} \int Q\left(\sqrt{\rho}\,|p_i R_{ii}|\right) p\left(|R_{ii}|\right) d|R_{ii}| \\ &= \frac{1}{4}\sum_{i=1}^{4} \int_{\mathbf{h}} \frac{1}{\pi} \int_0^{\pi/2} \exp\left(-\frac{\rho p_i^2 |R_{ii}|^2}{2\sin^2\theta}\right) \frac{1}{\pi^4} \exp\left(-\mathbf{h}^H\mathbf{h}\right) d\theta d\mathbf{h} \\ &= \frac{1}{4}\left\{ \underbrace{\sum_{i=1}^{2} \int_{\mathbf{h}} \frac{1}{\pi} \int_0^{\pi/2} \exp\left(-\frac{\rho p_i^2 |R_{11}|^2}{2\sin^2\theta}\right) \frac{1}{\pi^4} \exp\left(-\mathbf{h}^H\mathbf{h}\right) d\theta d\mathbf{h}}_{:=P_1} \right. \\ &\qquad \left. + \underbrace{\sum_{i=3}^{4} \int_{\mathbf{h}} \frac{1}{\pi} \int_0^{\pi/2} \exp\left(-\frac{\rho p_i^2 |R_{33}|^2}{2\sin^2\theta}\right) \frac{1}{\pi^4} \exp\left(-\mathbf{h}^H\mathbf{h}\right) d\theta d\mathbf{h}}_{:=P_2} \right\}. \end{aligned} \tag{4.31}$$

In what follows we will derive an analytic expression for P_1 and an upper bound for P_2, this in turn yields a closed-form upper bound of P_e.

1. An analytic Form of P_1: Inserting (4.26) into P_1 in Equation (4.31), the same derivation in Section 4.1 is exploited and P_1 can be obtained as follows:

$$\begin{aligned} P_1 &= \sum_{i=1}^{2} \int_{\mathbf{h}} \frac{1}{\pi} \int_0^{\pi/2} \exp\left(-\frac{\rho p_1^2 \mathbf{h}^H\mathbf{h}}{2\sin^2\theta}\right) \frac{1}{\pi^4} \exp\left(-\mathbf{h}^H\mathbf{h}\right) d\theta d\mathbf{h} \\ &= \sum_{i=1}^{2} \frac{1}{\pi} \int_0^{\pi/2} \int_{\mathbf{h}} \frac{1}{\pi^4} \exp\left(-\mathbf{h}^H \left(\frac{\rho p_1^2 \mathbf{I}_4}{2\sin^2\theta} + \mathbf{I}_4\right)\mathbf{h}\right) d\mathbf{h}\, d\theta \end{aligned}$$

$$
\begin{aligned}
&\underset{(a)}{=}\sum_{i=1}^{2}\frac{1}{\pi}\int_0^{\pi/2}\left\{\det\left[\frac{\rho p_i^2\mathbf{I}_4}{2\sin^2\theta}+\mathbf{I}_4\right]\right\}^{-1}d\theta \\
&=\sum_{i=1}^{2}\frac{1}{\pi}\int_0^{\pi/2}\left(\frac{\rho p_1^2}{2\sin^2\theta}+1\right)^{-4}d\theta \qquad (4.32)\\
&\underset{(b)}{=}\sum_{i=1}^{2}\sum_{k=0}^{3}\binom{3+k}{k}\left[1-G(\frac{\rho p_i^2}{2})\right]^k\left[G(\frac{\rho p_i^2}{2})\right]^4
\end{aligned}
$$

2. An Analytic Upper Bound of P_2: It is noted that the closed-form expression of P_1 in (4.32) hinges entirely on (4.26), in which $|R_{11}|^2$ is seen to been essentially quadratic in the channel gain vector ($\mathbf{h}=[h_1 \quad h_2 \quad h_3 \quad h_4]^T$). Such a property, however, no longer holds for $|R_{33}|^2$. As a result, there does not seem to exist an exact expression for P_2 analogue to (4.32). We shall then instead seek for a tractable upped bound for P_2. From Section 4.1, it is known that $|R_{33}|^2$ must satisfy either (4.22) or (4.24), depending on whether $\Lambda \geq 0$ or $\Lambda < 0$, where $\Lambda = \mathrm{Re}(h_1^* h_3 + h_2^* h_4)$. This results can be exploited for deriving a tractable upper bound of P_2. Indeed, we first note by definition that $P_2/2$ is the average BER of the 3rd and 4th component channels (see (4.31)). Let us denote by $P_{2|\Lambda\geq 0}/2$ the associated conditional probability given that the event $\{\Lambda \geq 0\}$ is true, and likewise by $P_{2|\Lambda<0}/2$ for the complement event $\{\Lambda < 0\}$. Then with (4.31) and (4.27), we have

$$
P_{2|\Lambda\geq 0}/2 \leq \frac{1}{2}\sum_{i=3}^{4}\int_{\mathbf{h}}\frac{1}{\pi}\int_0^{\pi/2}\exp\left(-\frac{\rho p_i^2\det(\mathbf{H}_1-\mathbf{H}_2)}{2\sin^2\theta}\right)\frac{1}{\pi^4}\exp\left(-\mathbf{h}^H\mathbf{h}\right)d\theta d\mathbf{h}\,; \qquad (4.33)
$$

also (4.31) and (4.28) together imply

$$P_{2|\Lambda<0}/2 \le \frac{1}{2}\sum_{i=3}^{4}\int_{\mathbf{h}}\frac{1}{\pi}\int_{0}^{\pi/2}\exp\left(-\frac{\rho p_i^2\det(\mathbf{H}_1+\mathbf{H}_2)}{2\sin^2\theta}\right)\frac{1}{\pi^4}\exp\left(-\mathbf{h}^H\mathbf{h}\right)d\theta d\mathbf{h}.$$

(4.34)

Since

$$P_2/2 = \left(P_{2|\Lambda\ge 0}/2\right)\Pr(\Lambda\ge 0) + \left(P_{2|\Lambda<0}/2\right)\Pr(\Lambda<0); \tag{4.35}$$

and assuming that the two outcomes $\{\Lambda\ge 0\}$ and $\{\Lambda<0\}$ are equally-probable, namely, $\Pr(\Lambda\ge 0)=\Pr(\Lambda<0)=1/2$, relations (4.33)-(4.35) then leads to the following key inequality

$$\begin{aligned}P_2 \le \frac{1}{2}\Bigg\{&\sum_{i=3}^{4}\int_{\mathbf{h}}\frac{1}{\pi}\int_{0}^{\pi/2}\exp\left(-\frac{\rho p_i^2\det(\mathbf{H}_1-\mathbf{H}_2)}{2\sin^2\theta}\right)\frac{1}{\pi^4}\exp\left(-\mathbf{h}^H\mathbf{h}\right)d\theta d\mathbf{h}\\ &+\sum_{i=3}^{4}\int_{\mathbf{h}}\frac{1}{\pi}\int_{0}^{\pi/2}\exp\left(-\frac{\rho p_i^2\det(\mathbf{H}_1+\mathbf{H}_2)}{2\sin^2\theta}\right)\frac{1}{\pi^4}\exp\left(-\mathbf{h}^H\mathbf{h}\right)d\theta d\mathbf{h}\Bigg\}.\end{aligned}$$

(4.36)

The significance of (4.36) lies in that the exponents in both summands are now quadratic in channel coefficients. Indeed, from (4.29) and (4.30), inequality (4.36) can be equivalently rewritten as

$$\begin{aligned}P_2 &\le \frac{1}{2}\Bigg\{\sum_{i=3}^{4}\int_{\mathbf{h}}\frac{1}{\pi}\int_{0}^{\pi/2}\exp\left(-\frac{\rho p_i^2\mathbf{h}^H\Delta_-\mathbf{h}}{2\sin^2\theta}\right)\frac{1}{\pi^4}\exp\left(-\mathbf{h}^H\mathbf{h}\right)d\theta d\mathbf{h}\\ &\quad+\sum_{i=3}^{4}\int_{\mathbf{h}}\frac{1}{\pi}\int_{0}^{\pi/2}\exp\left(-\frac{\rho p_i^2\mathbf{h}^H\Delta_+\mathbf{h}}{2\sin^2\theta}\right)\frac{1}{\pi^4}\exp\left(-\mathbf{h}^H\mathbf{h}\right)d\theta d\mathbf{h}\Bigg\}\\ &=\frac{1}{2}\Bigg\{\sum_{i=3}^{4}\int_{\mathbf{h}}\frac{1}{\pi}\int_{0}^{\pi/2}\exp\left(-\mathbf{h}^H\left(\frac{\rho p_i^2\Delta_-}{2\sin^2\theta}+\mathbf{I}_4\right)\mathbf{h}\right)d\theta d\mathbf{h}\\ &\quad+\sum_{i=3}^{4}\int_{\mathbf{h}}\frac{1}{\pi}\int_{0}^{\pi/2}\exp\left(-\mathbf{h}^H\left(\frac{\rho p_i^2\Delta_+}{2\sin^2\theta}+\mathbf{I}_4\right)\mathbf{h}\right)d\theta d\mathbf{h}\Bigg\}\end{aligned}$$

$$= \frac{1}{2}\left\{ \sum_{i=3}^{4} \frac{1}{\pi} \int_0^{\pi/2} \left\{ \det\left[\frac{\rho p_i^2 \Delta_-}{2\sin^2\theta} + \mathbf{I}_4 \right] \right\}^{-1} d\theta \right.$$
$$\left. + \sum_{i=3}^{4} \frac{1}{\pi} \int_0^{\pi/2} \left\{ \det\left[\frac{\rho p_i^2 \Delta_+}{2\sin^2\theta} + \mathbf{I}_4 \right] \right\}^{-1} d\theta \right\}. \tag{4.37}$$

where the last equality follows again from [23], [25]. Now, the eigenvalus of both Δ_+ and Δ_- are calculated as follows $\{0,0,2,2\}$, and (4.37) becomes

$$P_2 \le$$
$$\frac{1}{2}\left\{ \sum_{i=3}^{4} \frac{1}{\pi} \int_0^{\pi/2} \left(\frac{\rho p_i^2}{\sin^2\theta} + 1 \right)^{-2} d\theta + \sum_{i=3}^{4} \frac{1}{\pi} \int_0^{\pi/2} \left(\frac{\rho p_i^2}{\sin^2\theta} + 1 \right)^{-2} d\theta \right\}$$
$$= \frac{1}{\pi} \int_0^{\pi/2} \left(\frac{\rho p_3^2}{\sin^2\theta} + 1 \right)^{-2} d\theta + \frac{1}{\pi} \int_0^{\pi/2} \left(\frac{\rho p_4^2}{\sin^2\theta} + 1 \right)^{-2} d\theta$$
$$\underset{(c)}{=} \sum_{k=0}^{1} \binom{1+k}{k} \left[1 - G(\rho p_3^2)\right]^k \left[G(\rho p_3^2)\right]^2 + \sum_{k=0}^{1} \binom{1+k}{k} \left[1 - G(\rho p_4^2)\right]^k \left[G(\rho p_4^2)\right]^2$$
$$= \sum_{i=3}^{4} \sum_{k=0}^{1} \binom{1+k}{k} \left[1 - G(\rho p_i^2)\right]^k \left[G(\rho p_i^2)\right]^2, \tag{4.38}$$

where (c) follows again by using [25, e.q. (38)].

Combining (4.31), (4.32) and (4.38), the overall mean BER by averaging the channel distribution in (4.7) can thus be upper bounded by

$$P_e \le \frac{1}{4}\left\{ \sum_{i=1}^{2} \sum_{k=0}^{3} \binom{3+k}{k} \left[1 - G(\frac{\rho p_i^2}{2})\right]^k \left[G(\frac{\rho p_i^2}{2})\right]^4 \right.$$
$$\left. + \sum_{i=3}^{4} \sum_{k=0}^{1} \binom{1+k}{k} \left[1 - G(\rho p_i^2)\right]^k \left[G(\rho p_i^2)\right]^2 \right\}. \tag{4.39}$$

where $G(\cdot)$ is defined in (4.10).

An upper bound of mean BER averaged with respect to the channel distribution is derived in the error propagation free case. By exploiting this upper bound, the power

loading factors are determined by minimizing this upper bound. In the next section, the analysis is extended into imperfect channel estimation case.

4.3.2 Imperfect Channel Estimation Case

When the channel state information is not perfectly known at the transmitter, the above method can't be used. Therefore, it is assumed that the channel statistics are known and the similar method is derived. Assuming that channel estimate $\hat{\mathbf{h}}$ and channel estimation error $\mathbf{e}$, we have that $\hat{\mathbf{h}} = \mathbf{h} + \mathbf{e}$. The estimation error $\mathbf{e}$ has Gaussian distribution with zero mean and covariance matrix $\mathbf{C}_{\mathbf{ee}} = \Sigma_{\hat{\mathbf{h}}} - \Sigma_{\mathbf{h}}$, where $\Sigma_{\hat{\mathbf{h}}}$ and $\Sigma_{\mathbf{h}}$ are the covariance matrices of the channel estimate and channel state information, respectively. From [23], the estimation error can be modeled into noise covariance matrix. That is, the estimation error will enhance the noise as follows:

$$\mathbf{E} = \mathbf{C}_{\mathbf{ee}} E_s + N_0 \mathbf{I}_N, \tag{4.40}$$

where E_s is the symbol energy and $N_0 \mathbf{I}_N$ is i.i.d. Gaussian covariance matrix. Then, the derivations in Section 4.3.1 are revised and the mean BER averaged with respect to the channel distribution is given. From [23], the average BER can be obtained as

$$P_e = \frac{1}{4}\sum_{i=1}^{4} P_{ei} = \frac{1}{4}\sum_{i=1}^{4} \int Q\left(\sqrt{p_i^2 E_s \hat{\mathbf{h}}^H \mathbf{E}^{-1} \hat{\mathbf{h}}}\right) p\left(\hat{\mathbf{h}}\right) d\hat{\mathbf{h}}. \tag{4.41}$$

By exploiting (4.6), Equation (4.41) becomes

$$\begin{aligned} P_e &= \frac{1}{4}\sum_{i=1}^{4} \int_{\hat{\mathbf{h}}} \frac{1}{\pi} \int_0^{\pi/2} \exp\left(-\frac{p_i^2 E_s \hat{\mathbf{h}}^H \mathbf{E}^{-1} \hat{\mathbf{h}}}{2\sin^2\theta}\right) d\theta \frac{1}{\pi^4 \det(\Sigma)} \exp\left(-\hat{\mathbf{h}}^H \Sigma^{-1} \hat{\mathbf{h}}\right) d\hat{\mathbf{h}} \\ &= \frac{1}{4}\sum_{i=1}^{4} \frac{1}{\pi} \int_0^{\pi/2} \int_{\hat{\mathbf{h}}} \frac{1}{\pi^4 \det(\Sigma)} \exp\left(-\hat{\mathbf{h}}^H \left(\frac{p_i^2 E_s \mathbf{E}^{-1} \Sigma}{2\sin^2\theta} + \mathbf{I}_4\right) \Sigma^{-1} \hat{\mathbf{h}}\right) d\hat{\mathbf{h}} d\theta \\ &= \frac{1}{4}\sum_{i=1}^{4} \frac{1}{\pi} \int_0^{\pi/2} \left\{ \det\left[\frac{p_i^2 E_s \mathbf{E}^{-1} \Sigma}{2\sin^2\theta} + \mathbf{I}_4\right] \right\}^{-1} d\theta \end{aligned}$$

$$
\begin{aligned}
&= \frac{1}{4}\sum_{i=1}^{4}\frac{1}{\pi}\int_0^{\pi/2}\left\{\prod_{n=1}^{N}\left(\frac{\lambda_{i,n}p_i^2}{\sin^2\theta}+1\right)\right\}^{-1} d\theta \\
&= \frac{1}{4}\sum_{i=1}^{4}\frac{1}{\pi}\int_0^{\pi/2}\left[\sum_{k=1}^{K}\sum_{n=1}^{N_k}\mu_{k,n}\left(\frac{\lambda_{i,k}p_i^2}{\sin^2\theta}+1\right)^{-n}\right] d\theta \\
&= \frac{1}{4}\sum_{i=1}^{4}\sum_{k=1}^{K}\sum_{n=1}^{N_k}\mu_{k,n}\sum_{j=0}^{n-1}\binom{n-1+j}{j}\left[1-G(\lambda_{i,k}p_i^2)\right]^j\left[G(\lambda_{i,k}p_i^2)\right]^n.
\end{aligned}
\tag{4.42}
$$

These parameters are defined as that λ_k (k = 1, 2,…, K) are the eigenvalues of $\frac{E_s\mathbf{E}^{-1}\Sigma}{2}$, K is the number of distinct eigenvalues, N_i is the eigenvalue's multiplicity, $\mu_{i,n}$ is the ith residue associated with nth power in the partial-fraction expansion, and $G(\cdot)$ is defined in (4.10). We can see that Equation (4.42) is equivalent to Equation (4.9), except that the eigenvalues are not equal to each other. Therefore, the upper bound of average BER in Section 4.3.1 is only slightly revised. From (4.31) and (4.35), we have

$$
\begin{aligned}
P_e \le \frac{1}{4}\Bigg\{&\sum_{i=1}^{2}\int_{\hat{\mathbf{h}}}\frac{1}{\pi}\int_0^{\pi/2}\exp\left(-\frac{p_i^2E_s\hat{\mathbf{h}}^H\mathbf{E}^{-1}\hat{\mathbf{h}}}{2\sin^2\theta}\right)\frac{1}{\pi^4}\exp\left(-\hat{\mathbf{h}}^H\Sigma^{-1}\hat{\mathbf{h}}\right)d\theta d\hat{\mathbf{h}} \\
&+\Pr(\Lambda\ge 0)\sum_{i=3}^{4}\int_{\hat{\mathbf{h}}}\frac{1}{\pi}\int_0^{\pi/2}\exp\left(-\frac{p_i^2E_s\hat{\mathbf{h}}^H\mathbf{\Lambda}_{-}\mathbf{E}^{-1}\hat{\mathbf{h}}}{2\sin^2\theta}\right)\frac{1}{\pi^4}\exp\left(-\hat{\mathbf{h}}^H\Sigma^{-1}\hat{\mathbf{h}}\right)d\theta d\hat{\mathbf{h}} \\
&+\Pr(\Lambda< 0)\sum_{i=3}^{4}\int_{\hat{\mathbf{h}}}\frac{1}{\pi}\int_0^{\pi/2}\exp\left(-\frac{p_i^2E_s\hat{\mathbf{h}}^H\mathbf{\Lambda}_{+}\mathbf{E}^{-1}\hat{\mathbf{h}}}{2\sin^2\theta}\right)\frac{1}{\pi^4}\exp\left(-\hat{\mathbf{h}}^H\Sigma^{-1}\hat{\mathbf{h}}\right)d\theta d\hat{\mathbf{h}}\Bigg\}.
\end{aligned}
\tag{4.43}
$$

It is noted that the channel covariance matrix Σ will affect the probabilities $\Pr(\Lambda\ge 0)$ and $\Pr(\Lambda< 0)$, where $\Lambda = \mathrm{Re}(h_1^*h_3 + h_2^*h_4)$. After some observations of simulations, it is found that when the correlation between these channels is stronger, the probability $\Pr(\Lambda\ge 0)$ is larger and $\Pr(\Lambda< 0)$ is smaller. Therefore, it is assumed that the two outcomes $\{\Lambda\ge 0\}$ and $\{\Lambda< 0\}$ are equally-probable. In this condition, an upper bound of average BER which is a function of probabilities

$\Pr(\Lambda \geq 0)$ and $\Pr(\Lambda < 0)$ will be derived. For simplicity, it is assumed that channel pdf is i.i.d. Gaussian distribution ($\sum = \mathbf{I}$) and the two outcomes $\{\Lambda \geq 0\}$ and $\{\Lambda < 0\}$ are equally-probable ($\Pr(\Lambda \geq 0) = \Pr(\Lambda < 0) = 1/2$). Equation (4.43) can be obtained as

$$\begin{aligned} P_e \leq \frac{1}{4}\Bigg\{ & \sum_{i=1}^{2} \int_{\hat{\mathbf{h}}} \frac{1}{\pi} \int_0^{\pi/2} \exp\left(-\frac{p_i^2 E_s \hat{\mathbf{h}}^H \mathbf{E}^{-1} \hat{\mathbf{h}}}{2\sin^2\theta} \right) \frac{1}{\pi^4} \exp\left(-\hat{\mathbf{h}}^H \hat{\mathbf{h}}\right) d\theta d\hat{\mathbf{h}} \\ & + \frac{1}{2} \sum_{i=3}^{4} \int_{\hat{\mathbf{h}}} \frac{1}{\pi} \int_0^{\pi/2} \exp\left(-\frac{p_i^2 E_s \hat{\mathbf{h}}^H \boldsymbol{\Delta}_+ \mathbf{E}^{-1} \hat{\mathbf{h}}}{2\sin^2\theta} \right) \frac{1}{\pi^4} \exp\left(-\hat{\mathbf{h}}^H \hat{\mathbf{h}}\right) d\theta d\hat{\mathbf{h}} \\ & + \frac{1}{2} \sum_{i=3}^{4} \int_{\hat{\mathbf{h}}} \frac{1}{\pi} \int_0^{\pi/2} \exp\left(-\frac{p_i^2 E_s \hat{\mathbf{h}}^H \boldsymbol{\Delta}_- \mathbf{E}^{-1} \hat{\mathbf{h}}}{2\sin^2\theta} \right) \frac{1}{\pi^4} \exp\left(-\hat{\mathbf{h}}^H \hat{\mathbf{h}}\right) d\theta d\hat{\mathbf{h}} \Bigg\} \end{aligned} \quad . \quad (4.44)$$

From Equations (4.31)-(4.39), the same derivation procedure can be obtained as follows:

$$\begin{aligned} P_e \leq \frac{1}{4}\Bigg\{ & \sum_{i=1}^{2} \frac{1}{\pi} \int_0^{\pi/2} \int_{\hat{\mathbf{h}}} \frac{1}{\pi^4 \det(\sum)} \exp\left(-\hat{\mathbf{h}}^H \left(\frac{p_i^2 E_s \mathbf{E}^{-1}}{2\sin^2\theta} + \mathbf{I}_4 \right) \hat{\mathbf{h}} \right) d\hat{\mathbf{h}} d\theta \\ & + \frac{1}{2} \sum_{i=3}^{4} \frac{1}{\pi} \int_0^{\pi/2} \int_{\hat{\mathbf{h}}} \frac{1}{\pi^4 \det(\sum)} \exp\left(-\hat{\mathbf{h}}^H \left(\frac{p_i^2 E_s \boldsymbol{\Delta}_+ \mathbf{E}^{-1}}{2\sin^2\theta} + \mathbf{I}_4 \right) \hat{\mathbf{h}} \right) d\hat{\mathbf{h}} d\theta \\ & + \frac{1}{2} \sum_{i=3}^{4} \frac{1}{\pi} \int_0^{\pi/2} \int_{\hat{\mathbf{h}}} \frac{1}{\pi^4 \det(\sum)} \exp\left(-\hat{\mathbf{h}}^H \left(\frac{p_i^2 E_s \boldsymbol{\Delta}_- \mathbf{E}^{-1}}{2\sin^2\theta} + \mathbf{I}_4 \right) \hat{\mathbf{h}} \right) d\hat{\mathbf{h}} d\theta \Bigg\} \end{aligned}$$

$$\begin{aligned} = \frac{1}{4}\Bigg\{ & \sum_{i=1}^{2} \frac{1}{\pi} \int_0^{\pi/2} \left\{ \det\left[\frac{p_i^2 E_s \mathbf{E}^{-1}}{2\sin^2\theta} + \mathbf{I}_4 \right] \right\}^{-1} d\theta \\ & + \frac{1}{2} \sum_{i=3}^{4} \frac{1}{\pi} \int_0^{\pi/2} \left\{ \det\left[\frac{p_i^2 E_s \boldsymbol{\Delta}_+ \mathbf{E}^{-1}}{2\sin^2\theta} + \mathbf{I}_4 \right] \right\}^{-1} d\theta \\ & + \frac{1}{2} \sum_{i=3}^{4} \frac{1}{\pi} \int_0^{\pi/2} \left\{ \det\left[\frac{p_i^2 E_s \boldsymbol{\Delta}_- \mathbf{E}^{-1}}{2\sin^2\theta} + \mathbf{I}_4 \right] \right\}^{-1} d\theta \Bigg\} \end{aligned}$$

$$
\begin{aligned}
&= \frac{1}{4}\left\{ \sum_{i=1}^{2} \frac{1}{\pi} \int_0^{\pi/2} \left\{ \prod_{n=1}^{N_i} \left(\frac{\lambda_{i,n} p_i^2}{\sin^2\theta} + 1 \right) \right\}^{-1} d\theta \right. \\
&\quad + \frac{1}{2} \sum_{i=3}^{4} \frac{1}{\pi} \int_0^{\pi/2} \left\{ \prod_{n=1}^{N_i} \left(\frac{\lambda_{i,n} p_i^2}{\sin^2\theta} + 1 \right) \right\}^{-1} d\theta \\
&\quad \left. + \frac{1}{2} \sum_{i=3}^{4} \frac{1}{\pi} \int_0^{\pi/2} \left\{ \prod_{n=1}^{N_i} \left(\frac{\lambda_{i,n} p_i^2}{\sin^2\theta} + 1 \right) \right\}^{-1} d\theta \right\} \\
&= \frac{1}{4}\left\{ \sum_{i=1}^{2} \frac{1}{\pi} \int_0^{\pi/2} \left[\sum_{k=1}^{K} \sum_{n=1}^{N_{i,k}} \mu_{k,n} \left(\frac{\lambda_{i,k} p_i^2}{\sin^2\theta} + 1 \right)^{-n} \right] d\theta \right. \\
&\quad \left. + \sum_{i=3}^{4} \frac{1}{\pi} \int_0^{\pi/2} \left[\sum_{k=1}^{K} \sum_{n=1}^{N_{i,k}} \mu_{k,n} \left(\frac{\lambda_{i,k} p_i^2}{\sin^2\theta} + 1 \right)^{-n} \right] d\theta \right\} \qquad (4.45) \\
&= \frac{1}{4}\left\{ \sum_{i=1}^{2} \sum_{k=1}^{K} \sum_{n=1}^{N_{i,k}} \mu_{k,n} \sum_{j=0}^{n-1} \binom{n-1+j}{j} \left[1 - G(\lambda_{i,k} p_i^2) \right]^j \left[G(\lambda_{i,k} p_i^2) \right]^n \right. \\
&\quad \left. + \sum_{i=3}^{4} \sum_{k=1}^{K} \sum_{n=1}^{N_{i,k}} \mu_{k,n} \sum_{j=0}^{n-1} \binom{n-1+j}{j} \left[1 - G(\lambda_{i,k} p_i^2) \right]^j \left[G(\lambda_{i,k} p_i^2) \right]^n \right\}.
\end{aligned}
$$

These parameters are defined in the same manner previously. Summarizing Sections 4.3.1 and 4.3.2, the proposed power allocation scheme by minimizing this upper bound is then given in the next section.

4.4 Optimal Power Allocation for Minimum Upper Bound of BER

From the above section, we propose a method of determining power loading factors by minimizing the average BER upper bound in (4.39), subject to the power normalization constraint. Instead of considering channel realization at our design, the average BER for the channel distribution is evaluated. Determining power loading factors by minimizing the upper bound of the error probability averaged with respect to the channel distribution is proposed. As the cost function is highly nonlinear in p_i's,

there do not seem to exist closed-form optimal solutions. Instead, the problem is solved via numerical search (e.g. by using **fmincon** function in Matlab Optimization Toolbox).

4.5 Computer Simulations

First, Figure 4.1 shows the upper bound of average BER compared with the average BER. It is obvious that the upper bound of average BER is indeed larger than the average BER and the upper bound is tighter for low SNR than high SNR.

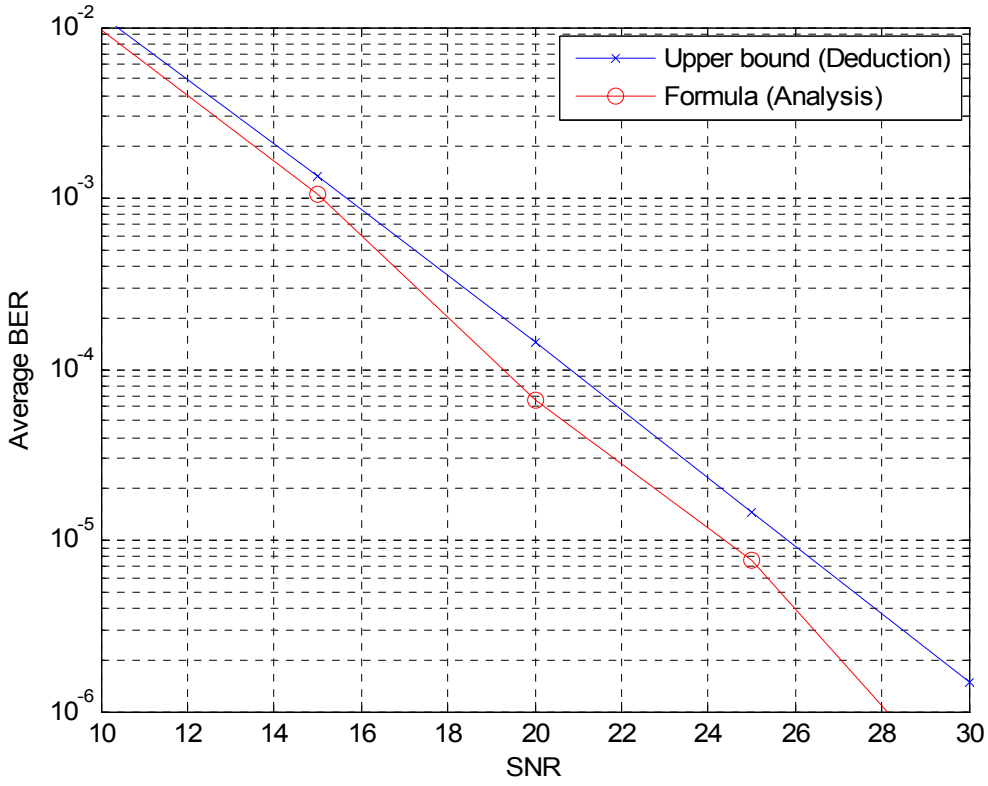

Figure 4.1: Upper bound of average BER performances

To illustrate the numerical performance of the proposed scheme, we compare the simulated average BER of the following receivers: linear MMSE equalizer, QR-based detectors with and without power loading, and the joint ML decoding; the results are

shown in Figure 4.2 (QPSK modulation is used) and the solutions at various SNR are listed in Table 4.1. As we can see, the QR-based solution without power allocation only slightly outperforms the linear MMSE equalizer. When combined with the proposed optimal power loading scheme, performance improvement up to about $2\,\text{dB}$ is achieved in the medium-to-high SNR region; in particular, the BER is almost identical to that attained by the optimal ML decoding for SNR above $22.5\,\text{dB}$. From Table 4.1, we can see the relationship of power loading factors as follows: $p_1 = p_2$, $p_3 = p_4$, and $p_3 > p_1$ because $R_{11} = R_{22}$, $R_{33} = R_{44}$, and $R_{11} \geq R_{33}$.

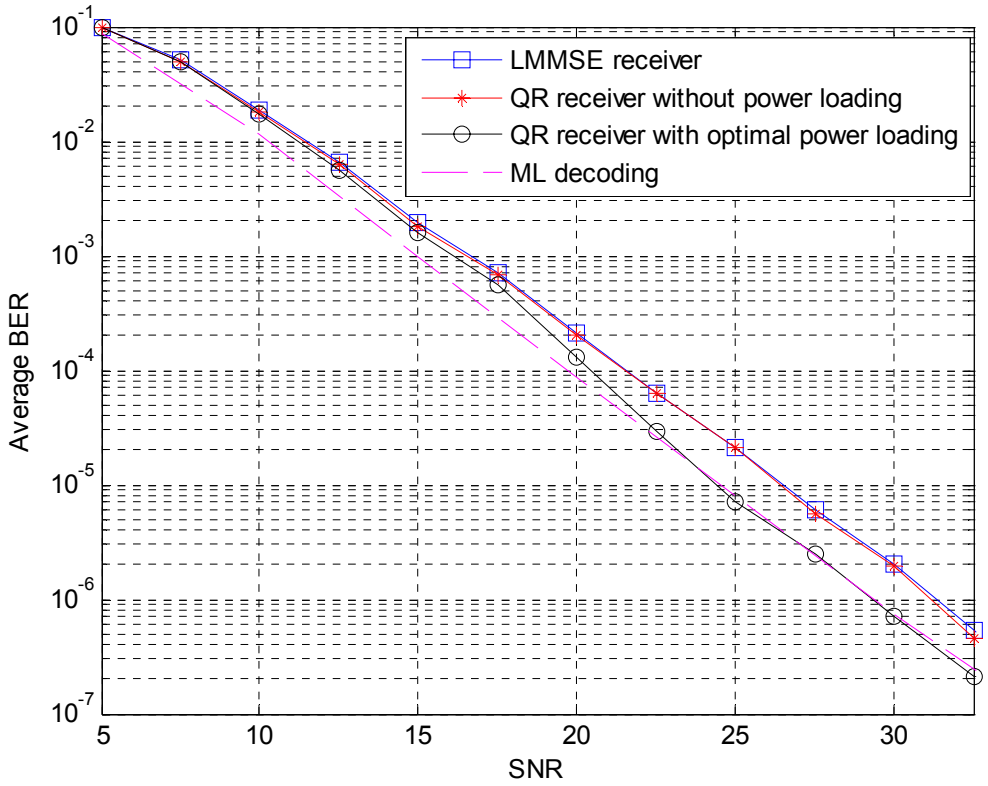

Figure 4.2: Average BER performances of Q-OSTBC with different receivers

Table 4.1: Computed optimal power loading factors in Figure 4.2

Power loading factors / SNR (dB)	p_1	p_2	p_3	p_4
5	0.9982	0.9982	1.0018	1.0018
7.5	0.9807	0.9807	1.0189	1.0189
10	0.9529	0.9529	1.0449	1.0449
12.5	0.9197	0.9197	1.0743	1.0743
15	0.7769	0.7769	1.1817	1.1817
17.5	0.7259	0.7259	1.2137	1.2137
20	0.6724	0.6724	1.2441	1.2441
22.5	0.6180	0.6180	1.2720	1.2720
25	0.5641	0.5641	1.2968	1.2968
27.5	0.5123	0.5123	1.3182	1.3182
30	0.4633	0.4632	1.3362	1.3362
32.5	0.4177	0.4177	1.3511	1.3511
35	0.3755	0.3755	1.3635	1.3635

In Figure 4.3, we show that when there is channel estimation error, our method can be still used. Considering that the channel estimation error covariance matrix is equal to $0.01\mathbf{I}$, the average BER performance is presented and it is found that the BER performance is dominated by the channel estimation error instead of SNR in the high SNR region. When the diagonal entries of the channel estimation error covariance matrix is much larger than the noise power, the BER performance exhibits slight saturation in the high SNR region.

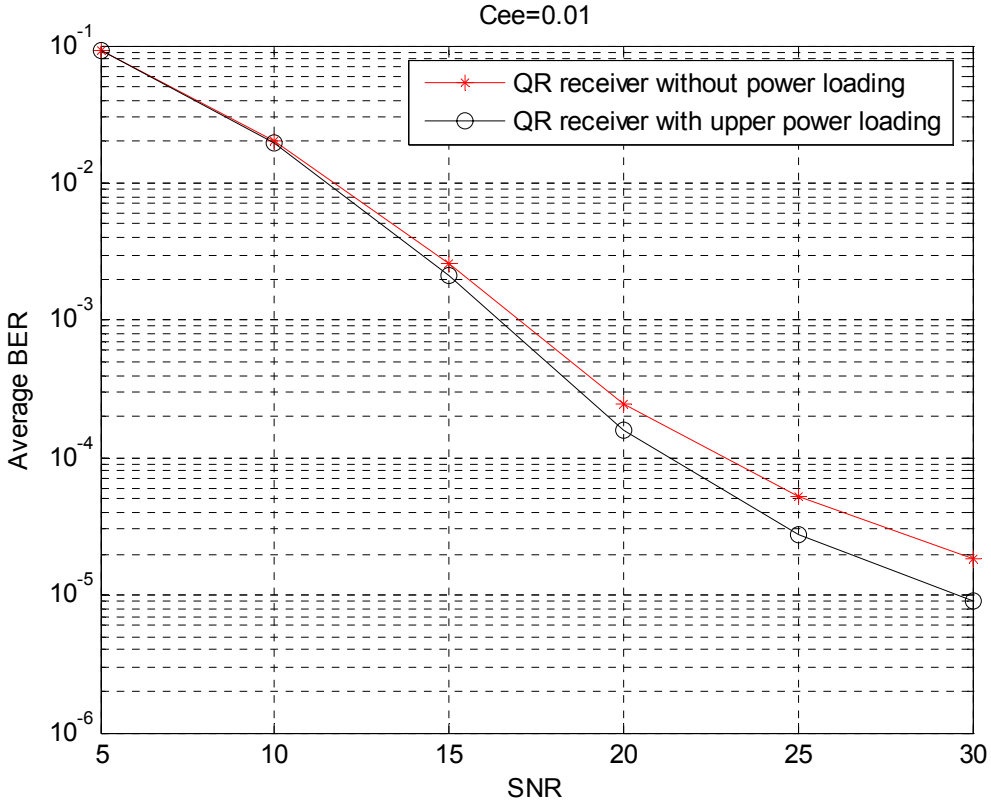

Figure 4.3: Average BER performances of Q-OSTBC with power loading in the channel estimation error case

4.6 Summary

In Section 4.1, we introduce the closed-form formula toward the upper bound of mean BER averaged with respect to the channel distribution. Because the diagonal entries of the upper triangular matrix are related to the channel determinant, we find the bound of the channel determinant in Section 4.2. Then, we exploit the bound of the channel determinant to derive the upper bound of average BER. The upper bound is written as a quadratic form, so we can evaluate the upper bound of the mean BER with respect to the channel distribution and obtain the corresponding closed-form formula. Considering perfect channel estimation, we determine our power loading factors by minimizing the corresponding closed-form formula. Furthermore, we consider imperfect channel estimation and derive the upper bound of the mean BER averaged

with respect to the channel distribution in closed-form. By minimizing this upper bound, we obtain the power loading factors. We compare the simulated average BER of the following receivers: linear MMSE equalizer, QR-based detectors with and without power loading, and the joint ML decoding. In Figure 4.2, we can see that when the QR-based solution is combined with the proposed optimal power loading scheme, performance improvement up to about 2 dB is achieved in the medium-to-high SNR region, in particular, and the BER is almost identical to that attained by the optimal ML decoding for SNR above 22.5 dB.

Chapter 5

Conclusion

In this thesis, we consider the transmission of the ABBA code over i.i.d. Rayleigh fading channels, and propose a symbol power allocation scheme for minimizing the average BER performance. In order to achieve a bit-error-rate (BER) performance compromise between linear equalization and joint maximum likelihood (ML) decoding, we propose to adopt QR-based successive detection with proper symbol power allocation. In Chapter 2, we introduce OSTBC and Q-OSTBC; their corresponding decoding methods are introduced. The QR decomposition of the channel matrix for the ABBA code is derived in Section 2.3.2. By exploiting a distinctive channel matrix structure induced by the ABBA code, we derive an explicit formula of the associated QR-decomposition. Then, we detect the received signals with QR-based successive detection. In Chapter 3, it is shown that the average BER with errorless front-layer decision feedback, although being merely a lower bound of the true mean error rate, remains simple to characterize and, moreover, is closely related to an upper bound of the block error probability when error-propagation occurs [10]. Motivated by this fact and to guarantee a performance improvement, the optimal power allocation schemes are introduced under a fixed channel realization without considering error propagation. Then, considering the case that when error propagation occurs, the corresponding

method is presented. The simulations show that the performance is improved by allocating transmit power via the minimum BER criterion.

In Chapter 4, the overall mean BER averaged with respect to the channel distribution is introduced first and the bound is derived for the channel determinant in Section 4.2. The exploitation of a symmetric channel matrix structure unique to the ABBA code leads to a closed-form upper bound of the overall mean BER (averaged over the channel distribution). The optimal power allocation factors obtained by minimizing this bound thus guarantee a universal performance regardless of the instantaneous channel characteristics. That is, we propose to determine the power loading weights toward minimizing the overall mean BER, averaged with respect to the channel distribution. Simulation results confirm the effectiveness of the proposed solution: the achievable BER result is almost identical to that of joint ML detection when SNR is high.

The study presented in the thesis has discussed a power allocation scheme by minimizing the average BER in the error propagation free case. In particular, we derive the upper bound of the mean BER averaged with respect to the channel distribution in closed-form. Instead of considering the channel realization, we only require to know SNR, the channel covariance matrix, and the estimation error covariance matrix. No error propagation is considered in the above discussions. We then take error propagation into account and derive the corresponding mean BER formula averaged with respect to the channel distribution. Considering error propagation, the multiplication of two Q-functions problem occurs. However, it is not easy for us to deal with the multiplication of two Q-functions problem averaged with respect to the channel distribution. The derivation of the corresponding upper bound is thus a problem worthy of investigation in the future.

Bibliography

[1] V. Tarokh, H. Jafarkhani, and A. R. Calderbank, "Space-time block codes from orthogonal designs," *IEEE Trans. Information Theory*, vol. 45, pp. 1456–1467, July 1999.

[2] H. Jafarkhani, *Space-Time Coding*, Cambridge University Press, 2005.

[3] E. G. Larsson and P. Stoica, *Space-Time Block Coding for Wireless Communications*, Cambridge University Press, 2003.

[4] H. Jafarkhani, **"**A quasi-orthogonal space-time block code," *IEEE Trans. on Communications***,** vol. 49, pp. 1-4, Jan. 2001.

[5] O. Tirkkonen, A. Boariu and A. Hottinen, "Minimal non-orthogonal rate 1 space-time block code for 3+ Tx antenna," *IEEE 6th Int. Symp. on Spread-Spectrum Tech. and Appli.*, NJIT, New Jersey, USA, pp. 429-432, Sept. 2000.

[6] S. Alamouti, "A simple transmit diversity technique for wireless communications", *IEEE Journal on Sel. Areas in Comm.,* vol. 16, pp. 1451-1458, Oct. 1998.

[7] L. Liu and H. Jafarkhani, "Application of quasi-orthogonal space-time block codes in beamforming," *IEEE Trans. Signal Processing*, vol. 53, no. 1, pp.54-63, Jan. 2005.

[8] R. Kalbasi, D. D. Falconer, and A. H. Banihashemi, "Optimal power allocation for a V-BLAST system with two antennas at the transmitter," *IEEE Communication Letters*, vol. 9, no.9, pp. 826–828, Sept. 2005.

[9] N. Prasad and M. K. Varanasi, "Analysis of decision feedback detection for MIMO Rayleigh-fading channels and optimization of power and rate allocation," *IEEE Trans. Information Theory*, vol. 50, no. 6, pp.1009-1025, June 2004.

[10] Z. Yan, K. M. Wong, and Z. Q. Luo, “Optimal diagonal precoder for multiantenna communication systems,” *IEEE Trans. Signal Processing*, vol. 53, no. 6, pp. 2089–2100, June 2005.

[11] H. Zhung, L. Dai, S. Zhou, and Y. Yao, “Low complexity per-antenna rate and power control approach for closed-loop V-BLAST,” *IEEE Trans. Communications*, vol. 51, no. 11, pp.1783-1787, Nov. 2003.

[12] S. H. Nam, O. S. Shin, and K. B. Lee, “Transmit power allocation for a modified V-BLAST system,” *IEEE Trans. Communications*, vol. 52, no. 7, pp.1074-1079, July 2004.

[13] N. Wang and S. D. Blostein, “Minimum BER power allocation for MIMO spatial multiplexing systems,” *Proc. IEEE ICC’05*, vol. 4, pp. 2282–2286, 2005.

[14] A. H. Sayed, W. M. Younis, and A. Tarighat, “An invariant matrix structure in multiantenna communications,” *IEEE. Signal Processing Letters*, vol. 12, no. 11, pp. 749–752, Nov. 2005.

[15] P. W. Wolnianaky, G. J. Foschini, G. D. Golden, and R. A. Valenzuela, “V-BLAST: An architecture for realizing very high data rates over rich-scattering wireless channels,” *Proc. IEEE ISSSE-98*, Italy, pp. 295-300, Sept. 1998.

[16] N. Wang and S. D. Blostein, “Power loading for CP-OFDM over frequency-selective fading channels,” *Proc. IEEE Globecom*, vol. 4, San Francisco, CA, pp. 2305–2309, Dec. 2003.

[17] N. Wang and S. D. Blostein, “Comparison of CP-based single carrier and OFDM with power allocation,” *IEEE Trans. Communications*, vol. 53, no. 3, pp.391-394, Mar. 2005.

[18] C. S. Park and K. B. Lee, “Transmit power allocation for BER performance improvement in multicarrier system,” *IEEE Trans. Communications*, vol. 52, no. 10, pp.1658-1663, Oct. 2004.

[19] E. N. Onggosanusi, A. M. Sayeed, and B. D. Van Veen, “Efficient signaling schemes for wideband space-time wireless channels using channel state information,” *IEEE Trans. on Vehicular Tech.,* vol. 52, no. 1, pp.1–13, Jan. 2003.

[20] A. Zanella, M. Chiani, and M. Z. Win, “MMSE reception and successive interference cancellation for MIMO systems with high spectral efficiency,” *IEEE Trans. Communications*, vol. 4, no. 3, pp.1244-1253, May 2005.

[21] N. Prasad and M. K. Varanasi, “Analysis of decision feedback detection for MIMO Rayleigh-fading channels and the optimization of power and rate allocations,” *IEEE Trans. Information Theory*, vol. 50, no. 6, pp. 1009–1025, June 2004.

[22] R. Kalbasi, D. D. Falconer, and A. H. Banihashemi, “Optimum power allocation for a V-BLAST system with two antennas at the transmitter,” *IEEE Trans. Communications*, vol. 9, no. 9, pp. 826–828, Sept. 2005.

[23] Y. Peng, S. Cui, and R. You, “Optimal pilot-to-data power ratio for diversity combining with imperfect channel estimation,” *IEEE Communication Letters*, vol. 10, no.2, pp. 97–99, Feb. 2006.

[24] M. K. Simon and M-S Alouini, *Digital Communication over Fading Channels: A Unified Approach to Performance Analysis*, John Wiley & Sons, 2000.

[25] R. You, H. Li, and Y Bar-Ness, “Diversity combining with imperfect channel estimation,” *IEEE Trans. Communications*, vol. 53, no. 10, pp.1655-1662, Oct. 2005.